CHEMICAL REVIEWS

pubs.acs.org/CR

Review

Electronic Structure Methods for the Description of Nonadiabatic Effects and Conical Intersections

Spiridoula Matsika*

Cite This: https://doi.org/10.1021/acs.chemrev.1c00074

Read Online

ACCESS | Metrics & More | Article Recommendations

ABSTRACT: Nonadiabatic effects are ubiquitous in photophysics and photochemistry, and therefore, many theoretical developments have been made to properly describe them. Conical intersections are central in nonadiabatic processes, as they promote efficient and ultrafast nonadiabatic transitions between electronic states. A proper theoretical description requires developments in electronic structure and specifically in methods that describe conical intersections between states and nonadiabatic coupling terms. This review focuses on the electronic structure aspects of nonadiabatic processes. We discuss the requirements of electronic structure methods to describe conical intersections and nonadiabatic couplings, how the most common excited state methods perform in describing these effects, and what the recent developments are in expanding the methodology and implementing nonadiabatic couplings.

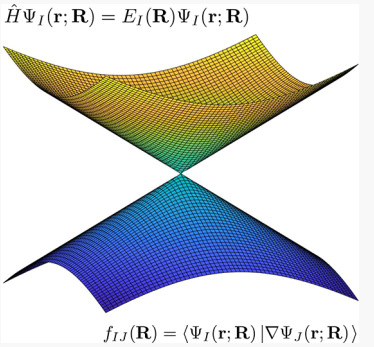

CONTENTS

Received: January 25, 2021

1. INTRODUCTION

The quantum mechanical study of molecules is primarily based on the Born−Oppenheimer (BO) approximation,[1] which separates the motion of electrons from that of nuclei. This approximation is based on the fact that the mass of electrons is much smaller than that of nuclei, so they are expected to move much faster than the nuclei. While this approximation is valid in many thermal reactions, it breaks down when more than one electronic state participates in a process, and the potential energy surfaces (PES) of the electronic states approach each other leading to coupling between electronic and nuclear motion. In this case, nonadiabatic events take place. Nonadiabatic events are ubiquitous in photophysics and photochemistry, and they play an important role in radicals and open shell systems when several electronic states are energetically in close proximity.

Despite the fact that there is a breakdown of the BO approximation, the study of nonadiabatic processes still involves a two step process: solving the electronic structure Schrödinger equation which generates PES for electronic states and the coupling terms between the PES of different electronic states and then using this information to solve for the motion of the nuclei. The second step can be done either using quantum mechanics or relying on classical mechanics. Enormous progress has been made in both of these steps during the last three decades, and many advances have been made in both the electronic structure theory and dynamics. Many reviews, and even books, have been written on nonadiabatic effects over the years.[2−19] Several chemical reviews of nonadiabatic dynamics using both classical and quantum models have also been written recently in this journal.[20−22]

The present review will focus on the electronic structure aspects of nonadiabatic processes. We will discuss the requirements for electronic structure methods to describe conical intersections (CoIns) and nonadiabatic couplings (NACs) and the recent developments in electronic structure methods for excited states, which aim at describing correctly CoIns and NACs. There has been an intense interest in developments in electronic structure theory focusing on methods applicable to nonadiabatic events during the past decade, accompanied by several implementations of NAC in a variety of methods. Our focus is on these recent developments.

The review is organized as follows. We will start with the fundamental theory based on the BO approximation and how it is expanded to nonadiabatic events. We introduce CoIns and how they are located and described. We will then discuss electronic structure methods that can be used for excited states and nonadiabatic dynamics and focus on their performance in describing CoIns. Finally, implementations and features of the NAC will be discussed.

2. BREAKDOWN OF THE BORN−OPPENHEIMER APPROXIMATION

We will start by the basic description of nonadiabatic events within the Born−Oppenheimer framework. The time-independent Schrödinger equation for molecules is given by

$$H^T\Psi^T(\mathbf{r}, \mathbf{R}) = E^T\Psi^T(\mathbf{r}, \mathbf{R}) \tag{1}$$

where $\mathbf{R}$ denotes all the nuclear coordinates and $\mathbf{r}$ are the electronic coordinates. The total nonrelativistic Hamiltonian is given by

$$H^T(\mathbf{r}, \mathbf{R}) = T^n(\mathbf{R}) + H^e(\mathbf{r}, \mathbf{R}) \tag{2}$$

where T^n is the nuclear kinetic energy operator and $H^e(\mathbf{r}; \mathbf{R})$ is the electronic nonrelativistic Hamiltonian, which includes the electronic kinetic energy and the Coulomb interactions between the particles. Since this review is focused on the electronic structure aspects, the superscript e will be dropped from now on.

The first step is to solve the electronic Schrödinger equation

$$H\Psi_I(\mathbf{r}; \mathbf{R}) = E_I(\mathbf{R})\Psi_I(\mathbf{r}; \mathbf{R}) \tag{3}$$

The eigenfunctions of H form a complete set in the electronic space at every value of $\mathbf{R}$, and they can be used to expand the total wave function

$$\Psi^T(\mathbf{r}, \mathbf{R}) = \sum_I \Psi_I(\mathbf{r}; \mathbf{R})\chi_I(\mathbf{R}) \tag{4}$$

where $\chi_I(\mathbf{R})$ are expansion coefficients. This expansion is called the Born−Oppenheimer expansion, and it is exact if the summation is not truncated. It becomes an approximation when it is truncated, which is what happens practically. Inserting it into the Schrödinger equation, multiplying on the left by Ψ_J^*, and integrating, we obtain

$$[T^n + E_I]\chi_I - \sum_J \sum_\alpha \frac{1}{2M_\alpha}(2f_{IJ}^\alpha \cdot \nabla_\alpha \chi_J + K_{IJ}^\alpha \chi_J) = E^T\chi_I \tag{5}$$

where α denotes nuclear degrees of freedom and J denotes electronic states. The terms K_{IJ} and $\mathbf{f}_{IJ}$ couple the electronic states I, J and originate from the nuclear kinetic energy operator operating on the electronic wave functions $\Psi_I(\mathbf{r}; \mathbf{R})$. They are given by

$$f_{IJ}^\alpha(\mathbf{R}) = \langle \Psi_I(\mathbf{r}; \mathbf{R}) | \nabla_\alpha \Psi_J(\mathbf{r}; \mathbf{R}) \rangle \tag{6}$$

and

$$K_{IJ}(\mathbf{R}) = \sum_\alpha \langle \Psi_I(\mathbf{r}; \mathbf{R}) | \nabla_\alpha^2 \Psi_J(\mathbf{r}; \mathbf{R}) \rangle \tag{7}$$

The brackets in eqs 6 and 7 denote integration over electronic coordinates $\mathbf{r}$, and ∇_α refers to the gradient over the nuclear coordinate R_α. The diagonal term K_{II} corresponds to nonadiabatic corrections to a single potential energy surface and is called the BO correction. In many cases, especially in ground state properties and reactivity of closed shell molecules, only one electronic state is important and it is well separated from all others. In that case, the couplings $\mathbf{f}_{IJ}$ and K_{IJ} are negligible, and they are neglected from the Schrödinger equation, eq 5, leading to the Born−Oppenheimer approximation. Often, however, especially in photochemistry, and when open shell species are involved, several electronic states are important and interact with each other, leading to important nonadiabatic processes. In that case the coupling terms need to be included.

The nonadiabatic or derivative coupling $\mathbf{f}_{IJ}$ between states I, J is the dominant term which is included in nonadiabatic dynamics and drives the nonadiabatic transitions. $\mathbf{f}_{IJ}(\mathbf{R})$ is a vector with dimensionality equal to the number of nuclear coordinates. The derivative coupling is a measure of the variation of the character of the electronic wave function with respect to the nuclear coordinates and is inversely proportional to the energy difference between states I and J,

$$\mathbf{f}_{IJ}(\mathbf{R}) = \frac{\langle \Psi_I | \nabla H | \Psi_J \rangle}{E_J - E_I} \tag{8}$$

https://doi.org/10.1021/acs.chemrev.1c00074
Chem. Rev. XXXX, XXX, XXX−XXX

This equation is informative in indicating when the derivative coupling is expected to be large. In particular, when the denominator, i.e., the energy difference between electronic energies, becomes small, then the derivative couplings become large, and the adiabatic approximation for the involved electronic states can be expected to break down. The derivative coupling $\mathbf{f}_{IJ}$ is responsible for coupling the different electronic states and drives radiationless transitions between them; that is why it plays a dominant role in nonadiabatic events and their study. Obtaining and using this term is essential in studying nonadiabatic processes and will be discussed in detail in section 5.

The K_{IJ} term may cause discontinuous behavior in calculations of nonadiabatic dynamics in the adiabatic representation, and it has been recommended that it is neglected when employing mixed quantum-classical methods and certain approximate quantum dynamical methods in the adiabatic representation.[23] Recently, Meek and Levine have shown that this term can be accurately accounted for when using multiple-spawning calculations on adiabatic surfaces by using locally diabatized Gaussian basis functions.[24] Nevertheless, the results agree with those of dynamics when the term is neglected, supporting the common practice of neglecting the term.[24]

In the discussion above, the total wave function is expanded in terms of the eigenfunctions of the electronic Hamiltonian. As a result, all the off-diagonal Hamiltonian coupling matrix elements $\langle \Psi_I | H | \Psi_J \rangle$ are zero, and the coupling between different electronic states is present in the nuclear kinetic energy terms, giving rise to the derivative coupling. This is the adiabatic representation.[17] In the adiabatic representation the derivative coupling is a vector whose magnitude can go to infinity, making the solution of the Schödinger equation for nuclei complicated. So for nuclear dynamics it is often desirable to have an alternative representation. Formally, this can be achieved by setting the derivative coupling to zero. Such a representation is called strictly diabatic,[25−29] and it causes the reappearance of the off-diagonal coupling in the potential term which is a scalar. The problem is that the derivative coupling cannot be removed completely at every nuclear degree of freedom when the expansion over electronic states is truncated,[30] so a true diabatic representation does not exist. However, we can aim at making $\mathbf{f}_{IJ}$ very small leading to a quasi-diabatic representation. The disadvantage of diabatic states is that there is no unique straightforward way to obtain them. Using electronic structure theory it is easy to obtain the eigenstates, i.e. the adiabatic states, but diabatization is more complicated. Physically, the diabatic representation maintains the character of the electronic wave functions, so that they are always smooth functions of the nuclear coordinates. Physical approaches can be used to "diabatize" the adiabatic states, such as maintaining a smooth dipole moment of another physical property. There are many approaches to generate diabatic states, and discussing them is beyond the scope of this review.

3. CONICAL INTERSECTIONS

3.1. Definitions and Noncrossing Rule

The efficiency of nonadiabatic transitions between two states depends on the derivative coupling $\mathbf{f}_{IJ}$ vector between the states, which in turn depends on the energetic proximity of the states, as shown in eq 8. When the two states become degenerate, the coupling is maximum (infinity), providing the most efficient way for radiationless transitions between states. These degeneracies, CoIns, play a crucial role in nonadiabatic chemistry, and they provide a means to study these processes using electronic structure tools. The conditions for the existence of CoIns were discussed in 1929 by von Neumann and Wigner,[31] while in 1937 Teller argued that CoIns may give rise to fast radiationless transitions.[32] But practical recognition of the importance of CoIns happened much later. The prevalence of CoIns was facilitated by developments in electronic structure theory in the early 1990s making the optimization of these points possible. Since then their importance in many areas of chemistry has become evident. In fact, CoIns are much more likely to occur than true avoided intersections, where there is a minimum on the energy gap.[33] The ubiquity of CoIns leads to a need for appropriate electronic structure theory, and there has been an intense effort in developing methods that can describe properly these features and consequently photochemistry and photophysics.

We will start with the basic description of CoIns, in order to understand how to locate them and how to characterize them using electronic structure methods. Instead of using the eigenfunctions of the electronic Hamiltonian to expand the total wave function, one may choose a different basis. We can consider a diabatic two-state basis ϕ_1, ϕ_2, leading to the Hamiltonian[5,34]

$$\mathbf{H} = \begin{pmatrix} H_{11}(\mathbf{R}) & H_{12}(\mathbf{R}) \\ H_{21}(\mathbf{R}) & H_{22}(\mathbf{R}) \end{pmatrix} \tag{9}$$

where $H_{ij} = \langle \phi_i | H | \phi_j \rangle$. The eigenvalues for this Hamiltonian are

$$E_{1,2} = \bar{H} \pm \sqrt{\Delta H^2 + H_{12}^2} \tag{10}$$

where $\bar{H} = (H_{11} + H_{22})/2$ and $\Delta H = (H_{11} - H_{22})/2$. The rotation angle α defines the transformation from diabatic to adiabatic states and is given by

$$\sin\alpha = \frac{H_{12}}{\sqrt{\Delta H^2 + H_{12}^2}} \tag{11}$$

$$\cos\alpha = \frac{\Delta H}{\sqrt{\Delta H^2 + H_{12}^2}} \tag{12}$$

For the eigenvalues of this matrix to be degenerate two conditions must be satisfied,

$$H_{11}(\mathbf{R}) - H_{22}(\mathbf{R}) = 0 \tag{13}$$

$$H_{12}(\mathbf{R}) = 0 \tag{14}$$

These conditions are satisfied in an $N^{int} - 2$ subspace, when a molecule has N^{int} degrees of freedom. The dimensionality and the conditions for degeneracy had been discussed in 1929 by Neumann and Wigner in their seminal work.[31] Diatomic molecules have only one degree of freedom, so the two conditions can never be satisfied, and it is not possible for two electronic states of the same symmetry to become degenerate. This leads to the noncrossing rule. Polyatomic molecules, however, have many nuclear degrees of freedom, making the conditions easy to satisfy and leading to degenerate electronic states.[32] The $N^{int} - 2$ subspace, where the states are degenerate, is called the seam or intersection space. The two-dimensional space orthogonal to it is called the branching or $g - h$ space.[5,34] In this space the degeneracy is lifted linearly in a first order approximation.

https://doi.org/10.1021/acs.chemrev.1c00074
Chem. Rev. XXXX, XXX, XXX−XXX

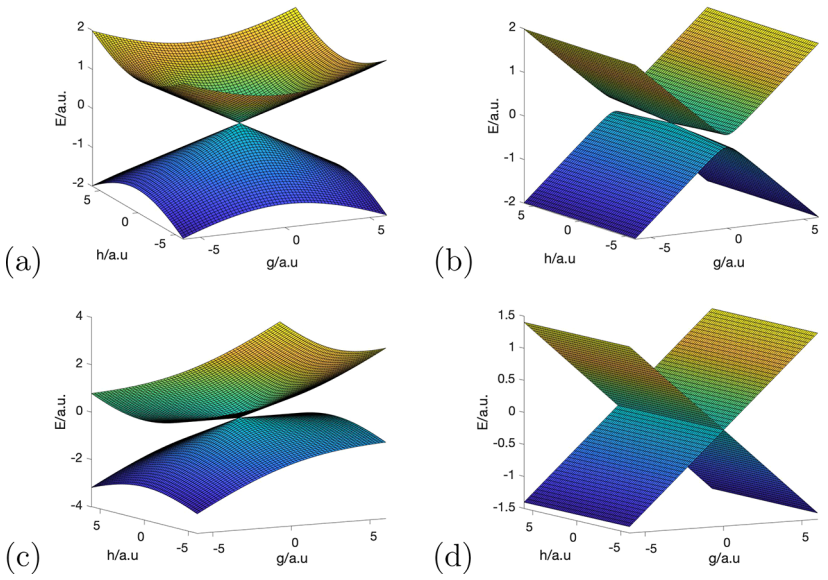

Figure 1. Energies of two states around CoIns (a−c) as a function of branching coordinates and (d) as a function of one branching coordinate and one seam coordinate. The energies are plotted using eq 22 with (a) $g = h = 0.234$ and $s_x = s_y = 0$ (vertical symmetrical cone); (b) $g = 0.3308$, $h = 0.0234$, and $s_x = s_y = 0$ (vertical asymmetric cone); (c) $g = h = 0.234$, $s_x = 0.2$, and $s_y = 0$ (tilted symmetric cone); (d) $g = 0.234$ and all other parameters 0 (h is a seam coordinate here). All parameters are in a.u. units.

The above description can be extended beyond two states, to describe degeneracies between three electronic states.[35−37] In that case, there are five conditions that need to be satisfied to reach degeneracy, and the branching space is five-dimensional. Three-state CoIns have been proven to be important in a variety of molecular systems.[35,37−48]

An important consequence of CoIns is that in the adiabatic representation a real electronic wave function changes sign around a CoIn.[49−52] This is called the geometric or Berry phase, and it is a signature of a true CoIn. The geometric phase effect can have an impact on nuclear dynamics around CoIns.[53−56]

3.2. Branching Space, Topology, and Topography

The ability of the various electronic structure methods to describe both the topography and the topology of CoIns is crucial and one of the fundamental problems with several electronic structure methods. In order to avoid confusion about the two terms, we define them here. Topology refers to the dimensionality of the CoIn seam space. As shown above, the correct dimensionality is $N^{int} - 2$, but there are electronic structure methods that fail to predict this correctly. This will be a focus when we discuss the suitability of electronic structure methods to describe CoIns. Topography refers to the shape of the surfaces around the CoIn. This is a more general issue, that applies to the correct description of potential energy surfaces and how a particular electronic structure method describes their shape. The shape of the CoIn is affected by how well an electronic structure method describes both states that are intersecting. Both of these properties have been examined for most of the methods used for excited states, and there is a great variation in their performance. Describing the topology and topography of a CoIn accurately is not trivial, and many electronic structure methods fail to do so.

In order to describe CoIns more quantitatively, a Taylor series expansion of the potential energy terms can be used. We assume a degeneracy at $\mathbf{R}_0$. At a nearby point $\mathbf{R} = \mathbf{R}_0 + \delta\mathbf{R}$ the matrix elements of the Hamiltonian, when expanded in a Taylor expansion to first order around the point of CoIn $\mathbf{R}_0$, can be written as[34,57]

$$\Delta H_{IJ}(\mathbf{R}) = 0 + \nabla(\Delta H_{IJ})(\mathbf{R}_0)\cdot\delta\mathbf{R} \tag{15}$$

$$H_{IJ}(\mathbf{R}) = 0 + \nabla H_{IJ}(\mathbf{R}_0)\cdot\delta\mathbf{R} \tag{16}$$

The requirements for a CoIn at $\mathbf{R}$ then become

$$\nabla(\Delta H_{IJ})\cdot\delta\mathbf{R} = \mathbf{g}_{IJ}\cdot\delta\mathbf{R} = 0 \tag{17}$$

$$\nabla H_{IJ}\cdot\delta\mathbf{R} = \mathbf{h}_{IJ}\cdot\delta\mathbf{R} = 0 \tag{18}$$

so that $\delta\mathbf{R}$ must be orthogonal to the subspace spanned by the vectors $\mathbf{g}_{IJ}$ and $\mathbf{h}_{IJ}$ (or defined also simply as $\mathbf{g}$ and $\mathbf{h}$; $\mathbf{g}$ is often also defined simply as the difference between the gradients without the factor of 2) for the degeneracy to remain. Other common names for the branching vectors in the literature are $\mathbf{x}_1$ and $\mathbf{x}_2$.[8,17,34] The degeneracy is lifted linearly, as seen in eqs 15 and 16, in the two-dimensional branching space defined by these two vectors. The subspace orthogonal to the branching space is the seam or intersection space. The branching vectors $\mathbf{g}_{IJ}$ and $\mathbf{h}_{IJ}$ represent nuclear motion leading to vibrational motion of the molecule.

The intersection adapted coordinates are defined as the unit vectors along the energy difference gradient and the coupling gradient,[34]

$$\mathbf{x} = \mathbf{g}_{IJ}/g \tag{19}$$

$$\mathbf{y} = \mathbf{h}_{IJ}/h \tag{20}$$

where g, h are the norms of the corresponding vectors.[5] Using these coordinates the Hamiltonian matrix of eq 9 becomes

$$\mathbf{H} = (s_1 x + s_2 y)\mathbf{I} + \begin{pmatrix} gx & hy \\ hy & -gx \end{pmatrix} \tag{21}$$

where x, y are displacements along the $\mathbf{g}_{IJ}$, $\mathbf{h}_{IJ}$ directions, respectively, s_1 and s_2 are the projections of $\frac{\mathbf{g}_I + \mathbf{g}_J}{2}$ onto the

https://doi.org/10.1021/acs.chemrev.1c00074
Chem. Rev. XXXX, XXX, XXX−XXX

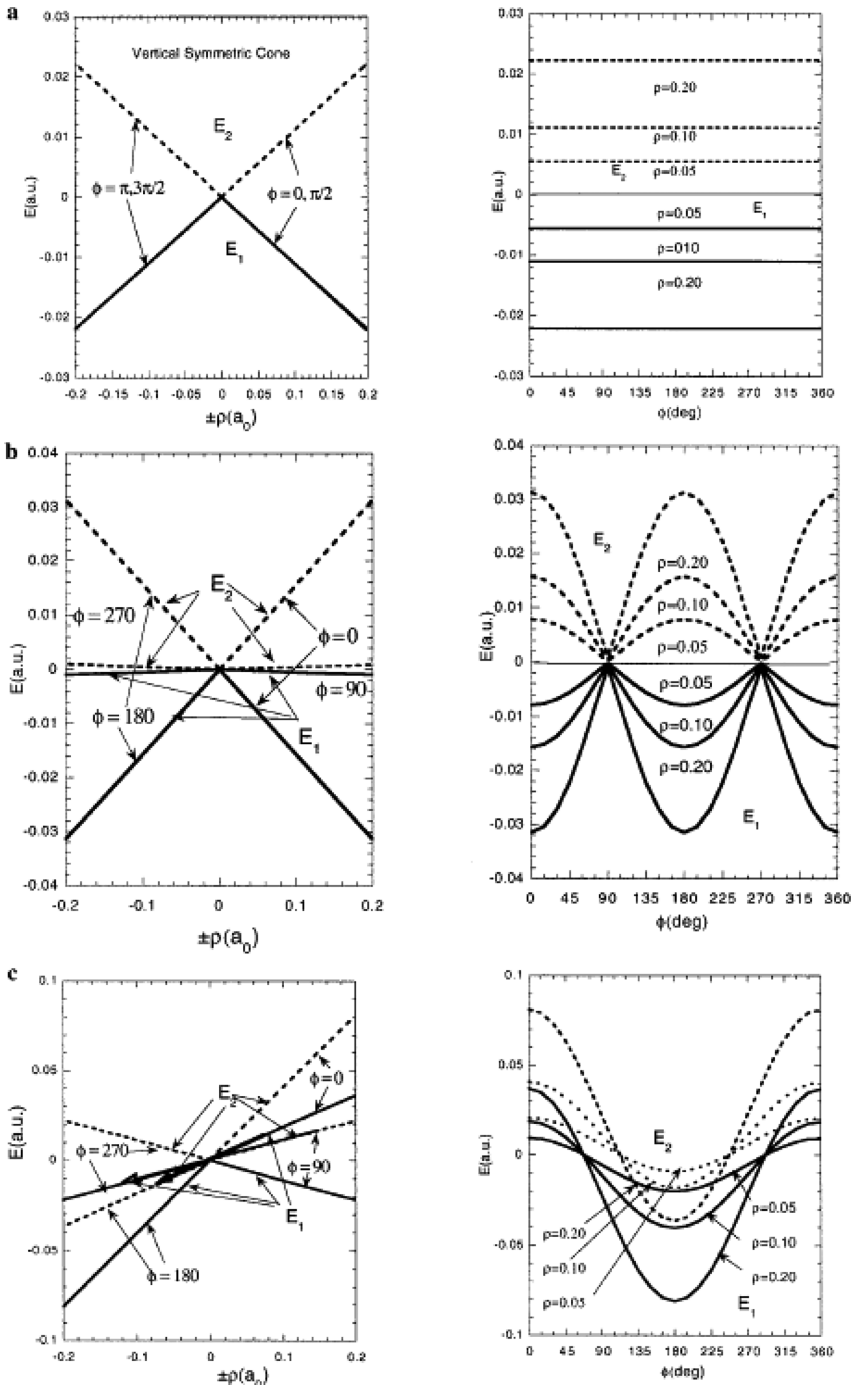

Figure 2. Sections of the potential energy surface for (a) a vertical symmetrical cone, $g = h = 0.234$ and $s_x = s_y = 0$; (b) vertical asymmetric cone, $g = 0.3308$, $h = 0.0234$, and $s_x = s_y = 0$; and (c) tilted symmetric cone, $g = h = 0.234$, $s_x = 0.2$, and $s_y = 0$. Dashed (solid) lines are upper (lower) cone. These are projections of the cones shown in Figure 1. All parameters are in a.u. units. Reprinted with permission from ref 5. Copyright 2001 American Chemical Society.

branching plane, and **I** is a 2 × 2 unit matrix. The energy at the CoIn point is set to zero. The eigenvalues are given by

$$E_{1,2}(x, y) = s_1 x + s_2 y \pm \sqrt{(gx)^2 + (hy)^2} \quad (22)$$

Using this equation we can plot the energy of the two states around the CoIn along the two special coordinates, and the potential will have the form of a double cone. The parameters g, h give the slope of the CoIn, while the parameters s_1, s_2 give the tilt. A vertical or peaked CoIn is a CoIn in which the s_1 and s_2 parameters are zero. When these parameters are nonzero, the CoIn is sloped or tilted. The CoIn is also characterized by the difference in the slopes, g and h. A symmetric CoIn is one in which the slopes g and h are equal, while an asymmetric one has different slopes. Figure 1 shows three different cases of CoIns plotted along the branching coordinates, depicting a vertical symmetric, vertical asymmetric, and a tilted cone. A plot along the seam coordinate is also shown to highlight the line of degenerate points in this case.

https://doi.org/10.1021/acs.chemrev.1c00074
Chem. Rev. XXXX, XXX, XXX−XXX

A different way to plot the energies along the two coordinates is to use polar coordinates instead, defined as $x = \rho \cos \phi$ and $y = \rho \sin \phi$. In this case the energies become

$$E_{1,2}(\rho, \phi) = \rho(s_1 \cos \phi + s_2 \sin \phi \pm \sqrt{(g \cos \phi)^2 + (h \sin \phi)^2}) \quad (23)$$

Plotting the energies using these polar coordinates is an alternative way to look at the topography. This approach has been used in several studies in applications but also when testing electronic structure methods, as will be discussed in section 4. Some representative plots are shown in Figure 2. The left side of the figure depicts the energies of the two states as a function of the distance from the CoIn, ρ, for different shapes of CoIns, while the right side shows the energies as a function of ϕ. For a symmetric cone, the energies are independent of ϕ, while for asymmetric and tilted cones they can change around the loop encircling the CoIn. So, these plots provide another visual way to depict the topography of a CoIn.

The CoIn parameters enable us to characterize a CoIn and determine the topography around it. The topography of the PESs in the vicinity of a CoIn plays a significant role in its ability to promote a nonadiabatic transition.[34,58−63] Time-dependent studies have verified this in model and real systems.[60,64] Details of the actual topography can cause significant differences in the subsequent dynamics. This had been shown in reduced dimensionality model studies initially.[60] But it can also be seen in more recent calculations of molecular systems including all degrees of freedom. In a study that applied a nonlinear dimensionality reduction scheme (diffusion mapping) to generate reaction coordinates directly from dynamics calculations, such an effect was shown for CoIns in polyatomic molecules involved in photoisomerization.[65] It was shown that a peaked CoIn was more efficient at transferring population, despite being higher in energy than a sloped CoIn. Other studies have looked into this effect as well, although they did not always see such a direct influence of the topography.[66,67]

The above description is a first-order description of CoIns. If one includes higher order terms, then the seam curvature is introduced. Analytical[68−70] or fitting methods[71,72] have been used to describe the second-order terms. While the first-order gradients enable the location of stationary points on the seam, second-order gradients, that is the Hessian, can help identify whether the points are minima or maxima.

The choice of the electronic structure method is very important for several reasons. Electronic structure methods provide information about the location and topography of a CoIn. Since the states crossing can be of very different character, the electronic structure methods have to provide a balanced description. Otherwise, the point of where the crossing occurs may change a lot or the topography of the CoIn will also change dramatically changing the efficiency for nonadiabatic transitions. The electronic structure method however may have a more fundamental effect: it may not describe the dimensionality of the cone correctly, that is the topology of the cone. There are several recent studies that have addressed both of these points for most of the methods used to describe excited states, and the findings will be discussed in section 4.

3.3. Orthogonal Branching Vectors

Even though the **g** and **h** vectors are uniquely defined at any point with no degeneracy, that changes at the points of degeneracy. At the CoIn the wave functions of the two degenerate states are not uniquely defined since any linear combination of them produces states that are still eigenfunctions of the Hamiltonian. The orthonormal eigenfunctions are arbitrary up to a rotation by an angle β. Consequently, the **g** and **h** vectors are also not uniquely defined. A unitary transformation however can rotate them so that orthogonal vectors $\tilde{\mathbf{g}}$ and $\tilde{\mathbf{h}}$ are produced,[5,73] where the requirement $\tilde{\mathbf{g}}\cdot\tilde{\mathbf{h}} = \mathbf{0}$ leads to the equation that provides β

$$\tan 4\beta_0 = \frac{2\mathbf{g}\cdot\mathbf{h}}{|\mathbf{h}|^2 - |\mathbf{g}|^2} \quad (24)$$

Using this value of β_0 to do the rotation, one obtains orthogonal branching vectors which can be used to define the topography and topology of the CoIn.[5,73]

3.4. Locating Conical Intersections

Several algorithms for locating CoIns have been developed.[74−87] The most efficient methods require the NAC. Since this coupling, however, is not available in many electronic structure packages, methods based on penalty functions that do not require the NAC have also been developed..[82,84] Since CoIns form a seam space, the search algorithms actually search for a CoIn point which has minimum energy on the seam space (MECI).

The algorithms that are now available can locate a stationary point along the seam or intersection space very efficiently. However, there is no proof that this is an energy minimum, unless the Hessian in the subspace is calculated and diagonalized. Another major issue is that the CoIns found depend on the initial guess, so intuition is necessary for such searches. Furthermore, one cannot be certain that all relevant MECIs have been found for polyatomic molecules. In order to address this problem, some efforts are being made to develop algorithms that can perform more automatic searches without intuition involved.[88−92] In a recent study, MECIs are found using driving coordinates that can be generated using a combinatorial search and subsequent optimization.[92] We are not going to discuss these approaches in detail here but rather discuss the traditional algorithms for locating MECIs starting from an initial guess.

3.4.1. Lagrange Multiplier Based Method. One of the first methods to locate minimum energy points on the seam of CoIns uses Lagrange multiplier techniques for constrained minimizations. The Lagrange multipliers are used to incorporate the constraints for CoIns and/or for geometrical constraints into a minimization procedure.[74−79] In the approach, first developed by Manaa and Yarkony,[77] the following Lagrangian is formed and minimized

$$L(\mathbf{R}, \lambda_1, \lambda_2) = E_I + \lambda_1 \Delta E_{IJ} + \lambda_2 H_{IJ} \quad (25)$$

where λ_1 and λ_2 are Lagrange multipliers. Additional geometrical constraints can be imposed by adding them to the Lagrangian. The advantage of this approach is that it can be easily extended to searches for three-state CoIns by adding more constraints.[36] A Newton−Raphson method can be used to locate extrema of the Lagrangian. The gradients of the constraints give $\mathbf{g}_{IJ}$ and $\mathbf{h}_{IJ}$. Instead of incorporating the energy E_I in the Lagrangian, the average of the two states can also be used.

3.4.2. Gradient Projection Method. A different approach to locate CoIns, developed by Robb and co-workers, uses projected gradient techniques instead of Lagrange multipliers.[80] The energy difference in the plane spanned by $\mathbf{g}_{IJ}$ and $\mathbf{h}_{IJ}$ is minimized while the upper state E_J is minimized in the

https://doi.org/10.1021/acs.chemrev.1c00074
Chem. Rev. XXXX, XXX, XXX−XXX

remaining N^{int} − 2-dimensional space orthogonal to the branching plane.[80]

The gradient that minimizes the energy difference is

$$\mathbf{f}_1 = 2(E_I - E_J)\frac{\mathbf{g}_{IJ}}{g_{IJ}} \tag{26}$$

The space orthogonal to the branching plane is defined by the projection matrix

$$\mathbf{P} = \mathbf{I} - \hat{\mathbf{g}}_{IJ}\hat{\mathbf{g}}_{IJ}^{\dagger} - \hat{\mathbf{h}}_{IJ}\hat{\mathbf{h}}_{IJ}^{\dagger} \tag{27}$$

$\hat{\mathbf{g}}$ and $\hat{\mathbf{h}}$ represent the orthonormalized vectors. The upper state gradient projection is

$$\mathbf{f}_2 = \mathbf{P}\frac{\partial E_J}{\partial \mathbf{R}} \tag{28}$$

The gradient to be minimized is a linear combination of $\mathbf{f}_1$ and $\mathbf{f}_2$. This algorithm has been used extensively, improved, and extended to three-state CoIns, over the years.[86,87,93−96]

3.4.3. Penalty Function Method. In addition to the above algorithms, there is a need to have algorithms for locating CoIns which do not require the derivative coupling vector, since this is not available for all electronic structure methods and it adds computational cost. The penalty function method is an approach to achieve this by adding a term to an objective function that monotonically increases as the energy gap increases.[82,84] In the method developed by Martinez and co-workers,[84] the objective function

$$L_{IJ}(\mathbf{R}; \sigma, \alpha) = \bar{E}_{IJ}(\mathbf{R}) + \sigma G_{IJ}(\Delta E_{IJ}(\mathbf{R}); \alpha) \tag{29}$$

is minimized. $\bar{E}_{IJ}$ and ΔE_{IJ} are the average energy and energy difference of the two states I and J, respectively, σ is a parameter used to lead the optimization toward the seam space minimum, and G_{IJ} is a penalty function which smooths discontinuities in the gradient of the potential surface. G_{IJ} has the form

$$G_{IJ}(\Delta E_{IJ}; \alpha) = \frac{\Delta E_{IJ}^2}{\Delta E_{IJ} + \alpha} \tag{30}$$

where α is a user defined smoothing parameter. Minimization of the objective function in eq 29 corresponds to minimizing $\bar{E}_{IJ}$ subject to the constraint that ΔE_{IJ} goes to zero. This method can also be used to locate three-state CoIns.[84] A penalty function based method to locate three-state CoIns using combined quantum and classical mechanics (QM/MM) methodology has also been developed.[97]

3.4.4. Comparisons. The three methods discussed above for optimizing the minimum energy point on the seam were compared by Thiel and co-workers.[95] The performance of the algorithms was tested on 12 well-known CoIns of small molecules. The Lagrange Newton method was found to be the most efficient. For example, when locating a CoIn in butadiene, the penalty function method needed 86 iterations to converge while the other two methods needed 15−16 iterations. Each iteration is much cheaper for the penalty function method, of course, since couplings are not needed, but when the number of iterations is so much larger, this advantage is diminished. In butadiene, the total time was 7.1 s when using the penalty function method while it was 1.9 s for the other methods. As a result, the penalty function method is not recommended when the couplings are available. Nevertheless, there are still many electronic structure methods and packages that do not have analytic derivative couplings implemented, and in that case this method is essential. Herbert and co-workers[98] also confirmed that methods that use the coupling make the convergence much faster, decreasing the number of iterations and the time it takes to converge by more than a factor of 2. Winslow et al.[99] have also compared the gradient projection method and penalty function method to optimize MECIs using a variety of electronic structure methods. They concluded that the penalty function method is reliable in predicting the MECI geometries, although they agree that in cases where derivative couplings are available the projected method is better.

3.4.5. Beyond MECI. In addition to algorithms for locating MECIs, other procedures have been developed to navigate the PES involving CoIns, which is critical for understanding the overall photochemical and photophysical events. These procedures include protocols that use steepest-descent paths from the Franck−Condon point toward a CoIn or from a CoIn toward products.[100−102] Minimum energy paths connecting CoIns to products on the ground state have been done starting from displacements along the branching plane.[100,103] Other more sophisticated approaches have also been developed, such as geometry optimization on a hypersphere.[104] An approach that can be used to find accessible CoIns from the Franck−Condon region is to use classical trajectories and specifically trajectories with zero initial velocities.[105,106] As an example, this approach has been used in locating CoIns in rhodopsin using QM/MM.[105]

Furthermore, the MECI is not necessarily the most important or most accessible CoIn, so it is important to explore the seam space and pathways along it. Various approaches have focused on exploring the seam space.[62,102,107] Steepest-descent paths within the seam space have been used.[102] Another approach is the recent seam space nudged elastic band (SS-NEB) method, which combines the nudged elastic band method with gradient projected MECI optimization. It provides an efficient approach to find minimum energy paths in the seam space.[107] Ultimately, dynamics studies provide the most complete picture, but since these are time-consuming, insight from the electronic structure calculations is important. Dynamics can be used to check how accurate the representations of reaction paths are.[106,108]

4. HOW ELECTRONIC STRUCTURE METHODS DESCRIBE CONICAL INTERSECTIONS

Based on the basics we have discussed so far, the requirements of electronic structure methods to properly describe CoIns are emerging. The description of nonadiabatic events and CoIns poses challenges to electronic structure methods. An equivalent description of the states involved in CoIns as well as proper description of their NACs is required for an adequate treatment. Availability of analytic gradients is crucial for being able to locate CoIns and for extending them to the calculation of NACs. When choosing an electronic structure method to study CoIns, there are some critical properties that need to be described properly: (i) location of CoIns (geometry and energy), (ii) topology/topography of CoIns, and (iii) NACs. It should further be highlighted once again that the type of states involved in the nonadiabatic transitions or CoIns is critical in determining whether an electronic structure method can describe these effects adequately. For example, coupling between excited states can be described by a greater variety of methods compared to coupling between the ground and an excited state in closed shell molecules because in several methods the ground state is not treated equivalently to the excited states creating problems when

https://doi.org/10.1021/acs.chemrev.1c00074
Chem. Rev. XXXX, XXX, XXX−XXX

the ground state is involved in the CoIn, as will be described in detail below. In another example, when symmetry is involved, the situation may become simpler, as in the case of the Jahn−Teller effect,[109−111] since symmetry dictates the location of CoIns and the symmetry of the coupling.

In this section, we will examine how common methods for excited states can describe CoIns based on recent research in this area. Methods for excited states which have been used in nonadiabatic studies will be summarized, and their advantages and disadvantages in describing CoIns will be described. Electronic structure methods can be divided broadly into single reference and multireference methods, and we discuss them separately.

4.1. Multireference Methods

Multireference methods have the ability to describe several electronic states equivalently, and they provide a natural way to describe coupling between them. These methods were the first to be used for the description of CoIns and nonadiabatic dynamics. Multireference methods and their usage in excited states have been discussed in detail in recent reviews in this journal.[112−114] Here the focus is on how electronic structure methods can describe CoIns and the recent developments of electronic structure methods in this direction. We only give a basic overview of the methods so that it will facilitate our discussion of them with respect to CoIns. The methods can be divided into the ones that are based on the variational method (multiconfigurational self-consistent field (MCSCF) and multireference configuration interaction (MRCI)) and the ones that are based on perturbation theory (MRPT). A third area has actually emerged in more recent years, which combines multireference approaches with DFT. These approaches have been recently reviewed in this journal and will not be considered in detail here.[115] We want to point out however that after the review by Ghosh et al.[115] was published there have been more developments toward efforts to describe CoIns. Specifically, the multiconfiguration pair-density functional theory (MC-PDFT) with multistate extensions has shown promise in describing CoIns accurately.[116,117]

4.1.1. MRCI. The easiest method to understand conceptually is configuration interaction, based on variational principle.[118] In this method the electronic wave function is expanded in terms of Slater determinants or configuration state functions (CSFs) that are formed from excitations of electrons from the occupied orbitals in the Hartree−Fock wave function to the virtual orbitals. The expansion can be written as

$$\Psi_I = \sum_{a=1}^{N^{CSF}} c_a^I \psi_a \tag{31}$$

CSFs are linear combinations of Slater determinants that are eigenfunctions of the spin operator and have the correct spatial symmetry and total spin of the electronic state.[118] This multielectron basis is constructed from molecular orbitals, which are obtained prior to the configuration interaction calculation. The energies and wave functions are provided by solving the eigenvalue equation

$$[\mathbf{H}(\mathbf{R}) - E_I(\mathbf{R})]\mathbf{c}^I(\mathbf{R}) = 0 \tag{32}$$

where $\mathbf{H}(\mathbf{R})$ is the electronic Hamiltonian in the CSF or Slater determinant basis. Usually the expansion includes only single and double excitations and is defined as CISD, which more specifically is

$$|\Psi_{CISD}\rangle = c_0|0\rangle + \sum_{i,a} c_i^a|\psi_i^a\rangle + \sum_{i>j,a>b} c_{ij}^{ab}|\psi_{ij}^{ab}\rangle \tag{33}$$

$|0\rangle$ is the Hartree−Fock reference, and $|\psi_i^a\rangle$, $|\psi_{ij}^{ab}\rangle$ denote single and double excitations from the reference, respectively.

In order to apply configuration interaction to nonadiabatic problems, it has to be extended to the multireference configuration interaction version, where instead of using a single reference, the Hartree−Fock Slater determinant, many references are used. In MRCI up to double excitations (MRCISD), the wave function is comprised of single and double excitations from these references,[112,113]

$$|\Psi_{MRCISD}\rangle = \sum_I c_I|I\rangle + \sum_{S,a} c_S^a|\psi_S^a\rangle + \sum_{D,a,b} c_D^{ab}|\psi_D^{ab}\rangle \tag{34}$$

$|\psi_S^a\rangle$ denotes all single excitations from the reference space defined by all $|I\rangle$, while $|\psi_D^{ab}\rangle$ denotes all single and double excitations from the references to the virtual orbitals (using notation used in ref 113).

The references can be chosen in a variety of ways. The most common procedure, however, is to choose an active space of important orbitals and allow all possible occupations within that space (full CI in that space). In the above expansion, redundancies may occur when the same configuration can be generated from two different references, and these redundant expansion terms need to be eliminated. Redundancies do not occur in an occupation based approach where a possible determinant either succeeds or fails to satisfy the occupation restrictions, and that alone determines its expansion index.[112] MRCI has been developed either uncontracted (where excitations from all references occur)[119] or internally contracted.[120−122] In the internally contracted version, which is used in order to reduce the expansion, single and double excitations are applied to the predetermined reference wave function as a whole keeping the coefficients mixing the references fixed as computed from a preceding multiconfiguration self-consistent field calculation.

A problem with CI and MRCI is that they are not size-consistent and size-extensive. A method is size-extensive when the energy is scaling properly with the size of a molecule, while a method is size-consistent when the sum of the energies of noninteracting monomers is equal to the energy of the entire system.[123,124] The Davidson correction, E_Q, is the simplest approach that can correct for this error using a simple formula depending only on the coefficient of the HF reference, or in MRCI the weight of all references combined, c_0, and the correlation energy ΔE ($E_Q = (1 - c_0^2)\Delta E$).[125] The corrected approach is often referred as MRCI+Q. More sophisticated corrections also exist.[112,113,126]

A major advantage of MRCI is that there are analytic gradients available in Columbus,[127,128] which has an uncontracted version based on the Graphical Unitary Group Approach (GUGA).[129−131] The gradients have been extended to the calculation of NACs, as will be discussed later.[132,133]

4.1.2. MCSCF/CASSCF. MCSCF is another variational approach using an expansion as shown in eq 31. In this approach, in addition to optimizing the linear coefficients of the expansion, the orbitals are also optimized. So, optimization of the MCSCF expansion is a more complicated problem compared to CI/MRCI, and several implementations exist.[112,134−136] The most popular choice for the selection of references to be included in the expansion is the complete active space (CAS) approach where all possible configurations in a

https://doi.org/10.1021/acs.chemrev.1c00074
Chem. Rev. XXXX, XXX, XXX−XXX

given orbital space are included.[137,138] This expansion is called CASSCF, although it was also introduced as the FORS (full optimized reaction space) model by Ruedenberg and co-workers.[138] This approach simplifies the definition of the wave function and has advantages both theoretical and practical. The drawback however is that the number of configurations increases exponentially with the number of active orbitals, severely limiting the size of active space that can be used. An alternative approach is the restricted active space (RAS) leading to RASSCF, where the active space is partitioned into three spaces.[139] The middle space is a complete active space, the first space has a restricted number of holes, while the third space has a restricted number of electrons. Figure 3 shows diagramatically this separation.

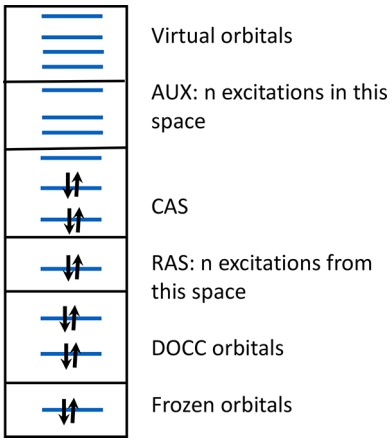

Figure 3. Orbital level diagram showing the division of orbitals in a RASSCF/CASSCF/MRCI calculation. Frozen orbitals are not reoptimized in the MCSCF procedure, doubly occupied orbitals (DOCC) are reoptimized but they always have an occupation of 2, orbitals in the RAS have *n* number of electrons being excited out of them, while orbitals in AUX allow for *n* electrons to be excited into them. All possible occupations are allowed in CAS (so, a FCI is performed in that space). Virtual orbitals are used in MRCI where the MCSCF is used as a reference, and one or two electrons are excited into the virtual space.

MCSCF does not include dynamical correlation. So the most accurate way to include multireference effects is to start with MCSCF and add dynamical correlation through configuration interaction (as in MRCI) or perturbation theory (as in multireference perturbation theory (MRPT) approaches). These methods however are often much more expensive, so, until recently, in practice optimizations and dynamics were mostly done using CASSCF.

Despite the complication of CASSCF, several efficient codes exist that can perform efficient calculations on larger systems. Recent implementation (including gradients and NACs) using graphical processing units (GPUs) and an algorithm for the CASSCF orbital optimization that uses sparsity in the atomic orbital (AO) basis set has allowed CASSCF computations on molecular systems containing more than 1000 atoms.[140−142]

4.1.2.1. Variations of MCSCF. An extension of the RASSCF method is the occupation-restricted-multiple-active-space (ORMAS).[143] This method allows for the arbitrary partitioning of the set of active orbitals instead of just three partitions, as in RASSCF. Furthermore, for each of these partitioned orbital groups, variations in their electron occupations are allowed through the specifications of minimum and maximum values. ORMAS allows for a more flexible way to define a wave function that includes nondynamical correlation. NACs have been developed and tested.[144] Overall, having no excitations between the ORMAS subspaces leads to qualitatively reasonable results for couplings, while single excitations significantly improve the energies and gradients. However, single excitation between the subspaces can lead to problems with the orbital subspaces. Derivative couplings with ORMAS are similar to the CASSCF ones.[144] ORMAS has also been used with spin-flip (SF) in order to solve the problem of spin contamination in SF approaches as will be discussed later.[145,146]

Several other variations on CASSCF/MCSCF have been discussed in the literature. Optimizing both the CI coefficients and the orbitals is a computationally intensive problem. A CASCI (complete active space configuration interaction) approach allows for the separation of these steps, since this approach only optimizes the CI coefficients and the orbitals can be obtained from a different procedure. This idea has been utilized in several approaches.[147−153]

Levine and co-workers have developed and tested a CASCI approach using orbitals obtained from state-averaged configuration interaction singles natural orbitals (CISNO).[151,154] This is a much more efficient approach compared to CASSCF since the orbitals and CI coefficients are optimized separately. The CISNO provide a reasonable description of the excited states and CASCI guarantees the proper multireference character of the system. As such, the topology around CoIns is correctly described by this approach, and this was demonstrated in the original publication using ethylene as the model.[151] Analytic gradients and NACs have also been developed.[154] Using GPUs the authors were able to demonstrate that it can be used to perform excited state dynamics simulations of molecules containing on the order of 100 atoms or CoIn optimization for systems with about 300 atoms.

Another choice of orbitals that has been explored in CASCI is high-multiplicity natural orbitals (HMNO) obtained from a correlated calculation on a high-multiplicity state.[149,155] In this case the high-multiplicity state is the ground state in that manifold, so any correlated method for the ground state can work. This approach provides good description of excitation energies and PES, but it is sensitive to the type of excited state described. It can also describe CoIns with similar accuracy as CASSCF.[155] It saves computational time in two ways, by skipping the orbital optimization step and by allowing virtual orbitals to be frozen in a subsequent MRCI calculation. A similar approach is the restricted active space spin-flip (RAS-SF), which uses orbitals from the Hartree−Fock (high-spin) determinant and a restricted active space.[153,156]

Another approach that has been used to describe CoIns is the Floating Occupation Molecular Orbitals (FOMO) method. In this method, a single determinant HF equation is used with fractional occupation numbers. The occupation numbers are determined via Fermi−Dirac or related distributions during the SCF procedure. Complete active space configuration interaction wave functions with floating occupation molecular orbitals (FOMO-CASCI) have also been implemented with ab initio and semiempirical Hamiltonians.[152,157] Gradients and derivative couplings have been implemented,[142,158] and they have also been used in dynamics.[159] A very recent review has summarized all the methods related to CASCI.[160]

Mazzioti and co-workers looked at CoIns using two-electron reduced density matrices methods from solutions of the anti-Hermitian contracted Schrödinger equation (ACSE) without

https://doi.org/10.1021/acs.chemrev.1c00074
Chem. Rev. XXXX, XXX, XXX−XXX

explicitly computing many-electron wave functions.[161] The ACSE can be initialized with a mean-field two-electron reduced density matrix (2-RDM) from Hartree−Fock theory or a correlated 2-RDM from MCSCF calculation. Conical intersections were located in methylene and water, as well as CoIns involved in the tautomerization of vinyl alcohol to acetylaldehyde.[162−164]

4.1.2.2. Density Matrix Renormalization Group. The density matrix renormalization group (DMRG) has emerged as a promising method for strongly correlated systems and consequently for excited states as well.[165,166] DMRG combined with SCF is able to approximate a CASSCF wave function to arbitrary accuracy with polynomial scaling by reducing the size of the configurational space by optimization of a matrix product state wave function. The main advantage is being able to extend to much larger active spaces since the exponential scaling of CASSCF is avoided leading to impressive expansions compared to traditional CASSCF. The method is especially suited for long conjugated molecules with strong correlation in which case more than 100 active orbitals can be included.[165] DMRG treats nondynamical correlation primarily, so it has been combined with correlated methods, complete active space second-order perturbation theory (CASPT2),[167,168] and MRCI,[169] to include dynamical correlation. Gradients[170,171] and nonadiabatic couplings have been developed using an approximate scheme.[172] The algorithm was tested with a MECI search on 1,2-dioxetanone. The results were identical to CASSCF. This is only a recent development, and more work is expected to add to the contributions of this promising approach to nonadiabatic processes and CoIns.

4.1.3. Multireference Perturbation Theory. Multireference perturbation theory, MRPT, has many variants. The application of perturbation theory in a contracted way to a zero order wave function calculated at the complete active space CAS level was developed by Roos giving rise to CASPT2,[173,174] and it was implemented in Molcas.[175] Later it was also implemented in Molpro,[176] and it is the most widely used approach to date. Although CASPT2 is very useful for describing excited states with the inclusion of both dynamical and nondynamical correlation, it is problematic around CoIns since it uses perturbation theory to correct one state at a time. The multistate CASPT2 (MS-CASPT2) was developed later,[177] which takes into account coupling between states and is thus more appropriate for CoIns between excited states. In this case the steps that are taken follow the order of "diagonalize, then perturb, then diagonalize". Even in that case care must be exercised if the underlying CASPT2 reference is not very good for the multistate procedure.[178]

Several other different variations have been developed.[179−186] A different formalism was developed by Nakano, Hirao, and Gordon based on Van Vleck perturbation theory and quasidegenerate perturbation theory with multiconfigurational self-consistent-field reference.[180−182] This approach is implemented in Gamess[187,188] and termed MCQDPT2 (multiconfiguration quasi-degenerate second-order perturbation theory). MCQDPT2 uses uncontracted configuration state functions to expand the first-order wave function and a diagonal approximation for the zeroth order Hamiltonian.[189] Even in the multistate case, Granovsky showed that there may be singular potential energy surfaces around avoided crossings and CoIns.[190] The extended multiconfiguration quasi-degenerate perturbation theory (XMCQDPT2) was developed by Granovsky to fix these problems.[190] The extended approach solves this problem by enforcing the states to be invariant under unitary transformations within the model space. XMCQDPT2 is available in the Firefly QC package,[191] which is partially based on the Gamess (US)[187] source code. An analogous extended MS-CASPT2 (XMS-CASPT2) has also been developed.[192] NEVPT2 (n-electron valence state perturbation theory) uses a contracted zero-order wave function but differs from CASPT2 in the nature of the zero-order Hamiltonian. In NEVPT2 the model Hamiltonian includes second-order terms in the form given by Dyall.[193] This operator does not give rise to intruder states, and it costs little more than other CASSCF perturbation theories. It has been implemented using contracted functions in both the single- and mutlistate models.[183,185,186] A quasidegenerate formulation of the second-order n-electron valence state perturbation theory approach, QD-NEVPT2, has also been developed.[186]

When using the standard Fock-matrix formulation for the zeroth-order Hamiltonian, a systematic error occurs in the description of processes that involve a change in the number of unpaired electrons.[194] The problem was associated with the zeroth-order Hamiltonian needed to yield diagonal elements that resemble negative ionization potentials and electron affinities for singly occupied orbitals. A shifted zeroth-order Hamiltonian has been introduced to account for this.[194] The empirical shift parameter, the IPEA shift, is based on benchmarks and is often taken to be 0.25 au.[194] A more recent study suggests that such a shift is not needed for moderate size organic chromophores.[195] Another problem encountered with CASPT2 is that sometimes the expectation values of doubly excited configurations are near the expectation value of the zeroth-order wave function, leading to singularities because of the denominators going to zero. In this case, an intruder state is introduced into the problem. In order to avoid intruder states, an imaginary shift is used in the denominators of the second-order perturbation theory expressions, which can replace the singularities with a small distortion of the potential energy function.[196]

A brief mathematical description focusing mostly on CASPT2 is given here, while an extensive discussion of all the details can be found in a recent review in this journal.[114] The zeroth-order Hamiltonian in multireference PT should resemble the single reference case. In most cases, including CASPT2, the Fock operator f of the spin-averaged first-order density matrix of the reference wave function is used, and the zeroth-order Hamiltonian is

$$H^{(0)} = PfP + QfQ \tag{35}$$

In CASPT2 $P = |0\rangle\langle 0|$ and $Q = 1 - P$ are projectors operators projecting onto the reference wave function $|0\rangle$ and its orthogonal compliment, respectively. The reference wave function is an MCSCF wave function. In most cases a CASSCF wave function is used as reference and this can be for a single state or a state-averaged one. The RASPT2 approach has also been developed more recently where a RASSCF wave function is used as a reference.[197]

The first-order wave function, $|\Psi_N^{(1)}\rangle$, is generated by single and double excitations to the reference function

$$|\Psi_N^{(1)}\rangle = \sum_j C_j^N |\Phi_j^{SD}\rangle \tag{36}$$

In CASPT2 the complementary space Q includes internally contracted configurations. The number of contracted config-

https://doi.org/10.1021/acs.chemrev.1c00074
Chem. Rev. XXXX, XXX, XXX−XXX

urations does not depend on the number of references, and this reduces the expansion significantly. On the other hand, the calculation of the matrix elements becomes more involved and requires higher order density matrices. The configurations are also nonorthogonal and are often linearly dependent. The amplitudes C_j^N are obtained by the equation

$$\sum_j C_j^N \langle \Phi_i^{SD}|H^{(0)} - E_N^{(0)}|\Phi_j^{SD}\rangle = -\langle \Phi_i^{SD}|H|0\rangle \tag{37}$$

In XMS-CASPT2 the projection operator includes all states in the multistate reference expansion, $P = \sum_N |\Psi_N^{(0)}\rangle\langle\Psi_N^{(0)}|$. The reference states $|\Psi_N^{(0)}\rangle$ are in general a subset of the states included in the state-averaged CASSCF. The difference between MS-CASPT2 and XMS-CASPT2 is in this term, wherein the MS-CASPT2 only diagonal terms $|\Psi_N^{(0)}\rangle f_{NN}\langle\Psi_N^{(0)}|$ are included so there is a $H^{(0)}$ for each state, while in XMS-CASPT2 all terms are included. In XMS-CASPT2 a state-averaged Fock operator is used while in MS-CASPT2 a state specific one is used. In general, the Fock operator is not diagonal in the space of reference wave functions, so it is diagonalized within the reference space producing a set of rotated reference functions.

Once the amplitudes are determined, an effective Hamiltonian is built and diagonalized,

$$H_{LM}^{eff} = \langle \Psi_L^{(0)}|H|\Psi_M^{(0)}\rangle + \frac{1}{2}[\langle \Psi_L^{(1)}|H|\Psi_M^{(0)}\rangle + \langle \Psi_L^{(0)}|H|\Psi_M^{(1)}\rangle] \tag{38}$$

The eigenvalues give the XMS energies while the resulting eigenfunctions u_M^I are used to build the corrected wave function

$$|\Psi_I\rangle = \sum_M u_M^I(|\Psi_M^{(0)}\rangle + |\Psi_M^{(1)}\rangle) \tag{39}$$

MS-CASPT2 excitation energies between states that are well separated are about 0.1−0.2 eV from the best theoretical estimates.[198,199] In contrast in XMS-CASPT2 the use of the state-averaged Fock operator may deteriorate the results of individual states, and the results depend on the number of states included in the XMS-CASPT2 model space. Very recently, a new approach was introduced by Battaglia and Lindh, the XDW-CASPT2, which aims at performing as MS-CASPT2 when the electronic states are well separated and as XMS-CASPT2 when underlying zeroth-order references are near-degenerate.[200,201] This approach is similar to XMS-CASPT2 to ensure approximate invariance under unitary transformations of the model states but uses a dynamic weighting scheme to smoothly interpolate the Fock operator between state-specific and state-average regimes.

Although analytic gradients in MRPT were not as readily available for a while, they are now available for many of the variants discussed. Shiozaki and co-workers developed and implemented analytic gradients for CASPT2,[202,203] MS-CASPT2, and XMS-CASPT2[204] and derivative coupling between (X)MS-CASPT2 states.[205,206] These are all available in Bagel.[207] Other analytic gradients for CASPT2 have also been developed using the Molrpo implementation,[208−211] and gradients for MCQDPT2 have been reported.[182] Analytic first-order derivatives for NEVPT2 and QD-NEVPT2 have also been developed recently.[212−214] Active spaces up to (12e,12o) in systems with about 1000 basis sets can be used in QD-NEVPT2, and the algorithm is parallelized.[214] Analytic gradients of CASPT2 using tensor hypercontraction have become available very recently, and they can treat molecules with more than 1000 basis functions very efficiently.[215]

4.1.4. Comparing MECI Structures and Energies Using Multireference Methods. In general, it is expected that there is at least qualitative agreement of locations of MECIs using the various multireference methods. Most MECIs are usually located using CASSCF, since gradients and NACs for CASSCF have been available for decades, while gradients for CASPT2 are much more recent. MRCI gradients have been available in some software, but usually MRCI is more expensive and cannot be used easily in many polyatomic molecules. Nevertheless, MRCI studies of polyatomic molecules, such as DNA bases and polyaromatic hydrocarbons, have been performed providing valuable insight on the effect of dynamical correlation on CoIns.[41,216−219]

We are not attempting to list all the publications that have compared the structures between CASSCF and MRCI or MRPT, but we are discussing a couple of representative examples to show how dynamical correlation can affect the location of MECIs. In a study of several organic molecules, the geometries of MECIs obtained at the CASSCF level were compared to those at the XMS-CASPT2 level, confirming that CASSCF performs qualitatively similar to XMS-CASPT2.[99] The structures differed by 0.01 Å in bond lengths and 7° in dihedral angles, although the maximum deviation in a dihedral angle was 35°. A contrary example that highlights the importance of dynamical correlation is cytosine, where it was found that energies of CoIns can change by more than 1 eV when dynamical correlation is added.[41,220−224] A different study focused on uracil and thymine cations and the two- and three-state CoIns in their electronic manifolds.[225] Here, again by using XMS-CASPT2 to optimize the CoIns and comparing them to CASSCF ones, it was found that dynamical correlation can be important in the relative energies of CoIns. In general, it is hard to predict when dynamical correlation will be important for the location of CoIns. This will most likely occur when dynamical correlation is much more important for one of the two crossing states, which is often referred to as the differential correlation energy effect. The problem could be even more severe when the ordering of states changes with dynamical correlation.

The performance of locating CoIns does not seem to depend as much on which multireference method is used to include dynamical correlation.[214,226] Quasidegenerate partially and strongly contracted NEVPT2 (QD-PC-NEVPT2 and QD-SC-NEVPT2) approaches have been recently explored and applied on benzene, and it was found that they agree well with XMS-CASPT2.[226] QD-NEVPT2 MECIs results have also been compared to MRCISD+Q (MRCISD with Davidson correction) and XMS-CASPT2, and overall the optimized geometries and energies were in good agreement.[214]

Other choices however can affect the location of MECIs. In a study the basis set as well as an active space dependence on the location of MECIs was explored.[214] It was found that geometries obtained with basis sets cc-pVTZ were accurate and agreed well with the cc-pV5Z geometries. On the other hand, the cc-pVDZ geometries showed larger deviations, with a maximum deviation in the bond lengths of 0.03 Å. This study suggests that using the cc-pVTZ basis set is preferable for MECIs, but often this is not possible for many photochemical reactions. As expected the energies are more sensitive to basis functions, and the MECI energies change significantly with increasing the number of basis functions. The size of the active space can also have an important

https://doi.org/10.1021/acs.chemrev.1c00074
Chem. Rev. XXXX, XXX, XXX−XXX

effect on the structure of MECIs, as well as the number of states included in the state average.

Overall, in choosing multireference methods one has to be careful of the various choices that need to be made, since they can all have an effect on the predicted MECIs. Inclusion of dynamical correlation, size of active space, basis set, and number of states averaged can all have an impact, although the magnitude of the impact depends on the specific molecules and nature of states investigated. Even more importantly, there is a danger to bias the outcome of a calculation by selecting different combinations of active space, basis sets, and methods. It is therefore advisible to use these methodologies with great care.

4.1.5. Topography and Topology of CoIns Using Multireference Methods. The most important advantage of multireference methods in describing CoIns is their ability to correctly describe the topology of a CoIn, because they treat all states equivalently. For this reason, they have been the default methods to use for nonadiabatic effects. Nevertheless, a more careful consideration of topology and topography of CoIns reveals that not all multireference methods are equally applicable, and some of them exhibit problems.

A model system that has been used in a series of studies to explore the topology and topography around CoIns is the penta-2,4-dieniminium cation (PSB3) (see Figure 4). PSB3 is a smaller model of the retinal chromophore of rhodopsin proteins (also shown in Figure 4), where the length of the system has been significantly reduced, but the main characteristics of double bonds and dieniminium cation remain. In recent years, PSB3 has been used to study the topography of CoIns, and the dimensionality (topology) of the branching space predicted by several electronic structure methods.[227−233] PSB3 is a very good candidate for such a study because of the very different character of the states involved in the CoIn. One of the states at the S_0/S_1 CoIn has a predominantly biradical electronic structure, while the other has a predominantly charge-transfer character. The weights of these configurations vary along different displacements, making the shape of the potential energy surface sensitive to a balanced description of nondynamical and dynamical correlation. This provides for a very sensitive tool to test the different behaviors of the electronic structure methods. Figure 4 shows the two coordinates defining the branching plane in this CoIn. One of the coordinates, the bond length alternation (BLA) coordinate, has been used in this work as the main coordinate to plot the energies of the two states using a variety of methods. The ground state potential energy surface of PSB3 is characterized by two transition states, denoted TS_{CT} and TS_{DIR}, which can be seen along the BLA scans, and both connect cis-PSB3 to trans-PSB3. Therefore, both transition states mediate the thermal isomerization of cis-PSB3 to trans-PSB3. Their location along BLA is another comparison that can be used to test the performance of the various methods.

A series of papers have been published using the S_0/S_1 CoIn in the PSB3 test system, and here we discuss the ones focusing on multireference methods and specifically comparing CASSCF to multireference methods with dynamical correlation, namely MRCISD, MR CISD+Q, and various MRPT2 variants.[227,231] Figure 5 shows scans along the BLA coordinate using all the multireference methods used in ref 227. Figure 5C illustrates best the importance of dynamical correlation in this system by comparing CASSCF to MRCISD+Q. CASSCF predicts the crossing between the two states much earlier along the BLA coordinate. It also changes completely the shape of the CoIn

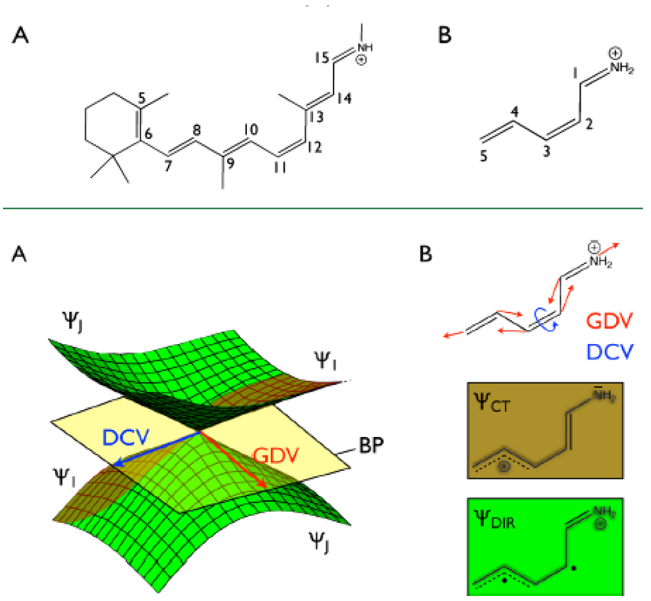

Figure 4. Top: (A) Structure of retinal protonated Schiff base and (B) its reduced penta-2,4-dieniminium cation model (PSB3). Bottom: (A) Double-cone representation of the potential energy surfaces around the CoIn. The gradient difference vector (GDV or **g**) and the derivative coupling vector (DCV or **h**) that lift the degeneracy at a CoIn are shown as red and blue arrows, respectively. The two vectors define the branching plane (BP) shown in yellow. The surfaces in the panel are colored brown or green to distinguish regions of the potential energy surface dominated by different electronic configurations, represented by the adiabatic wave functions ψ_I or ψ_J. (B) Characteristics of PSB3 at its minimum energy CoIn. On the top structure, the red and blue arrows indicate the GDV and DCV, respectively. The DCV corresponds to a torsional motion corresponding to the reaction coordinate (RC) driving the isomerization, and GDV is a bond length alternation coordinate corresponding to a lengthening of double bonds and shortening of single bonds along the backbone (BLA). The bottom two structures display bond-line diagrams of the two electronic configurations determining the character of the two states: one represents a charge-transfer electronic character, ψ_{CT}, and the other a diradical electronic character, ψ_{DIR}. Reprinted with permission from ref 231. Copyright 2014 American Chemical Society.

because of the very different relative stability of the two states. CASSCF predicts a vertical/peaked CoIn, while MRCISD+Q predicts a very sloped/tilted CoIn. Finally, the relative energies of the two transition states are reversed in the two methods. CASSCF predicts TS_{DIR} to be lower in energy while including correlation stabilizes TS_{CT} relative to TS_{DIR}. Turning our attention to Figure 5A,B we can see that the different correlated methods also give different predictions of the location of CoIn. Most of them predict a sloped CoIn, although the exact location and shape differ. It is shown that the incorporation of the IPEA shift yields CASPT2(IPEA = 0.25) and MS-CASPT2(IPEA = 0.25) results very similar to MRCISD+Q, while without IPEA the results were different. The best performing methods are shown in panel B. The choice of the active space can have an effect, as can be seen when comparing QD-NEVPT2 with (6,6) in panel A with QD-NEVPT2(6,8) in panel B, where the latter shows a much better agreement with MRCISD+Q. Overall, it is shown that adding correlation to CASSCF can affect the qualitative shape of the PES leading to CoIn. When dynamic electron correlation is included, it leads to a stabilization of the regions with charge-transfer character and to a significant reshaping of the reference CASSCF potential energy surface. In

https://doi.org/10.1021/acs.chemrev.1c00074
Chem. Rev. XXXX, XXX, XXX−XXX

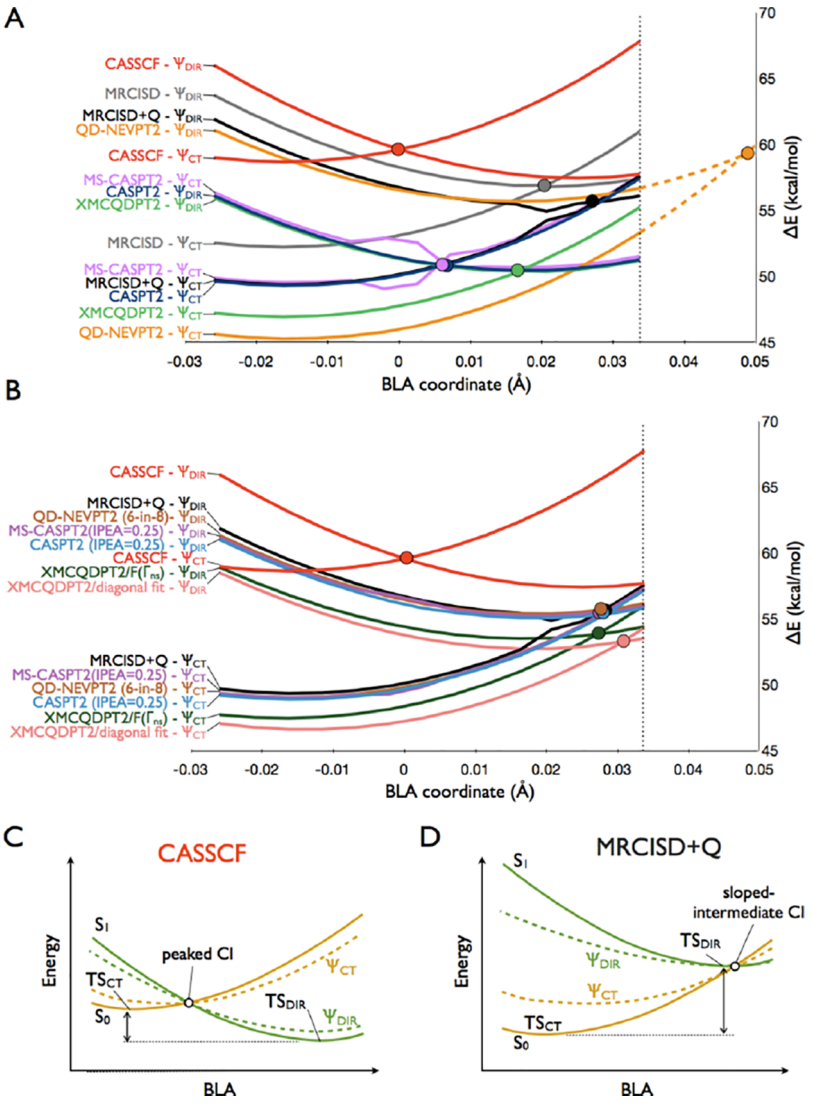

Figure 5. Energy profiles along the BLA coordinate compared with two-root SA-CASSCF (red) and MRCISD+Q (black) which are present in both parts A and B. The active space was (6,6). The energy values are relative to the reactant (cis-PSB3). The position of the CoIn for each method is indicated with a filled circle. The curves are labeled at the left margin to distinguish between diabatic curves with predominantly charge transfer (ψ_{CT}) and covalent-diradical (ψ_{DIR}) character for each method. (A) S_0 and S_1 energies for MRCISD (gray), CASPT2 (dark blue), MS-CASPT2 (magenta), QD-NEVPT2 (orange), and XMCQDPT2 (green). The QD-NEVPT2 CoIn does not lie within the selected BLA coordinate values, and so its position is estimated by extrapolating the QD-NEVPT2 curve using a polynomial fit (dashed line). (B) S_0 and S_1 energies for CASPT2(IPEA = 0.25) (blue), MS-CASPT2(IPEA = 0.25) (violet), QD-NEVPT2 with 6-in-8 active space (brown), XMCQDPT2 with a diagonal fit (pink), and XMCQDPT2/F(Γ_{ns}) (obtained using slightly different definitions of the model Fock-like operator used to define the zero-order Hamiltonian within the XMCQDPT2 formalism) (dark green). (C and D) Schematic valence bond-like state mixing diagrams for the S_0 and S_1 energy profiles along the BLA coordinate at the CASSCF and MRCISD+Q levels of theory, respectively. The diabatic states are represented with dashed lines. Mixing of the diabatic states produces the adiabatic states represented with solid lines. Brown curves are dominated by a charge-transfer wave function, while green curves are dominated by a covalent one. Reprinted with permission from ref 227. Copyright 2012 American Chemical Society.

some cases, accounting for these effects can have important implications when applied to basic photobiological problems.[234]

There are, however, some artifacts that can be seen in these curves. The MRCISD+Q curve shows an artifact at the point where MRCISD has a crossing. This artifact is due to the mixing of the CI wave functions at the CoIn which can lead to small overlaps with the CASSCF references and small coefficients in the Davidson correction.[235] The artifact can be reduced when using a Davidson correction with a relaxed or rotated reference.[227,235] Another important artifact appears at the CASPT2 and MS-CASPT2 curves at a different point along the BLA coordinate, although it is much more obvious for MS-CASPT2. This artifact is caused by the underlying CoIn at the CASSCF level at that point, and it occurs whenever the CASSCF wave functions are highly mixed, e.g. near a CoIn, and are used as the reference for CASPT2. XMCQDPT2 and XMS-CASPT2 do not have this problem.[190,192]

The artifact at the perturbation theory has been highlighted by another study that used PSB3 as well.[214] Figure 6 shows a contour plot of PESs around the S_1/S_0 CoIn. This figure illustrates again that using perturbation theory near a CASSCF CoIn can lead to discontinuities. The problem occurs at the positions of CASSCF CoIn, and it is mostly pronounced for MS-CASPT2. It is also present to a smaller degree for state specific NEVPT2 (SS-NEVPT2) and QD-NEVPT2. The QD-NEVPT2

https://doi.org/10.1021/acs.chemrev.1c00074
Chem. Rev. XXXX, XXX, XXX−XXX

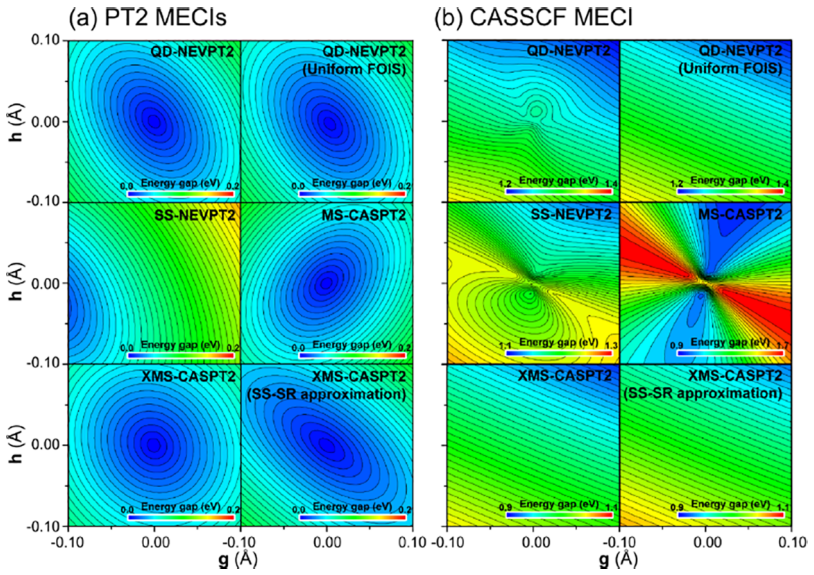

Figure 6. Contour plots of the S_1-S_0 energy gap near the (a) PT2 MECIs and (b) CASSCF MECI. In part a, the QD-NEVPT2 CoIn obtained with the state-averaged Dyall's Hamiltonian and state-specific projection manifold were also used for testing SS-NEVPT2 and QD-NEVPT2 with uniform projection manifold. In part b, note that the scale of the energy gap is different for the MS-CASPT2 method because of severe artifacts. The vectors **g** and **h** denote the normalized gradient difference vector and interstate coupling vector, respectively, obtained using the (a) PT2 methods and (b) SA-CASSCF method. Reprinted with permission from ref 214. Copyright 2020 American Chemical Society.

with uniform first-order interaction space does not exhibit such spurious behavior near the CASSCF MECI.

The above discussion shows how the topography changes when using different methods. In order to explore more the topology of the CoIn, it is best to examine the PES in loops around the CoIn. The definition of the loops in this case is shown in Figure 7 and resembles the polar coordinates of the branching plane, discussed in section 3.2. These loops were used in ref 231 to examine further the topography and topology of CoIns. This approach can distinguish between a dimensionality of $N^{int} - 1$ and $N^{int} - 2$, but it cannot distinguish $N^{int} - 3$ from the correct behavior $N^{int} - 2$. CASSCF branching vectors were used. Figure 8 shows the energy difference between the two states, S_0 and S_1, for the various methods tested around the loop. CASSCF and MRCISD have the correct dimensionality as expected, as well as MS-CASPT2, XMCQDPT2, and QD-NEVPT2. Some other multireference methods however do not show the correct dimensionality and specifically SS-CASPT2 and MRCISD+Q. In MRCISD+Q the crossing is linear rather than conical because the Davidson correction corrects the energies but not the couplings. SS-CASPT2 also does not display the correct dimensionality since the two states are not coupled correctly. This was first pointed out in earlier discussions of PT based methods by Malrieu et al.[189] The problem is corrected with MS-CASPT2, which includes coupling between the states, and it has the correct dimensionality.[236] But it may overestimate the coupling, as is shown in Figure 8, which shows that the gap is much larger than the other methods. This implies a very steep CoIn, and it has been noted in other work as well.[190,227] Furthermore, the MS-CASPT2 Hamiltonian matrix is generally nonsymmetric, so it is thought to produce a CoIn with a $(N^{int} - 3)$-dimensionality (more discussion on nonsymmetric Hamiltonians is given later). Symmetrization of the MS-CASPT2 Hamiltonian is needed to produce the correct $(N^{int} - 2)$-dimensionality. What is very important in this work is the demonstration that multireference methods are not always correct, and there are some multireference methods that do not describe the CoIns properly. Preliminary tests using surface hopping however reveal that the correct dimensionality may not be as crucial as one would expect.[231]

Schapiro and Neese used the same model to test the spectroscopy oriented configuration interaction (SORCI) method.[233] The SORCI method was introduced in 2003 by Neese as an efficient multireference method focused on providing accurate excitation energies.[237] The approach combines MRCI and MRPT. The first-order interaction space is divided into two subspaces, a strongly and a weakly interacting subspace. The configurations of the strongly interacting subspace can be treated variationally, while those of the latter space are treated using multireference perturbation theory to second order. The problem with this approach is that there are three threshold cutoffs involved in the procedure, and this makes it hard to obtain a smooth PES. In a study by Schapiro and Neese[233] these thresholds were varied starting from the default values up to complete removal of the thresholds. The study showed that making the threshold very tight can produce smooth PES and CoIns. In that study SORCI produced energy differences and energy profiles in good agreement with the MRCISD + Q method.

4.2. Single Reference Methods

In single reference methods the excited/ionic states can be obtained through linear response or equation of motion equations. These methods can in principle describe CoIns between excited states, but they cannot describe CoIns between the ground and excited state, so they have not been historically used in nonadiabatic effects. More recently, however, there have been many efforts to modify or update them to be used in such processes, since they are easier to use and often much more efficient, so they can be applied to larger molecular systems. Spin-flip is a general approach that has been used widely with single reference methods. Given its applicability to all single reference methods, it will be discussed separately after discussing

https://doi.org/10.1021/acs.chemrev.1c00074
Chem. Rev. XXXX, XXX, XXX−XXX

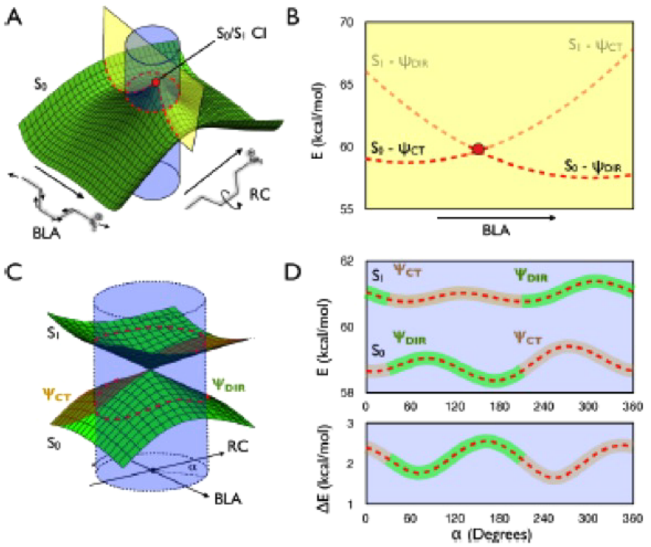

Figure 7. (A) Schematic representation of the PSB3 S_0 PES in the region of a S_0/S_1 CoIn and along a two-dimensional space defined by BLA and reaction coordinate (RC) that roughly correspond to the branching plane. The BLA coordinate and the CoIn loop cross sections are shown in yellow and blue, respectively. (B) S_0 (opaque) and S_1 (translucent) CASSCF energy profiles along the BLA coordinate. (C) More detailed scheme of the CoIn loop scan. Both the S_0 and S_1 surfaces are shown. The loop is at the intersection of the circumference of the blue cylinder with the S_0 and S_1 PESs (shown as red dashed lines) and lies in the branching plane defined by RC and BLA, assumed to be parallel to the DCV and GDV, respectively. Along the loop, the wave function of each state is expected to change electronic character twice. Areas of the surface shaded brown have a predominantly charge-transfer wave function, ψ_{CT}, while green regions have a predominately diradical wave function, ψ_{DIR}. (D) S_0 and S_1 CASSCF energies (top) and S_0-S_1 energy gap (bottom) along the CoIn loop as a function of α (as labeled in panel C). The energy profiles are shaded green or brown to show the dominant electronic character of the wave function for each state at that point (for the energy gap, only the character of the S_0 wave function is shown). Reprinted with permission from ref 231. Copyright 2014 American Chemical Society.

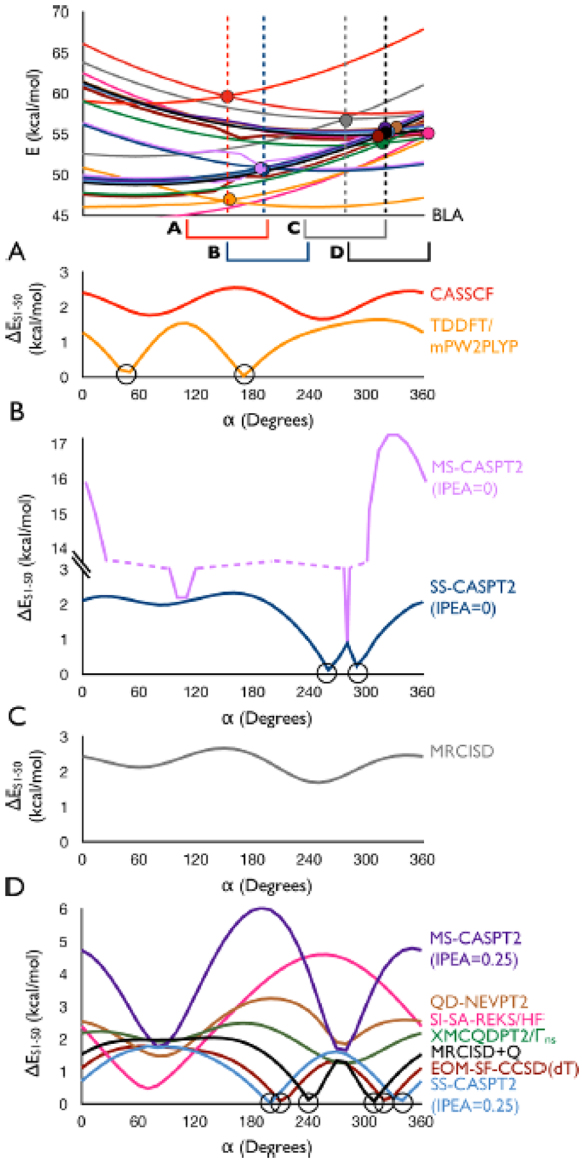

Figure 8. BLA and CoIn loop energy profiles for CASSCF (red), MRCISD (gray), MRCISD+Q (black), SS-CASPT2(IPEA = 0) (dark blue), MS-CASPT2(IPEA = 0) (violet), SS-CASPT2(IPEA = 0.25) (light blue), MS-CASPT2(IPEA = 0.25) (violet), XMCQDPT2/Γ_{ns} (green), QD-NEVPT2 (brown), TDDFT/mPW2PLYP (orange), and SI-SA-REKS-HF (fuchsia). (Top) S_0 and S_1 energy profiles along the BLA scan, relative to cis-PSB3. The positions of the crossings are shown as filled circles. Due to the different geometries of the crossings at different levels of theory, several CoIn loops were constructed, each centered at a different BLA value, to incorporate the crossings of all tested methods. One loop was centered at the CASSCF crossing (panel A), one around the MRCISD crossing (panel B), one around the CASPT2(IPEA = 0) crossing (panel C), and one around the MRCISD +Q crossing (panel D). Note that MRCISD+Q, SS-CASPT2- (IPEA = 0.25), MS-CASPT2 (IPEA = 0.25), XMCQDPT2, QD-NEVPT2, EOM-SF-CCSD(dT), and SI-SA-REKS all have similar energy profiles along the BLA and a similar geometry for the crossing, and therefore, only one loop is used to test all seven methods. Along the loops, only the energy differences between S_0 and S_1 are shown for all methods. An energy difference of about 0 kcal/mol means that the two states cross at that point. Such crossing points are indicated by black circles. Reprinted with permission from ref 231. Copyright 2014 American Chemical Society.

single reference methods that have been involved in the description of CoIns.

4.2.1. CIS and Corrections. CIS is the simplest method which gives a qualitative description of excited states. Configuration interaction was already discussed in the framework of MRCI. In this case a single HF reference is used and single excitations to the virtual space are included. The CIS solution is obtained by diagonalizing the Hamiltonian in the single excitations space. Because of the Brillouin theorem there is no coupling between the single excitations and the HF ground state, so CIS is not appropriate to describe CoIn between S_0 and S_1, but it can be used to describe CoIns between excited states, and that is the cheapest approach to describe these features.

Some efforts have been made in recent years to improve CIS, particularly by Subotnik and co-workers. The perturbative orbital optimized CIS (OO-CIS) attempts improving CIS using partial orbital optimization.[238] Recognizing that the orbitals in CIS are optimized for the ground state, an optimization of the energy for each excited state with respect to orbital rotations is introduced. The OO-CIS method improves dramatically the description of CT states, but it has deficiencies in describing couplings between excited states. The Variationally Orbital-Adapted Configuration Interaction Singles (VOA-CIS) method

https://doi.org/10.1021/acs.chemrev.1c00074
Chem. Rev. XXXX, XXX, XXX−XXX

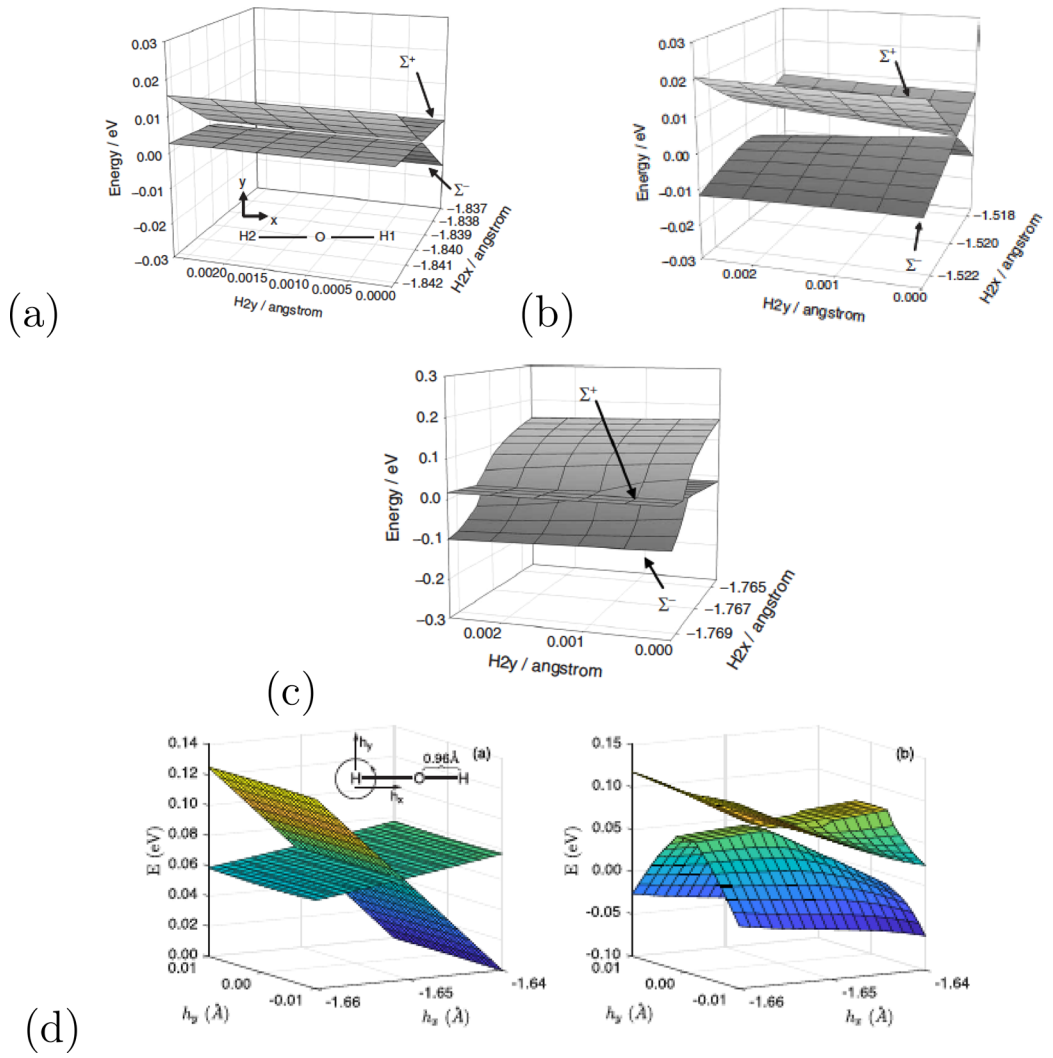

Figure 9. Potential energy surfaces of H_2O in the region surrounding a CoIn calculated using (a) CIS/6-31G, (b) SA3-CAS(6/4)/6-31G, (c) TD-B3LYP/6-31G, (d) TDDFT(B3LYP) (left), and TDDFT-1D (right) with optimized Kohn−Sham orbitals. (a−c) Reprinted with permission from ref 242. Copyright 2006 Taylor & Francis. (d) Reprinted with permission from ref 241. Copyright 2019 American Chemical Society. At the CASSCF and TDDFT-1D levels the degeneracy is lifted along two coordinates, while only one of the three independent displacement coordinates splits the degeneracy at the CIS and TDDFT levels.

aims at improving the description of the coupling.[239,240] It uses the orthogonalization to generate a set of corrected states and then rediagonalizes the Hamiltonian in that space. Orbital optimization should capture the most important doubles correction for excited states. Using this approach one may achieve improved couplings between excited states or between the ground and excited states. VOA-CIS vastly outperforms CIS, and quite often, VOA-CIS closely follows CIS(D).[239]

The most direct way to correctly describe CoIns with the ground state uses a vey simple idea to expand CIS (and TDDFT as will be discussed in detail below).[241] In an approach denoted as CIS-1D one doubly excited configuration is added to the expansion. This is clearly shown in the equation below which shows the CIS Hamiltonian expanded by addition of one doubly excited configuration.

$$\mathbf{H} = \begin{pmatrix} \langle \Psi_0|H|\Psi_0\rangle & 0 & \langle \Psi_0|H|\Psi_{h\bar{h}}^{l\bar{l}}\rangle \\ 0 & \langle \Psi_i^a|H|\Psi_j^b\rangle & \langle \Psi_i^a|H|\Psi_{h\bar{h}}^{l\bar{l}}\rangle \\ \langle \Psi_{h\bar{h}}^{l\bar{l}}|H|\Psi_0\rangle & \langle \Psi_{h\bar{h}}^{l\bar{l}}|H|\Psi_j^b\rangle & \langle \Psi_{h\bar{h}}^{l\bar{l}}|H|\Psi_{h\bar{h}}^{l\bar{l}}\rangle \end{pmatrix} \quad (40)$$

The important point in this approach is how to choose the virtual orbital where double excitations are allowed. Both the occupied and the unoccupied molecular orbital are optimized to minimize the energy of the corresponding double excitation state. It will be shown below that CIS-1D predicts the correct topology of CoIn.

4.2.1.1. Topography and Topology of CoIns Using CIS and Corrected Versions. The problem of the wrong dimensionality of the CoIn at the CIS level is the easiest to anticipate, since the coupling between the ground state and single excitation states is always zero according to the Brillouin theorem. Numerical results highlighting this were first shown by Martinez and co-workers in 2006.[242] CIS only describes states which are predominantly singly excited in character, and it can only

https://doi.org/10.1021/acs.chemrev.1c00074
Chem. Rev. XXXX, XXX, XXX−XXX

produce qualitatively correct results when the ground state is accurately modeled as a single determinant. Figure 9 shows two-dimensional potential energy surfaces of H_2O around a CoIn between the ground S_0 and the S_1 excited states. The PES of S_0 and S_1 along Cartesian coordinates of the H atoms are shown. The CoIn exists at a linear geometry of H_2O. The top panel shows the PES obtained from CIS, showing that the degeneracy is only lifted along one coordinate, since the two states are not interacting at any geometry at the CIS level. On the other hand, the correct behavior is demonstrated at Figure 9b at the CASSCF level, showing the lifting of the degeneracy along two dimensions.

4.2.2. Post-CIS Methods. In this section we discuss single reference methods that go beyond CIS and include dynamical correlation, mostly through perturbation theory. EOM-CCSD, which is superior to the methods in this section, will be discussed separately.

A natural way to go beyond CIS for excited states is to include electron correlation via perturbation theory through second order. A size-consistent MP2 correction to CIS leads to CIS(D).[243] Standard perturbation theory is applied to the double excitations while triples are included as a product of CIS single excitations and ground state MP2 double excitations. The method scales as $O(N^5)$, and it is a substantial improvement over CIS, but errors of excitation energies can still be around 0.5 eV.[239,243] A main disadvantage for the topic of interest however is that it does not work when the excited states approach each other. In that case degenerate perturbation theory has to be used. For this reason, the CIS(D_n) family of methods was introduced by Head-Gordon and co-workers which is based on quasi-degenerate perturbation theory.[244] In this approach corrections are obtained by diagonalizing a perturbative approximation to the second-order response matrix for the MP2 ground state. The doubles−doubles block of the response matrix is approximated by excitations of the diagonal Fock matrix. Furthermore, a Taylor series expansion in the self-energy of the doubles−doubles block is used. n takes values from 0 to ∞ according to the number of terms kept in the expansion. When $n = 0$ or $n = 1$, the method involves the diagonalization of a dressed response matrix with singles-only, where the dressing is state-independent. The resulting methods, CIS(D_0) and CIS(D_1), behave much better relative to CIS(D) in cases of near-degeneracy between excited states, but they are considerably more expensive. For $n = \infty$ CIS(D_∞) can be shown to be related to CC2 and ADC(2), as will be discussed below.[245]

Although CIS(D_n) methods can describe CoIns between excited states, the problem with the CoIns involving the ground state remains. CIS(2) is another approach based on quasidegenerate perturbation theory that has been developed to treat the S_0/S_1 CoIns.[246] In that approach a dressed Hamiltonian including the ground state and excited states is diagonalized to obtain the coupled states. It has been shown to give results qualitatively similar to MRCI for a small set of CoIns. The drawback is that it is not size-extensive anymore.

The approximate coupled-cluster method of second order (CC2) was formulated by Christiansen, Koch, and Jorgensen as an approximation of the CCSD method.[247] This method scales as N^5 instead of N^6 which is the scaling of CCSD (where N is the number of basis functions). The singles equation used to obtain the amplitudes remains the same as in CCSD and provides an approximate description of orbital relaxation, while the doubles equations are approximated to be correct through first order only, with the singles treated as zeroth-order parameters. One important result of this approximation is that an analytic expression for the doubles amplitudes is available that depends only on the singles amplitudes, electron repulsion integrals, and Fock operator, so there is no need to iteratively solve for the doubles amplitudes. Although the ground state CC2 energy is equivalent to MP2, the main advantage is that it can be used to apply linear response theory to obtain excitation energies. Excitation energies and transition moments are obtained as poles and residues of the CC2 linear response function. CIS(D_∞) is obtained from CC2 if the CC2 ground state converged cluster amplitudes are substituted by the amplitudes from first-order perturbation theory.[245] Linear-response CC2 combined with the resolution of the identity approximation for two-electron integrals (RI-CC2) has also been developed and extensively used for the investigation of electronically excited states of medium-sized organic molecules.[248] Recently, Martínez and co-workers developed a tensor-hypercontracted variant of equation-of-motion CC2, which also reduces the scaling of the method to N.[4249,250]

Another approach that includes dynamical correlation and has been used extensively for excited states is the algebraic-diagrammatic-construction (ADC) method.[251] The ADC scheme of the polarization propagator was originally proposed by Schirmer.[252−254] The polarization propagator describes the time evolution of the polarization of a many body system, which corresponds to time-dependent fluctuations of the ground state electron density or wave function of the unperturbed system. It contains information about the excited state wave functions. Using diagrammatic perturbation theory, a family of methods can be derived for the approximate calculation of excited states. Furthermore, using an intermediate state representation, one can obtain excited state wave functions and properties. The ground state for ADC(2) is MP2, while ADC(3) is obtained when MP3 is chosen as the ground state. In principle ADC(n) converges to the full-CI limit. ADC(2) (or ADC(2)-s) is the most commonly used variation. The method scales as N^5, making it quite efficient for larger systems, while the error in excitation energies is around 0.22 ± 0.38 eV using the Thiel benchmark set for testing.[251] ADC(2)-x differs from ADC(2)-s in the order at which the two-particle-two-hole block in the ADC matrix is treated, leading to the correct description of doubly excited states. The ADC(2)-x and ADC(3) methods scale as N^6. It has been demonstrated that ADC(2) is related to CC2 and CIS(D).[245] Neglect of the t_1 amplitudes present in the CC2 Jacobian gives the CIS(D_∞) Jacobian $A^{CIS}(D_\infty)$. The ADC(2)-s matrix is related to CIS(D_∞) by symmetrization

$$\mathbf{M}^{ADC(2)} = \frac{1}{2}[\mathbf{A}^{CIS(D_\infty)} + \mathbf{A}^{CIS(D_\infty)^\dagger}] \tag{41}$$

The above symmetrization results in ADC(2)-s being a Hermitian matrix, making it a more suitable method near avoided crossings and CoIns compared to the other CC2 and CIS(D) methods. CC2 yields somewhat better excitation energies, while CIS(D_∞) gives very similar energies to ADC(2)-s.[245,251]

Spin-scaling approaches have also been developed for these methods.[255−257] The spin-scaling approach was first introduced by Grimme in 2003, who partitioned the correlation energy into parallel and antiparallel spin components and used semi-empirical parameters to scale the weights of these two contributions or just scale the opposite spin part of the energy (SCS vs SOS).[258] It was initially used in MP2 but has been

https://doi.org/10.1021/acs.chemrev.1c00074
Chem. Rev. XXXX, XXX, XXX−XXX

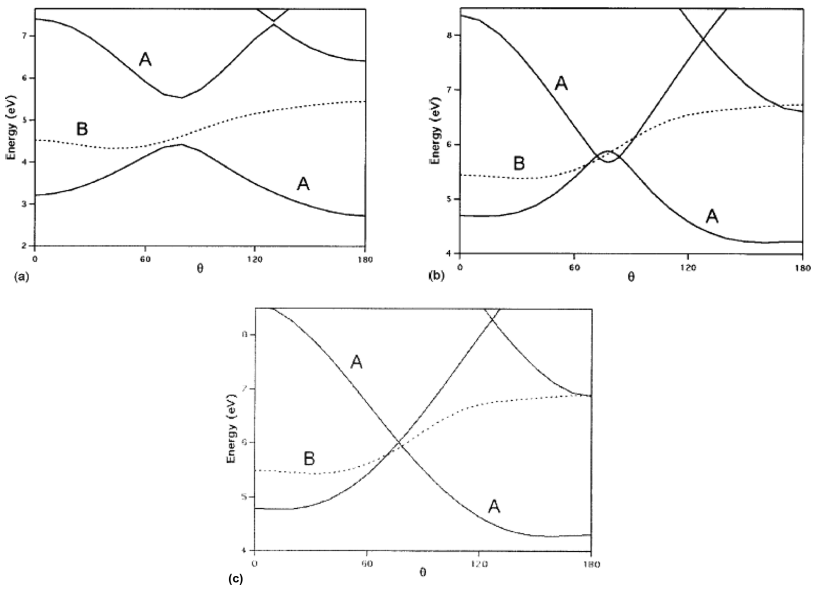

Figure 10. Energy profile of the three lowest excited states (A,B,A) in bent acetylene along its molecular torsion, at the (top left) CIS, (top right) SOS-CIS(D), and (bottom) SOS-CIS(D_0) levels. Reprinted with permission from ref 259. Copyright 2008 AIP Publishing.

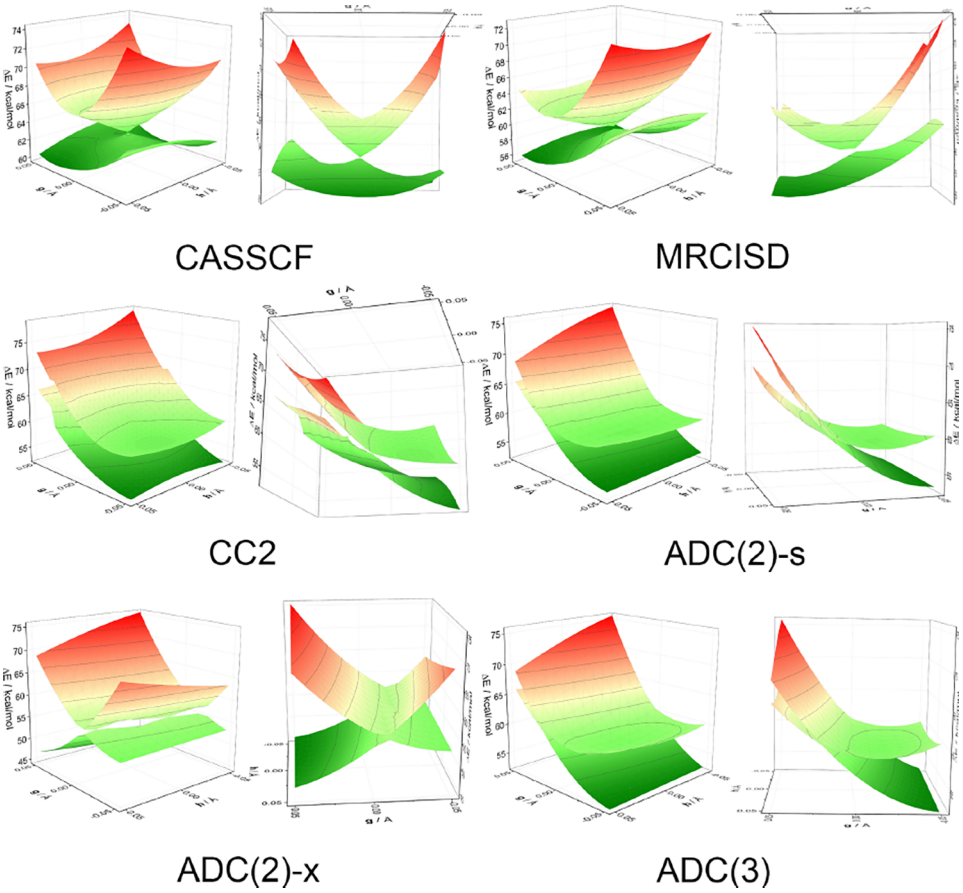

Figure 11. Energy profiles (in kcal/mol) of the S_0 and S_1 adiabatic potential-energy surfaces in the 2D branching space of the CoIn of PSB3 (note that the energy scales are different for each plot). The **g** vector corresponds roughly to the BLA coordinate, whereas the **h** vector corresponds roughly to the isomerization coordinate. For each method, the plot is shown from two different perspectives. For the CC2 method, a roughly three times finer grid was used and a few points are missing due to nonconvergence. Reprinted with permission from ref 232. Copyright 2015 American Chemical Society.

extended to other methods, including CC2, ADC(2), and CIS(D_n).[255,259]

4.2.2.1. Locating CoIns with Post-CIS Methods. The main problem with this set of methods is their inability to describe CoIns with the ground state. CIS(2) is the only exception, since it was designed specifically to fix this problem. The performance of CIS(2) to locate CoIns between S_0/S_1 and S_1/S_2 was tested in the organic molecules uracil and cytosine..[246] Most of the

https://doi.org/10.1021/acs.chemrev.1c00074
Chem. Rev. XXXX, XXX, XXX−XXX

geometry parameters are very similar to MRCIS except a few of them which involve atoms directly related to the excitation process. The most important deviations in the bond lengths were for the carbonyl groups in both molecules, with an overestimation of these bond lengths by up to 0.1 Å.

CoIns between excited states can also be problematic for some methods. Figure 10, taken from ref 259, demonstrates the differences in describing CoIns between excited states using some of the single reference methods. The figure plots the energies of the first three excited states of bent acetylene along the torsional coordinate that transforms it from cis to trans configuration. CIS is qualitatively correct, but the states are well separated because of the luck of the dynamical correlation. When dynamical correlation is added at the SOS-CIS(D) level, the states approach each other, but artificial crossings between the two A states are shown. At the SOS-CIS(D_0) level quasi-degenerate perturbation theory allows for a proper description of the states near their crossing. This reinforces again the fact that CIS(D) cannot describe properly CoIns even between excited states.

Within the set of methods discussed in this section, CC2 and ADC(2) have been the methods mostly employed in CoIns and nonadiabatic dynamics. Despite the fact that the S_0/S_1 CoIn are not expected to be properly described by these methods, the problem is mostly at describing the topology. The geometries of MECI located with these methods may still be well described. As an example, optimizations of the MECI for PSB3 were carried out at the CC2 and ADC(2) levels and compared to CASPT2 and MRCISD. In that system the structures obtained at the CC2 and ADC(2)-s/MP2 levels agree with the multireference methods.[232]

CC2 and other single reference methods have also been tested in the excited state dynamics of polyatomic molecules using surface hopping.[260−264] In single reference methods coupling with the ground state is not possible, so usually a hopping to the ground state is assumed when the gap between S_1 and S_0 is smaller than a threshold. In a test study ADC(2) performed better than CC2 and TDDFT to predict the nonadiabatic dynamics in adenine.[260] This however cannot be generalized, and further studies are needed. The results showed that dynamics with ADC(2) were more stable than CC2 dynamics which failed within 100 fs, because of numerical instabilities present in the case of quasi-degenerate excited states.

4.2.2.2. Topography and Topology of CoIns Using Post-CIS Methods. Based on theoretical arguments the topology of surface crossings between excited states by CC2 is demonstrated to be incorrectly described.[245,265] One of the problems with non-Hermitian approaches is that complex energies are possible, which will be elaborated in our discussion on EOM-CCSD.

Numerical demonstration of the deficiency of CC2 and ADC(2) has also been done. CoIns between the ground and an excited state using CC2 and ADC(2) were described more recently computationally using the retinal chromophore model used as a test for many methods by Olivucci and co-workers.[232,266] ADC(2)-s, ADC(2)-x, and third-order ADC, ADC(3), were tested. In addition, for both CC2 and ADC methods, the spin component-scaled (SCS) and spin-opposite-scaled (SOS) variants were also considered. Figure 11 shows plots of the CoIns produced using CC2 and the variants of ADC(2) for PSB3 and compared to CASSCF and MRCISD plots. The branching plane coordinates used for all methods in the plots (except MRCISD) are taken from CASSCF. CASSCF and MRCISD both show the correct topology of the CoIn, showing lifting of the degeneracy along both coordinates, as was discussed in the corresponding section in this review. The other plots in that figure show that only CC2 also predicts the correct topology of the CoIn. There is lifting of the degeneracy along both coordinates, even though not at the same degree as in MRCISD. A closer look at the energies around the CoIn however shows that they are not always smooth. On the other hand, all variants of the ADC method produce the wrong linear intersection topology as shown in Figure 11. The degeneracy is lifted only along the **g** branching coordinate. This is expected since the electronic ground state is described at a different level of theory, i.e. the MP2 or MP3 level, so coupling between the states is excluded.

It should also be pointed out that using the branching vectors obtained at one level of theory to calculate the shape of the cone at a different level of theory is tricky and can lead to misleading results if the vectors predicted by the two methods differ. This approach however is being used commonly mainly because many methods do not have implementations to calculate the **h** (nonadiabatic) vector. In the paper testing CC2 and ADC(2) the approach was tested by comparing the **g** vector obtained with CC2 to the one from CASSCF.[232]

4.2.3. EOM-CCSD. Coupled cluster theory is often considered the golden standard for ground state properties.[267−269] Its extension to excited states is a powerful and accurate method,[270−273] which can be successfully used as long as CC can describe correctly the ground state. In CC theory the ground state is described as an exponential wave function:

$$|\Psi_0^{CC}\rangle = e^T|0\rangle \tag{42}$$

where $|0\rangle$ is the reference determinant (usually Hartree−Fock) and $T = \sum t_\mu \tau_\mu$ is the cluster operator which includes single, double, etc. excitation operators τ_μ with amplitudes t_μ. The most common form uses the expansion up to second order leading to CCSD. The energy is given by

$$E_0^{CC} = \langle 0|e^{-T} H e^T|0\rangle \tag{43}$$

and the CC amplitudes are obtained from

$$\langle \Phi_i^a|e^{-T} H e^T|0\rangle = 0 \tag{44}$$

$$\langle \Phi_{ij}^{ab}|e^{-T} H e^T|0\rangle = 0 \tag{45}$$

Φ_i^a, Φ_{ij}^{ab} denote the single and double excitation manifold, respectively.

In EOM-EE-CC[270,273] the electronically excited states are described as

$$|\Psi_I^{EOM}\rangle = R_I e^T|0\rangle \tag{46}$$

$$\langle \tilde{\Psi}_I^{EOM}| = \langle 0|L_I e^{-T} \tag{47}$$

where R and L are excitation and de-excitation operators, respectively.

In the commonly used EOM-CCSD T, R, and L are all truncated to double excitations. The excitation energy and amplitudes R and L are obtained by solving the nonhermitian eigenproblem

$$E_I^{EOM} = \langle 0|L_I e^{-T} H e^T R_I|0\rangle = \langle 0|L_I \tilde{H} R_I|0\rangle \tag{48}$$

The operator R can be an excitation operator (in EOM-EE), a particle annihilation operator (in EOM-IP), a particle creation operator (in EOM-EA), or a particle spin-flipping operator (in EOM-SF). EOM-EE-CCSD is equivalent to linear response

https://doi.org/10.1021/acs.chemrev.1c00074
Chem. Rev. XXXX, XXX, XXX−XXX

CCSD for the excitation energies but not for transition properties.[272] Even though EOM-CCSD can treat a wide variety of states, it cannot treat doubly excited states, and this is a problem in some systems where doubly excited states are important in vertical excitation, such as polyenes. But more important for the present discussion, doubly excited states often become important when the S_0 wave function has some multiconfigurational character, and near-degeneracies exist.

4.2.3.1. Locating CoIns Using EOM-CCSD. Locating CoIns using EOM-CCSD has not been extensively used since derivative couplings have not been available until recently, and EOM-CCSD is a rather computationally expensive method. There have been however some tests on its performance, and we only offer some examples here.

Two- and three-state CoIns between excited states in adenine were located at the CC2, CCSD, and MRCIS levels and compared.[274] While the S_1/S_2 CoIns were similar in all three methods, there was a larger difference between the MRCIS and CCSD geometries and energies for the three state $S_1/S_2/S_3$ CoIn. This is most likely an effect of dynamical correlation, since the S_3 state was much more sensitive to dynamical correlation. This demonstrates again that accurate location of CoIns is a sensitive interplay between dynamical and nondynamical correlation, and it is system dependent and even within the same system can be state dependent.

4.2.3.2. Topography of CoIns Using EOM-CCSD. The question about whether the topology of a CoIn can be described by EOM-CCSD was first studied in detail by Köhn and Tajti in 2007.[265] The underlying problem however was first raised by Hättig in 2005.[245] In that review he noted that the topology of a CoIn is affected by the non-Hermitian nature of the Hamiltonian. In a nonsymmetric matrix there are three rather than two conditions that need to be satisfied in order to obtain degeneracy. In addition, complex energies can be obtained in this case. Nonhermitian matrices lead to unphysical complex energies, as was shown for CCSD and CCSDT.[265,275]

The crossing conditions for a non-Hermitian matrix can be obtained by considering the Wigner-Neumann derivation for the dimensionality (discussed in section 3.1). For a non-Hermitian method the Jacobian has the general form

$$\mathbf{A} = \begin{pmatrix} \Delta & X + Y \\ X - Y & -\Delta \end{pmatrix} \tag{49}$$

The eigenvalues are given by

$$E_{1,2} = \pm\sqrt{\Delta^2 + X^2 - Y^2} \tag{50}$$

For a nonsymmetric matrix a number of different cases can be distinguished, depending on the magnitude of the antisymmetric contribution to the coupling Y:

1. $Y^2 < \Delta^2 + X^2$, two real eigenvalues are obtained;
2. $Y^2 > \Delta^2 + X^2$, this leads to a conjugated pair of degenerate roots with eigenvalues

$$E_{1,2} = \pm i\sqrt{Y^2 - \Delta^2 - X^2} \tag{51}$$

3. $Y^2 = \Delta^2 + X^2$. This condition is fulfilled in $N^{int} - 1$ dimensions, for states of the same symmetry;
4. $Y = \Delta = X = 0$. This condition is fulfilled in $N^{int} - 3$ dimensions.

The picture that emerges from the relationships above is that the points at which the two states become degenerate with a nonsymmetric Jacobian ($Y^2 = \Delta^2 + X^2$) form a tube around the intersection seam obtained with a symmetric matrix. On the surface of the cylinder the eigenvectors are parallel, and in its interior the energies are complex. Figure 12 shows pictorially what happens. Köhn and Tajti demonstrated that indeed complex energies and parallel eigenvectors exist near a CoIn when using EOM-CCSD.[265] This behavior was illustrated by the EOM-EE calculations of formaldehyde, where in a small region around a CoIn, EOM-EE-CCSD roots become complex and the real parts of the energies degenerate.

Hättig identified the true CoIn as the case when $Y = \Delta = X = 0$ in which case the cylinder shrinks to a point. If there are three conditions that need to be satisfied, it has been assumed that the dimensionality of the CoIn is not correct with coupled cluster.[245,265] However, the exact EOM-CC theory, which is equivalent to FCI, describes the intersections correctly, leading to a paradox. This paradox has been recently explained by Kjønstad et al.[275] The explanation relies on the idea that the Jacobian matrix is nondefective away from CoIns, but it can be defective when degeneracies occur. At the limit of all excitation operators included (equivalent to FCI) it becomes nondefective again even at degeneracies. A nondefective matrix is one that can be diagonalized, while a defective matrix does not have a complete basis of eigenvectors. A symmetric matrix can always be diagonalized, while a nonsymmetric one is guaranteed to be nondefective only when the eigenvalues are distinct. For a nondefective matrix it can be shown that the three conditions are not independent, and there are only two independent conditions for an inherently real Hamiltonian,[275] so in this case the correct dimensionality of the CoIn is restored.[275] Therefore, at the limit of all excitations included both EOM-CC and FCI will give the same eigenvalues and the correct dimensionality of a CoIn. When CC is truncated, however, at accidental CoIns the Jacobian is a defective matrix. In that case degeneracy is obtained either via $Y^2 = \Delta^2 + X^2$ or $Y = \Delta = X = 0$. While Hättig[245] and Köhn and Tajti[265] argued that the true CoIn occurs in the second case, Kjønstad et al.[275] explain that the seam occurs using the first conditions leading to an $N^{int} - 1$-dimensional space which becomes $N^{int} - 2$ at the limit of all excitations. The cylinder shrinks to the $N^{int} - 2$ seam space when the energies become real at the complete T limit, as shown in Figure 12. The intersection though resembles a $N^{int} - 2$ CoIn for large distances away from the seam. At accidental symmetry allowed intersections CCSD is nondefective.

A possible solution has also been suggested through a modified theory, called similarity constrained coupled cluster theory.[276] In that approach CCSD is constrained to be nondefective. The wave function of similarity constrained CCSD (SCCSD) is defined by including an additional triple excitation in cluster operator T

$$T = \sum_{ai} t_i^a \tau_i^a + \frac{1}{2}\sum_{aibj} t_{ij}^{ab}\tau_{ij}^{ab} + \zeta\tau_{IJK}^{ABC} \tag{52}$$

The amplitudes t_i^a, t_{ij}^{ab}, and ζ are determined by imposing that the eigenvectors for the two intersecting states are orthogonal (in addition to satisfying the CCSD equations). This leads to a coupled set of equations that may be solved self-consistently. SCCSD was applied to the CoIn of 2^1A_1 and 3^1A_1 excited states of formaldehyde. Figure 12c illustrates the results. At the CCSD level the states cross at two points 1.3515 and 1.3570 Å giving a complex pair of states between those two points. At the SCCSD level the intersection becomes an avoided crossing. A CoIn at

https://doi.org/10.1021/acs.chemrev.1c00074
Chem. Rev. XXXX, XXX, XXX−XXX

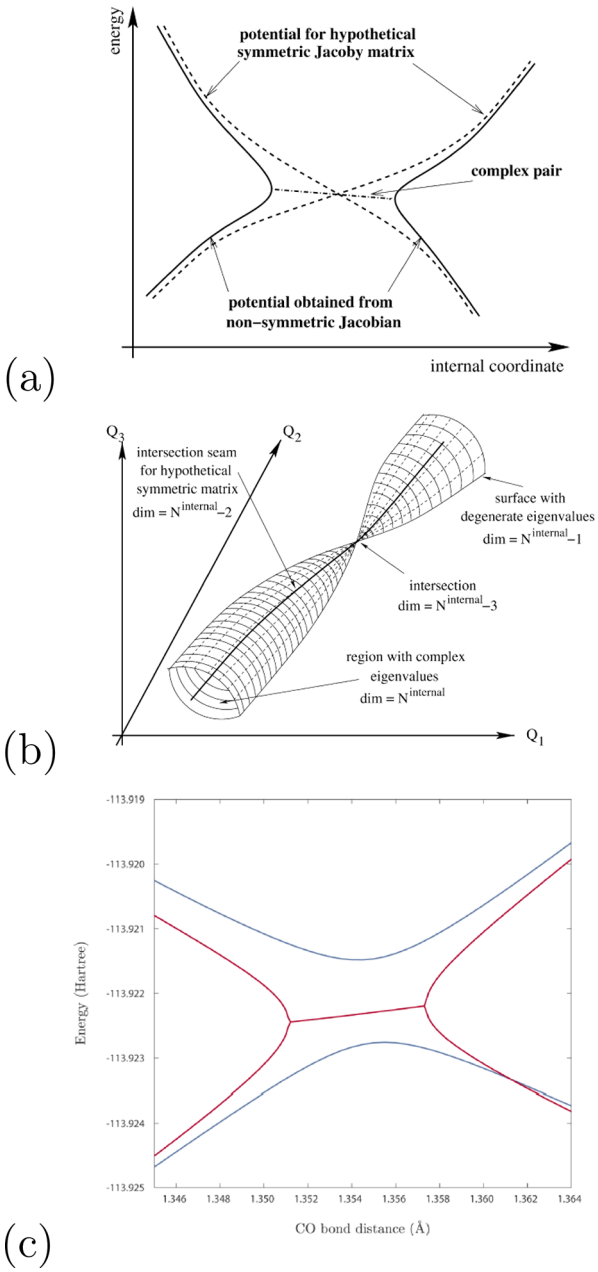

Figure 12. (a) Intersection of two states of the same symmetry as described by a symmetric and a nonsymmetric secular matrix. The potential curves obtained with a symmetric secular matrix are shown as broken lines. The full lines are the potential curves for a nonsymmetric secular matrix in the region where both eigenvalues are real, while for the region where the eigenvalues are complex only the real part is shown as a dashed and dotted line. (b) Intersection of two states shown in a space spanned by the two tuning coordinates of the CoIn and one coordinate along the intersection seam. The thick line is the intersection seam obtained with a symmetric secular matrix. For the nonsymmetric matrix the surface on which the two eigenvalues are degenerate is plotted. (c) 2^1A_1 and 3^1A_1 excited states of formaldehyde using CCSD (red) and SCCSD (blue) with an aug-cc-pVDZ basis. The real part of the CCSD energies is shown. A complex pair of energies is obtained for C═O bond distances of 1.3515−1.3570 Å. (a,b) Reprinted with permission from ref 245. Copyright 2005 Elsevier Books. (c) Reprinted with permission from ref 276. Copyright 2017 American Chemical Society.

this level of theory may exist at a different coordinate. This fix to the CCSD theory introduces some problems. The orbital invariance is lost and the PES is not continuous anymore. Alternative approaches can be used to maintain the continuity of PES and orbital invariance.[276]

A different issue with EOM-CCSD, which is common with all single reference methods, is the difficulty to describe CoIns involving the ground state.[277,278] This problem can be addressed with the spin-flip variant of EOM-CCSD. Spin-flip methods are discussed separately in section 4.2.6.

4.2.4. TDDFT. The method that has seen substantial progress in recent years in developments related to excited states and nonadiabatic events is TDDFT.[279] The most common implementation of TDDFT uses the adiabatic approximation which assumes that the self-consistent field responds instantaneously to changes in the charge density, and there is no memory. Excitations are obtained from the linear response formulation of TDDFT (LR-TDDFT), from the poles of the ground state density−density response function.

The TDDFT and time-dependent Hartree−Fock (TDHF) excitation energies ω are given by solving the eigenvalue equation

$$\begin{pmatrix} \mathbf{A} & \mathbf{B} \\ \mathbf{B}^* & \mathbf{A}^* \end{pmatrix} \begin{pmatrix} \mathbf{X} \\ \mathbf{Y} \end{pmatrix} = \omega \begin{pmatrix} \mathbf{1} & \mathbf{0} \\ \mathbf{0} & -\mathbf{1} \end{pmatrix} \begin{pmatrix} \mathbf{X} \\ \mathbf{Y} \end{pmatrix} \tag{53}$$

where the matrix elements are given by

$$A_{ia,jb} = (\epsilon_a - \epsilon_i)\delta_{ij}\delta_{ab} + (ia|jb) - c_{HF}(ij|ab) + (1 - c_{HF})(ia|f_{xc}|jb)$$

$$B_{ia,jb} = (ia|bj) - c_{HF}(ib|aj) + (1 - c_{HF})(ia|f_{xc}|bj)$$

ϵ_a is the ground state orbital energy for orbital a, i, j are ground state occupied orbitals, while a, b are virtual orbitals. $(i(1)a(1)|j(2)b(2))$ are two-electron integrals following the conventional chemists' (Mulliken) notation. f_{xc} is the kernel of the exchange-correlation functional, c_{HF} is the coefficient of the exact HF exchange present in a given functional. For TDHF $c_{HF} = 1$. For some typical functionals the values of c_{HF} are $c_{HF} = 0$ for LSDA, $c_{HF} = 0.2$ for B3LYP, and $c_{HF} = 0.25$ for PBE1PBE. When the **B** matrix is set to 0, one obtains the Tamm−Dancoff approximation (TDA).[280] When $c_{HF} = 1$, we obtain the CIS expressions.

4.2.4.1. Topography and Topology of CoIn Using TDDFT. The problem of the wrong dimensionality of the CoIn between ground and excited states at the TDDFT level was initially highlighted by Martinez and co-workers.[242] It was demonstrated in that study that even though TDDFT in the linear response and adiabatic approximations can predict geometries and energetics of MECIs quite accurately (as long as the excited state is not dominated by doubly excited character), it does not predict the shape of CoIns correctly. Since there are no matrix elements coupling the ground and excited states in TDDFT, similarly to CIS, TDDFT intersections between the ground state and a response state occur in $N^{int} - 1$ dimensions. CoIns between excited states however are described correctly. Figure 9 shows the PES around the CoIn of linear water using TDDFT and compared to CIS and CASSCF PES. It is clear that TDDFT behaves similarly to CIS and lifts the degeneracy only along one dimension, deviating from the correct behavior which is seen using CASSCF.

https://doi.org/10.1021/acs.chemrev.1c00074
Chem. Rev. XXXX, XXX, XXX−XXX

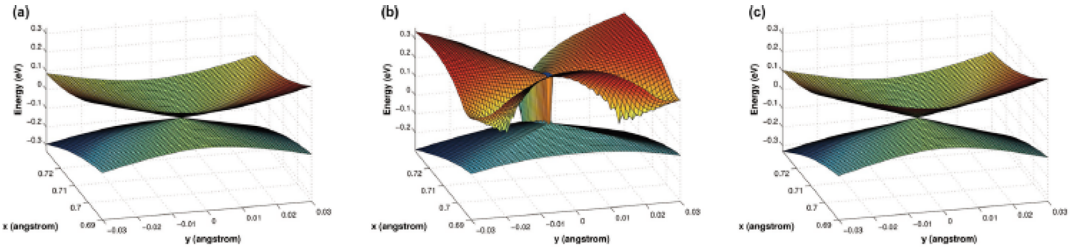

Figure 13. Potential energy surfaces of H_3 around a CoIn by (a) CASSCF (3,6), (b) TDDFT-B3LYP, and (c) pp-RPA/TDA-B3LYP. Two atoms are fixed on the *y* axis at (0, 0.409) and (0, −0.409), respectively, whereas the position of the third atom is varied along the x and y axes. TDDFT gives an unphysical butterfly shape for the excited state surface, whereas the pp-RPA, which reduces to the pp-TDA in this three-electron case, correctly describes the CoIn with potential energy surfaces closely resembling CASSCF. Reprinted with permission from ref 292. Copyright 2016 American Chemical Society.

Further benchmarks have tested the performance of TDDFT in photochemistry, such as those using the photochemical ring opening of oxirane as a test system.[281−283] It was initially shown that regular TDDFT does not give a good description of the photochemical path, showing in particular triplet instabilities (i.e., the energy of the triplet states becomes more stable than the ground singlet state at some points along the path). TDA gave better results than conventional TDDFT in cases like this, where bond breaking occurs.[281,282] The wrong dimensionality of CoIns was also confirmed in these studies. The performance of TDDFT in the description of CoIns was also explored in the series of benchmarks by Olivucci and co-workers using the retinal chromophore,[230,231] which also confirmed the wrong dimensionality of CoIns between the ground and the excited states. A volume in *Topics of Current Chemistry* on excited states using TDDFT published in 2015 reviews the performance of TDDFT both in describing CoIns[284] and in using it for surface hopping dynamics.[285]

4.2.5. Corrections and Alternatives to TDDFT. Despite the deficiencies of TDDFT to describe CoIns with S_0, its computational efficiency makes it a very attractive approach, so much effort has been directed into developing approaches to correct the wrong dimensionality of the CoIns predicted by linear response TDDFT. Other methods which try to add static correlation or doubly excited states in TDDFT have been developed to treat excited states and can be useful in treating CoIns.[286,287] Here we focus on methods that have been tested for their description of CoIns, so we are not explicitly considering all these methods. Methods combining DFT with wave function approaches have been recently reviewed in this journal and will also not be considered further here.[115]

A common theme among many methods is to find a way to include a coupling between the ground and excited state. Truhlar and co-workers proposed a way to introduce such a coupling in the Configuration Interaction-Corrected Tamm−Dancoff Approximation (CIC-TDA).[288] In that approach, they used the TDA approximation to TDDFT since it is more stable near state intersections and calculated a coupling between the reference and intersecting state, $A_{0,ia}$. $A_{0,ia}$ vanishes in regular TDA when using the KS operator. But, assuming that the reference KS determinant and the TDA response written as a linear combination of singly excited Slater determinants are approximate wave functions of the real system, the authors calculated the coupling using wave function theory as

$$A_{0,ia}^{CIC} = \langle \Phi_0^{KS} | H | \Phi_i^a \rangle = \langle a | h + \sum_j^{N^{occ}} 2J_j - \sum_j^{N^{occ}} K_j | i \rangle \quad (54)$$

where Φ_i^a is the dominant determinant in the intersecting excited state. This term is small because it depends on the difference between the KS orbitals and the HF orbitals, which is small. But it does not vanish and if included corrects the dimensionality of a CoIn. More specifically, $A_{0,ia}^{CIC}$ is equal to the difference between the matrix elements of the HF exchange potential and the KS xc potential. This approach was tested on NH_3 and PSB3, and it produced CoIns with the correct dimensionality.

Another approach similar in spirit, called the Dual-Functional Tamm−Dancoff Approximation (DF-TDA), has also been explored by the same group and uses different type of orbitals to avoid the zero coupling between S_1 and the reference state.[289] If Kohn−Sham orbitals are used in TDA, there is no coupling between the ground state and excited states. If different orbitals are used, this coupling is not zero anymore. In the DF-TDA method the strategy is to optimize the orbitals with one exchange-correlation functional and build the KS-TDA Hamiltonian with a different functional. As a result, the correct topology in the vicinity of S_1/S_0 CoIn is restored, although there are variations when compared to MS-CASPT2. The overall accuracy of DF-TDA is mostly determined by the functional that is used to build the TDA Hamiltonian.

The Particle−Particle Random Phase (pp-RPA) and Tamm−Dancoff Approximations (pp-TDA) start from a +2 cation reference and target the neutral (N) states by adding two electrons, so they naturally can describe the ground and excited states on the same footing.[290,291] For that reason it is expected that they can describe properly the dimension of CoIns since they account for the interstate interaction. The methods were tested and were found to describe correctly the surface in the vicinity of CoIns.[292] The basic equations for pp-RPA are

$$\begin{pmatrix} \mathbf{A} & \mathbf{B} \\ \mathbf{B}^* & \mathbf{C} \end{pmatrix} \begin{pmatrix} \mathbf{X} \\ \mathbf{Y} \end{pmatrix} = \omega^{\pm 2e} \begin{pmatrix} \mathbf{1} & \mathbf{0} \\ \mathbf{0} & -\mathbf{1} \end{pmatrix} \begin{pmatrix} \mathbf{X} \\ \mathbf{Y} \end{pmatrix} \quad (55)$$

where the matrix elements A are defined using occupied orbitals and those of C using only virtual orbitals

$$A_{ab,cd} = (\epsilon_a + \epsilon_b)\delta_{ac}\delta_{bd} + (ac|bd) - (ad|bc)$$
$$C_{ij,kl} = -(\epsilon_i + \epsilon_j)\delta_{ik}\delta_{jl} + (ik|jl) - (il|jk)$$

where *a*, *b*, *c*, and *d* are virtual orbital indices and *i*, *j*, *k*, and *l* are occupied orbital indices with the restrictions that $a > b$, $c > d$, $i > j$, and $k > l$. Eigenvectors **X** describe the two-electron addition system, while eigenvectors **Y** describe a two-electron removal system. Applying TDA sets **B** = 0. pp-TDA is recommended over pp-RPA because of the Hermitian matrix used which

https://doi.org/10.1021/acs.chemrev.1c00074
Chem. Rev. XXXX, XXX, XXX−XXX

guarantees real eigenvalues. CoIns for H_3 and NH_3 were tested. Figure 13 shows results for H_3, comparing the pp-TDA approach to regular TDDFT and CASSCF. It is obvious that pp-TDA predicts the correct topology, similar to CASSCF, whereas TDDFT fails to predict the correct shape of the CoIn. One shortcoming of these methods is that they may underestimate the bond lengths for CoIns because of the contracted cationic molecular orbitals, although different orbitals may correct this deficiency.

The hh-TDA method is the hole−hole equivalent to the pp-TDA method. In this case, the *N*-electron ground state and excited states are generated through double annihilations from an $(N + 2)$-electron reference in which the lowest unoccupied molecular orbital (LUMO) has two additional electrons.[291] As a result the hh-TDA treats ground and excited states on equal footing and can be used to describe CoIns involving the ground state.[293,294] The advantage of the hh-TDA approach compared to pp-TDA is that it can treat some cases that cannot be treated with pp-TDA, such as describing simultaneously low-lying $\pi\pi^*$ and $n\pi^*$ excited states. Since the reference includes two electrons in the LUMO, care has to be taken for SCF convergence and to avoid continuum-like solutions. It has been suggested that the method should be combined with range-separated density functionals that have 100% asymptotic Fock exchange and to avoid diffuse basis functions. hh-TDA has been benchmarked and used in dynamics recently by the Martinez group.[294,295]

Very recently, another approach was proposed aimed to be simple enough for dynamics while efficient and accurate in regions of CoIns.[241] This approach is the equivalent of CIS-1D described in section 4.2.1. In this approach, inspired by the work of Maitra et al.,[286] an ensemble is created using the ground state DFT wave function, the set of single excitation states, and one doubly excited configuration (with a pair of electrons excited from a specific KS spatial orbital to another specific KS spatial orbital, denoted TDDFT-1D ansatz). The important point in this ansatz is how to choose the virtual orbital where double excitations are allowed. The method was tested in several typical systems with CoIns, such as ethylene and water. Figure 9d (right) shows the plot of PES around the water CoIn that was initially used to test TDDFT by Levine et al.[242] and demonstrates that the new approach correctly describes the topology. Analytic gradients and derivative couplings were also implemented recently.[296]

Van Voorhis's group developed configuration interaction based on constrained density functional theory (CDFT-CI),[297,298] which has been used to describe ground state potential energy surfaces and barriers for a while. CDFT-CI was also tested for its performance on CoIns and showed that it can describe CoIns if some information is known about the target system.[299] CDFT-CI introduces an active space whose states are built from distinct constrained SCF calculations. A CI matrix is then constructed by calculating the fully ab initio energies and couplings, and it is diagonalized to produce the energies and coefficient vectors for the adiabatic states. CDFT relies on a partitioning of the system into multiple fragments and a means for assigning spin density to individual atoms. The DFT energy of a given state is then minimized subject to the constraint that the average spin and charge on each fragment take on specified values. In CDFT-CI both ground and excited states arise from the same CI diagonalization and are thus treated on an equal footing. A disadvantage of this method is that the results are very sensitive to the selection of the states used to build the CI matrix, and one has to use some chemical intuition in this choice. Analytic gradients have also been developed, making it easier to find stationary points and CoIns.[300] Figure 14 shows the performance of CDFT-CI in describing correctly the CoIn in H_3. While TDDFT fails, CDFT-CI reproduces the correct topology around the CoIn, producing a PES similar to full CI.

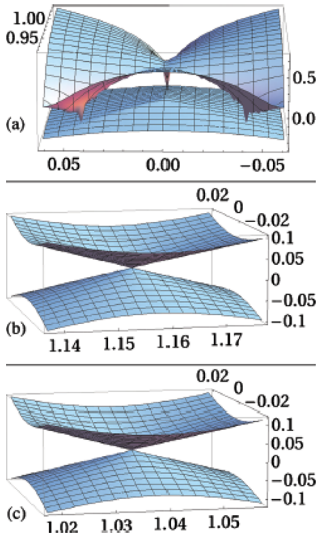

Figure 14. Potential energy surfaces of H_3 as computed by (a) TDDFT, (b) CDFT-CI, and (c) full CI. Reprinted with permission from ref 299. Copyright 2010 AIP Publishing.

A different approach from the response formalism to obtain excited states in the context of DFT includes the ensemble DFT approaches.[301−304] In was proved by Lieb[301] that the density and the ground state energy of a strongly correlated system are exactly represented by a weighted sum (ensemble) of the densities of several electronic configurations. Ensemble DFT can be used to obtain excitation energies from a variational calculation, instead of linear response as in LR-TDDFT. The weighting factors in the ensembles can be determined either by symmetry requirements, leading to the spin-restricted open-shell Kohn−Sham (ROKS) method, or by variational minimization of the energy, leading to the spin-restricted ensemble referenced Kohn−Sham (REKS) method.[305−308] An extension to ROKS is based on optimizing a single set of KS orbitals and an associated reference density, called the Slater transition state density, which represents both states under consideration equally well. NACs have been developed for this extension.[307,309]

The excited states in the REKS methodology are obtained by applying the ensemble variational principle proven by Gross et al.[302] In state-averaged REKS (SA-REKS) an ensemble including the ground state and a state created by a single excitation is used, and more specifically, a weighted sum of the energies of the ground state described by the REKS method and of the excited state described by the ROKS method. Within the Kohn−Sham approach, the ensemble representation leads to fractional occupation numbers of the Kohn−Sham orbitals. So, an optimization can be used for both the orbitals and the fractional occupation numbers.[310] The SA-REKS method treats S_0 and S_1 as uncoupled states, which is true when interaction is prevented by symmetry. But when the two states belong to the same symmetry, the states interact with each other and this interaction should be taken into account. In the state-interaction

https://doi.org/10.1021/acs.chemrev.1c00074
Chem. Rev. XXXX, XXX, XXX−XXX

SA-REKS (SI-SA-REKS) the S_0 and S_1 states can be obtained by diagonalizing a 2×2 secular matrix where the diagonal elements are the E^{REKS} and E^{ROKS} and a coupling matrix element between the two is introduced. The SI-SA-REKS method predicts the correct topology and topography of CoIns.[230,284,311] In addition to the topology, the performance of REKS to describe geometries of CoIns has also been tested.[312] It was shown that the BH&HLYP density functional yields the best results for the CoIn geometries and energetics when compared with multireference methods.[308] Overall, REKS and more specifically SI-SA-REKS seems quite promising for the description of CoIns and has been applied for nonadiabatic dynamics.[230,231,308,310,313−316] Very recently, the analytic gradient and nonadiabatic couplings for SI-SA-REKS have been derived, implemented,[314,317] and used in dynamics,[318,319] increasing its applicability in problems involving CoIns.

Another recent method combined Fermi smearing DFT with a fractional-occupation variant of the TDA version of TDDFT to be able to be used in nonadiabatic dynamics involving the ground state.[320]

4.2.6. Spin-Flip Approaches. A quite successful approach that has been used extensively with most single reference methods in order to overcome the issues with CoIns is the spin-flip (SF) approach.[277,278,321] The approach was first introduced in 2001 by Krylov[277] and has been expanded to several methods since then.[266,322−327] The idea behind it is to use a different reference from the states of interest. In SF singlet states are generated via excitation from a high-spin triplet reference state, doublets from a quartet, etc. Figure 15 shows pictorially how the

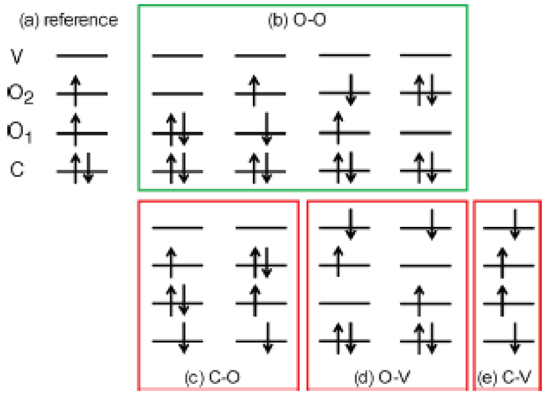

Figure 15. Example of spin-flip from a high-spin triplet reference state, for a model system consisting of four electrons in four orbitals. Configuration a is the reference state. Configurations in part b are obtained by a single flip-down excitation within the open-shell orbitals; only these configurations are able to form spin eigenstates. Configurations in parts c−e are obtained by closed- to open-shell excitations, open-shell to virtual excitations, and closed-shell to virtual excitations, respectively, each with a $\alpha \rightarrow \beta$ spin-flip excitation. These configurations are missing their complementary spin configurations and lead to spin-contaminated solutions in conventional SF-TDDFT. Reprinted with permission from ref 329. Copyright 2015 AIP Publishing.

SF approach works starting from a triplet reference. By an $\alpha \rightarrow \beta$ spin-flip the various singlet states of interest are generated. If one is interested in computing MECI between S_0 and S_1, then both of these states are described as spin-flipping excitations and are thus treated equivalently. As a result the topology of the CoIn is predicted correctly. This approach has been used to describe CoIns and/or NACs in combination with CIS,[98] TDDFT,[98,323,327−329] CCSD,[326] and ADC.[266,330] SF-TDDFT has been used in ab initio surface-hopping dynamics.[331] Spin-flip TDDFT has also been combined with the effective fragment methods for incorporating solvation in the study of CoIns.[332] A double spin-flip approach has also been implemented.[333]

The correct dimensionality of the CoIn using SF-TDDFT has been shown numerous times.[231,283,328] Figure 16 shows a

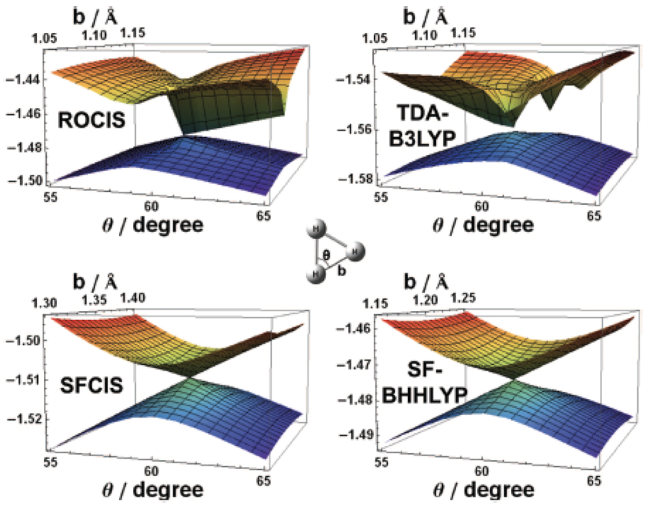

Figure 16. Potential energy surfaces around the CoIns of D_{3h} H_3 calculated by restricted open-shell CIS, unrestricted TD-B3LYP within the Tamm−Dancoff approximation, SF-CIS, and SF-BH&HLYP. All calculations employ the 6-31G* basis set, and energies are shown in atomic units. Reprinted with permission from ref 98. Copyright 2014 AIP Publishing.

comparison between the regular and the SF version of CIS and TDDFT in the description of a CoIn in H_3. It is clear in this comparison that CIS and TDDFT fail to describe the CoIn while their SF versions produce the correct shape of the cone. The spin-flip variant of ADC(3) has also been tested and shows the correct topology of S_1/S_0 CoIns,[330] unlike the conventional ADC methods. SF-EOM-CCSD with perturbative inclusion of triple excitations (dT or fT) was used in PSB3, and it was found that it produces potential energy profiles of the two lowest electronic states that agree well with MRCISD+Q.[228,229] ROHF references are preferred in the SF calculations in order to minimize the problem of spin-contamination. A recent perspective summarizes the advances of spin-flip approaches.[334] Initially algorithms for locating CoIns using SF-TDDFT were developed and used without the availability of couplings,[328] but NACs have become available since then.[98,335] SF-TDDFT overall demonstrated better performance than CASSCF for relative energies and optimized structures in benzene.[226]

The performance of SF-TDDFT in locating MECIs has been examined. Minezawa and Gordon were the first to report MECI geometries obtained with SF-TDDFT for ethylene and compared them to those obtained using MRCI and MS-CASPT2.[328] They found that SF-TDDFT correctly predicting the MECI geometries determined by the multireference methods. Zhang and Herbert compared SF-TDDFT MECI geometries of 9H-adenine to MRCIS results and found small differences.[98] Furthermore, they recommended BH&HLYP as the best functional when using SF-TDDFT. A comparison between SF-TDDFT, XMS-CASPT2, and CASSCF was made recently, focusing on MECI geometries and energies of a series

https://doi.org/10.1021/acs.chemrev.1c00074
Chem. Rev. XXXX, XXX, XXX−XXX

of biologically relevant organic molecules.[99] The differences in the energies of MECIs in most cases were found to be within 1 eV, and the comparison revealed a more qualitative rather than quantitative accuracy for SF-TDDFT.

A serious problem in spin-flip approaches is that the states are frequently spin contaminated. Figure 15 demonstrates the problem using a model consisting of four electrons in four orbitals.[329] The excitations within the open-shell space are able to generate spin-pure solutions, but all the involving closed shell or virtual excitations cannot be grouped into CSFs, and therefore the resulting wave function will not be an eigenfunction of the S^2 operator. In order to correct this problem, several approaches have been proposed which aim at adding missing determinants in order to produce spin eigenfunctions.[145,153,329,336−342] In order to overcome this deficiency, the CI space has been expanded to complete the spin-adapted CSFs leading to the spin-complete SF-CIS (SC-SF-CIS) and spin-flip extended configuration interaction singles (SF-XCIS).[336,337] An alternative approach developed by Tsuchimochi, called SFPCIS (Spin-Flip Projected CIS), uses an exact spin projection operator.[340] The topology of the CoIn has been tested with this approach, and it has been shown that it produces the correct topology. Zhang and Herbert used a tensor equation-of-motion approach and developed the spin-adapted SF-CIS (SA-SFCIS) method. This method has also been also extended to DFT, called SA-SF-DFT.[329] In the spin adapted version the minimum number of additional determinants required to construct the S^2 eigenstates is generated. As a result, spin becomes a good quantum number and the spin multiplicity is preserved.[329,342] The approach was tested in optimizing MECI and showed an improved efficiency in the optimization process reducing the number of iterations needed since the spin contamination was not an issue.[329]

The spin-flip approach can be generalized (and avoid spin contamination) by dividing the orbital space into three subsets based on the orbital occupations in the reference high-spin configuration: doubly occupied, singly occupied, and virtual. Schemes, such as RAS-SF and SF-ORMAS, have been developed this way.[145,153,338] SF-ORMAS is a single reference CI method that uses a high-spin restricted open shell determinant, where the wave function that has a given multiplicity is generated by an arbitrary amount of spin-flip excitations.[145,146] SF-ORMAS has been developed further with gradients and derivative couplings in order to focus on CoIns.[145,146,343] It has been shown to produce MECI geometries that are similar to MRCI.[146] Dynamical correlation has also been included with perturbation theory, labeled SF-MRMP2.[145]

Even when derivative couplings are not available, approximate schemes have been developed that estimate the couplings from the norm of one-particle transition density matrices,[344,345] and they have been used to estimate the rates of nonadiabatic transitions using RAS-SF wave functions in singlet fission.

The mixed-reference spin-flip time-dependent density functional theory (MRSF-TDDFT) method is another proposed method that eliminates the spin contamination of the SF-TDDFT methodology by using a mixed reference reduced density matrix, which combines reduced density matrices of the $M_S = +1$ and -1 triplet-ground states.[346] It has been shown that this approach can retain the correct topology of the CoIns and describes the geometry of the MECIs and their energies accurately.[347]

4.3. Semiempirical Methods

Semiempirical methods were used in locating CoIns in molecules as early as 2000.[94] Their advantage is that they are efficient, so they can be applied to large molecules. On the other hand, their performance cannot be predictive.[348] Semiempirical methods for CoIns are based on single reference and multireference methods and accordingly have similar advantages and disadvantages as their ab initio counterparts. The topology problems also are similar to these methods.

A widely used semiempirical method to describe CoIns is the OMx approach (orthogonalization models OM1, OM2, and OM3) developed by Thiel and co-workers.[348−350] The OMx methods include valence orthogonalization corrections into the core Hamiltonian, going beyond the standard modified neglect of diatomic overlap (MNDO) methods, and this leads to the correct asymmetric splitting of bonding and antibonding orbitals. OM1 includes these corrections only in the one-center one-electron part, while OM2 and OM3 include them also in the two-center one-electron terms. OM3 disregards some of the smaller corrections.[348] The molecular orbitals obtained from OMx are used in a GUGA-MRCI calculation. This OMx/MRCI approach has been used extensively to study CoIns and nonadiabatic dynamics, and an extensive list of publications can be found in previous work.[350,351] The OM2/MRCI has been tested on a small number of organic molecules for its performance on locating MECIs.[311,350] Compared to ab initio MRCISD, it was found that the root-mean-square deviation between the Cartesian coordinates of the ab initio and OM2/MRCI MECI structures was 0.1 Å. The branching-plane vectors between the two methods were also similar.[311] MECI geometries and branching vectors were also compared with SF-TDDFT and SI-SA-REKS, and they were all found to perform similarly.[311] OMx methods were parametrized using ground state properties, so better performance can be obtained by reparametrizing using excited state properties.

OMx has also been combined with CIS. Gradients and NACs have been developed for nonadiabatic dynamics between excited states, where CIS can be appropriate.[352] OMx/CIS is much more efficient than OMx/MRCI, so it can be extended to larger molecules. The method was applied on a molecule consisting of 2-, 3-, and 4-ring linear poly(phenylene ethynylene) units linked by meta-substitution as a proof of principle. Trajectory surface hopping nonadiabatic dynamics was used, and it was found to predict well energy transfer between excited states. Of course, this approach cannot be used for nonadiabatic processes involving the ground state since it is based on CIS. OMx has also been combined more recently with the SF-XCIS method to describe CoIns.[335] Its performance has been statistically evaluated for vertical singlet excitation energies, and analytic gradients and NACs have been implemented.[335]

The FOMO-CASCI method has also been implemented with semiempirical Hamiltonians.[157] The semiempirical FOMO-CASCI method using AM1, PM3, and MNDO has been extended to locate CoIn using an MECI search algorithm, and the resulting CoIn locations, energetics, and topographies were compared with those obtained from ab initio methods.[93] The topographies of CoIns generally agree very well with the ab initio results, but the relative energies are not very accurate. The method has been applied in various studies of excited states both in the gas phase and in solution.[93,353−355]

Another very popular semiempirical method used for excited states and CoIn is the DFT/MRCI method.[356−358] The

https://doi.org/10.1021/acs.chemrev.1c00074
Chem. Rev. XXXX, XXX, XXX−XXX

approach was originally derived by Grimme and Waletzke.[356] In DFT/MRCI Kohn−Sham, instead of HF, orbitals are used as the one-electron basis from which the configuration space is constructed. The original formulation by Grimme and Waletzke employed different parameters for singlet and triplet excitations whereas a new redesigned approach[357,359] uses identical parameter sets for all multiplicities. A major problem with DFT/MRCI is that gradients cannot be obtained analytically, so its application to CoIn is limited. They can however be determined numerically using finite differences and can be used to locate MECI points.[360]

5. DERIVATIVE COUPLING

The derivative or nonadiabatic coupling (NAC), responsible for coupling between different electronic states I, J and nonadiabatic transitions between them, is given by

$$f_{IJ}^{\alpha}(\mathbf{R}) = \langle \Psi_I(\mathbf{r};\mathbf{R})|\nabla_\alpha \Psi_J(\mathbf{r};\mathbf{R})\rangle \tag{56}$$

The brackets denote integration over electronic coordinates $\mathbf{r}$, and ∇_α refers to the gradient over the nuclear coordinate R_α. $\mathbf{f}_{IJ}(\mathbf{R})$ is a vector of dimension equal to the number of nuclear coordinates and a measure of the variation of the electronic wave function with respect to nuclear coordinates. For an exact solution to the Schrödinger equation it can easily be shown that it is equivalent to the expression

$$\mathbf{f}_{IJ}(\mathbf{R}) = \frac{\langle \Psi_I|\nabla H|\Psi_J\rangle}{E_J - E_I} \tag{57}$$

This relation shows that it is inversely proportional to the energy difference between states I and J, and it goes to infinity when the gap goes to zero (at the CoIns). That is why CoIns are so important in nonadiabatic processes. Derivative couplings are needed in dynamics, and they are also often used to locate CoIns, as was seen in previous sections. Finally, they are needed to compute rigorous diabatic states.[16]

In the case of the exact wave functions, NAC is a strictly one-electron operator and can be computed using unrelaxed one electron density matrices. The two-electron contributions to NAC are artifacts of using atom-centered incomplete basis sets; they vanish in the complete basis set limit or when using non-AO bases, such as plane wave or grid representations.[345,361]

If an analytic implementation is not available, the nonadiabatic coupling can be evaluated numerically by evaluating the overlap of the wave functions between small displacements,[362−364]

$$\langle \Psi_I|\nabla \Psi_J\rangle = \frac{\langle \Psi_I(x)|\Psi_J(x+\Delta x)\rangle - \langle \Psi_I(x)|\Psi_J(x-\Delta x)\rangle}{2\Delta x} \tag{58}$$

As in all cases of numerical derivatives, the cost becomes very expensive when many degrees of freedom are involved and one has to make displacements in every direction.

In semiclassical dynamics the derivative coupling vector appears as time derivative

$$\sigma_{IJ} = \langle \Psi_I|\frac{\partial \Psi_J}{\partial t}\rangle = \mathbf{f}_{IJ}(\mathbf{R})\cdot\dot{\mathbf{R}} \tag{59}$$

where $\dot{\mathbf{R}}$ is the velocity (time derivative of nuclear coordinates). The time derivative coupling can be calculated using the Hammes-Schiffer−Tully formula[365] using overlap integrals between the adiabatic wave functions at times t and $t + dt$

$$\sigma_{IJ} \approx \frac{\langle \Psi_I(t)|\Psi_J(t+\Delta t)\rangle - \langle \Psi_I(t+\Delta t)|\Psi_J(t)\rangle}{2\Delta t} \tag{60}$$

The advantage of the above expression utilized in semiclassical dynamics is that analytic expressions for NAC are not needed. This is advantageous in semiclassical methods such as surface hopping that only require the NAC dotted into the velocity. In more complete semiclassical methods (or in full quantum calculations) one requires the NAC in all directions, not just the component along the velocity. It was recently shown that time derivatives can nevertheless still be useful for such more complete semiclassical methods.[366] Other approaches have also been explored for the evaluation of the time derivatives coupling.[367,368] Since these approaches are more specific to dynamics, we will not explore them further here.

Equation 57 can be used practically when analytic expressions for the derivative coupling are evaluated for ab initio approximate solution to the Schrödinger equation, as will be described below for various methods. That relationship indicates how gradients of states can be explored when calculating nonadiabatic couplings. For two electronic states, Ψ_I and Ψ_J, we can construct the wave function of a fictitious mixed state $\Psi_I + \Psi_J$

$$\begin{aligned}&\langle \Psi_I + \Psi_J|\nabla H|\Psi_I + \Psi_J\rangle \\ &\quad = \langle \Psi_I|\nabla H|\Psi_I\rangle + \langle \Psi_J|\nabla H|\Psi_J\rangle + 2\langle \Psi_I|\nabla H|\Psi_J\rangle\end{aligned} \tag{61}$$

Knowing the densities or gradients of each state and of the mixed state, one can obtain the transition density or $\langle \Psi_I|\nabla H|\Psi_J\rangle$ (which for nonexact wave functions corresponds to the Hellmann−Feynman component of the coupling). This procedure has been used in MRCI[132] (in Columbus), MS-CASPT2,[211] and CCSD[361] (in QChem).

It was noted early on that the NAC is origin dependent and lacks translational and rotational invariance.[369−371] The lack of rotational invariance results in a dynamical coupling, between states of different symmetry in diatomic molecules and between the components of a Renner−Teller pair of states in polyatomic molecules.[372−374] When the derivative involves only overall nuclear rotation, i.e. $\mathbf{R}$ corresponds to overall nuclear rotation, then the derivative coupling matrix elements are equal to the total electronic angular momentum matrix elements[372,374]

$$-i\langle \Psi_I|\frac{\partial}{\partial \mathbf{R}}|\Psi_J\rangle = \langle \Psi_I|\mathbf{L}^{nuc}|\Psi_J\rangle = -\langle \Psi_I|\mathbf{L}^{el}|\Psi_J\rangle \tag{62}$$

The lack of translational invariance[371,375−377] can be an important problem when using NACs. Motivated by earlier literature on atom−atom scattering calculations,[376] Fatehi et al.[378,379] recently introduced corrections, electron translation factors (ETFs), for analytic derivative couplings. These authors found that for a range of representative organic molecules ETF correction is often small but can be qualitatively important, especially for few-atom systems. Later, Herbert and co-workers showed that the ETF correction exactly cancels the orbital contribution part in the expression for the derivative coupling.[98]

We continue by examining the basic facts of how some of the basic electronic structure methods have implemented NAC.

5.1. Derivative Coupling in Multireference Methods

First implementations of NAC appeared about 35 years ago.[370,375,380] The derivative coupling was first implemented for multireference wave functions, MCSCF[375] and

https://doi.org/10.1021/acs.chemrev.1c00074
Chem. Rev. XXXX, XXX, XXX−XXX

MRCI,[132,133,370,380] while implementations for MRPT appeared much later.

5.1.1. Derivative Coupling in CASSCF/MRCI. The expressions for evaluating analytical derivative couplings with CASSCF and MRCI wave functions were developed first.[375,380,381] They were shown by Lengsfield et al.[375] to be very similar to those of analytic gradients. This enables their computation by taking advantage of the developments in gradient theory. Specifically, gradients can be calculated as inner products of effective density matrices and derivatives of the atomic orbitals.[382] In the case of NACs the densities are replaced by transition densities. Furthermore, the coupled perturbed CP-MCSCF is solved, either once for each degree of freedom[383] or invoking the Z-matrix approach by Handy and Schaefer.[384] The basic equations for deriving NAC are illustrated here based on Lengsfield and Yarkony for MRCI.[380] Discussion of other methods will only highlight important elements specific to a given method that are missing from this derivation.

As discussed in section 4.1.1 the CI wave function for state I can be written as

$$\Psi_I(\mathbf{R}) = \sum_{a=1}^{N^{CSF}} c_a^I \psi_a(\mathbf{R}) \tag{63}$$

where ψ_a represents CSFs and c_a^I are the coefficients of the expansion. Using this wave function, the derivative coupling can be split into two parts, one coming from the derivative of the CSFs and one from the derivative of the coefficients.

$$\mathbf{f}_{IJ}(\mathbf{R}) = {}^{CSF}\mathbf{f}_{IJ}(\mathbf{R}) + {}^{CI}\mathbf{f}_{IJ}(\mathbf{R}) \tag{64}$$

$${}^{CI}\mathbf{f}_{IJ}(\mathbf{R}) = \langle c^I|\nabla c^J\rangle = \frac{1}{E_J - E_I}\langle c^I|\nabla H|c^J\rangle \tag{65}$$

$$= \frac{\mathbf{h}^{IJ}}{\Delta E_{JI}} \tag{66}$$

$${}^{CSF}\mathbf{f}_{IJ}(\mathbf{R}) = \sum_a \sum_b c_a^I c_b^J \langle \psi_a(\mathbf{R})|\nabla \psi_b(\mathbf{R})\rangle \tag{67}$$

∇ corresponds to derivatives with respect to all components of $\mathbf{R}$, and E_I is the energy of state I. Using the one particle (γ_{ij}) and two particle (Γ_{ijkl}) density matrices in the molecular orbital (MO) basis and one (h_{ij}) and two electron (g_{ijkl}) integrals in the MO basis, the energy E_I can be written as

$$E_I = \sum_{i,j} h_{ij}\gamma_{ij}^{II} + \sum_{i,j,k,l} g_{ijkl}\Gamma_{ijkl}^{II} + V_N \tag{68}$$

V_N is the nuclear repulsion energy. The gradient for component R_α is then written as

$$\frac{\partial E_I}{\partial R_\alpha} = \sum_{i,j}\left(\frac{\partial}{\partial R_\alpha}h_{ij}\right)\gamma_{ij}^{II} + \sum_{i,j,k,l}\left(\frac{\partial}{\partial R_\alpha}g_{ijkl}\right)\Gamma_{ijkl}^{II} + \frac{\partial V_N}{\partial R_\alpha} \tag{69}$$

It can be shown that the CI component of the derivative coupling ${}^{CI}\mathbf{f}_{IJ}(\mathbf{R})$ can be written in a similar way as

$${}^{CI}f_{IJ}^{\alpha}(\mathbf{R}) = \left\{\sum_{i,j}\left(\frac{\partial}{\partial R_\alpha}h_{ij}\right)\gamma_{ij}^{IJ} + \sum_{i,j,k,l}\left(\frac{\partial}{\partial R_\alpha}g_{ijkl}\right)\Gamma_{ijkl}^{IJ}\right\}\frac{1}{\Delta E_{JI}} \tag{70}$$

where γ_{ij}^{IJ} and Γ_{ijkl}^{IJ} are the transition density matrix elements between states I and J in the MO basis. Transforming to the AO basis (p, q, r, and s are indices over AOs), the equation becomes

$${}^{CI}f_{IJ}^{\alpha}(\mathbf{R}) = \left\{\sum_{p,q}\left(\frac{\partial}{\partial R_\alpha}h_{pq}\right)\gamma_{pq}^{IJ} + \sum_{p,q,r,s}\left(\frac{\partial}{\partial R_\alpha}g_{pqrs}\right)\Gamma_{pqrs}^{IJ} + \sum_{i,j}L_{ij}^{IJ}U_{ij}^{\alpha}\right\}\frac{1}{\Delta E_{JI}} \tag{71}$$

L_{ij}^{IJ} is a transition Lagrangian given by $L_{ij}^{IJ} = 2\sum_m \gamma_{jm}^{IJ}h_{im} + 4\sum_{m,k,l}\Gamma_{jmkl}^{IJ}g_{imkl}$. Similarly the CSF part can be shown to be

$${}^{CSF}f_{IJ}^{\alpha}(\mathbf{R}) = \sum_{i,j}\gamma_{ij}^{IJ}(\sigma_{ij}^{\alpha} + U_{ij}^{\alpha}) \tag{72}$$

U_{ij}^{α} represents the MO response terms (derivatives of molecular orbital coefficients) and is obtained from the CP-MCSCF or CP-SAMCSCF equations. σ_{ij}^{α} comes from differentiation of the overlap of atomic orbitals.

Implementations of analytic gradients and derivative couplings at the MRCI level are not as widespread as CASSCF ones. The Columbus software is a main publicly distributed software that has analytic gradients readily available and extended them to NAC.[127,128,132,385] The NAC in Columbus has also been expanded recently to the relativistic MRCI-SD method.[386,387] MRCISD NAC has also been developed by Hoffmann and co-workers extending to state-averaged MCSCF where the states do not need to have the same weights.[388]

Implementations of CASSCF NAC are the most widespread and exist in most packages with MCSCF capabilities, such as Columbus,[132] Gamess,[187,188] Gaussian,[389] Molpro,[176] Molcas,[175] and openMolcas.[390] A recent implementation of derivative couplings using state-averaged CASSCF within Molcas[175] uses density-fitted two-electron integrals to speed up the calculations.[391] Recently NAC was also implemented for CASSCF wave functions on graphical processing units,[141] and the software is available in Terachem.[392−394] Using this algorithm, the authors were able to do the largest to date MECI searches, such as locating an MECI of butadiene solvated in 50 methanol molecules at the SA-3-CAS(4,4)/6-31G* level of theory.[141]

NAC has been implemented in other variants of CASSCF, such as in ORMAS.[144] A comparison between ORMAS and CASSCF was made, not only examining CoIn geometries but also the behavior of NAC around the CoIn. It was found that ORMAS with single excitations can often reproduce CASSCF results but can have difficulty maintaining correct orbital subspaces. Also, CAS and ORMAS NAC vectors are very similar at most geometries. More recently the NACs have been implemented in the SF-ORMAS approach as well.[343]

For an example of the utility of the derivative coupling beyond dynamics, Figure 17 shows the components of the derivative coupling along one of the branching coordinates or the polar coordinate of the branching plane θ. The derivative coupling in that work was obtained using the implementation of CASSCF in Molcas.[391] Integration of f_θ along θ gives π, which is another way to confirm the existence of a CoIn inside the loop defined by θ. An analytic expression of f_θ^{AB} can be obtained in first order using the polar coordinates of the branching plane,

https://doi.org/10.1021/acs.chemrev.1c00074
Chem. Rev. XXXX, XXX, XXX−XXX

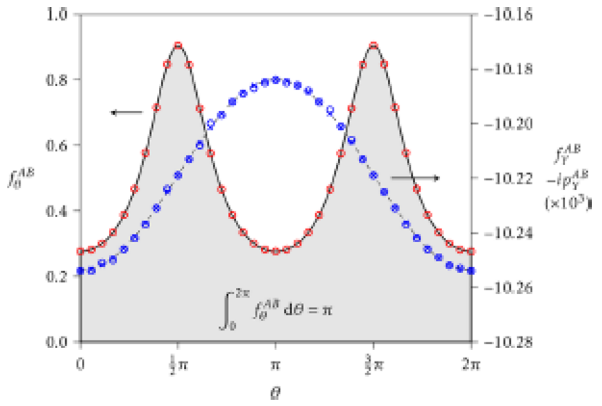

Figure 17. Values of f_θ^{AB} (red circles, left axis) and f_Y^{AB} (blue circles, right axis) for a circle surrounding the ethylene intersection. For comparison, the analytical result (from eq 73) is shown as a solid line, and the matrix elements of the electronic momentum operator are shown with blue crosses. The area below the solid line integrates to π, a sign that there is a CoIn inside the loop. Reprinted with permission from ref 391. Copyright 2016 American Chemical Society.

$$f_{IJ}^{\theta} = \rho \frac{gh}{g^2 \cos^2\theta + h^2 \sin^2\theta} \tag{73}$$

5.1.2. Derivative Coupling in CASPT2. Multireference methods based on perturbation theory were delayed in their development of analytic gradients and NACs, even though they have been heavily used in studying nonadiabatic problems. The NAC in MS-CASPT2 was initially evaluated numerically in an efficient procedure that only calculated the projection to the velocity needed in dynamics and was used in ab initio multiple-spawning dynamics.[395] Analytic implementations, for the full coupling or for the most important contributions, have been since developed for the various versions, MS-CASPT2,[205,209−211] XMS-CASPT2,[205] and NEVPT2.[214] Also, analytical NACs are derived and implemented for the generalized Van Vleck perturbation theory (GVVPT).[396,397]

The derivative coupling is separated into three different contributions,

$$\mathbf{f}_{IJ} = \mathbf{f}_{IJ}^{mix} + \mathbf{f}_{IJ}^{CAS} + \mathbf{f}_{IJ}^{PT2} \tag{74}$$

where $\mathbf{f}_{IJ}^{mix}$ includes the derivative of the (X)MS-CASPT2 mixing coefficients, $\mathbf{f}_{IJ}^{CAS}$ accounts for the coupling between reference CASSCF functions, and $\mathbf{f}_{IJ}^{PT2}$ accounts for the coupling between the reference function and the first-order correction. The first term is the dominant near CoIns and can be evaluated as

$$\mathbf{f}_{IJ}^{mix} = \sum_M u_M^I \frac{d}{d\mathbf{R}} u_M^J = (E_J - E_I)^{-1} \sum_{M,N} u_M^I \frac{dH_{MN}^{eff}}{d\mathbf{R}} u_N^J \tag{75}$$

using the wave function in eq 39. This term can be evaluated with techniques available for the gradients of states, similarly to what was discussed in the MRCI approach.

The availability of NAC with methods with dynamical correlation enables studying the effect of dynamical correlation on the coupling. In most cases, the differences highlight the differences in the underlying wave functions of the states. In addition, a proper comparison between NAC should take into account the fact that NAC is a vector, so both the magnitude and the direction are important. The **g** and **h** vectors define which vibrations are activated as molecules go through CoIns. The importance of the direction in the dynamics can be seen in the surface hopping approach, where the probability for nonadiabatic transitions is proportional to the dot product of the derivative coupling and the velocity vector, so the direction of the derivative coupling is crucial. MS-CASPT2 analytic gradients for the coupling vector were applied to cyclohexadiene, and the CoIns and energetics were compared to results from CASSCF in order to determine the effect of dynamical correlation. For cyclohexadiene, dynamical correlation is very important and creates big differences in the results.[209] Figure 18 shows the direction of **g** and **h** vectors for the S_1/S_0 MECI point in cyclohexadiene obtained at the MS-CASPT2 and CASSCF methods. It is clear that the vectors are affected by the addition of dynamical correlation.

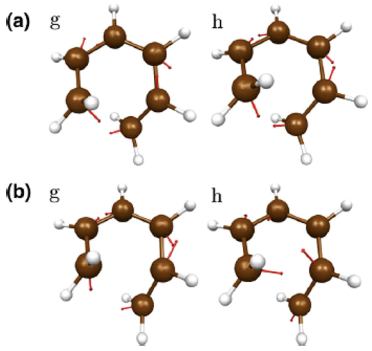

Figure 18. Direction of the **g** and **h** vectors for the S_1/S_0 MECI point in cyclohexadiene obtained at the (a) MS-CASPT2 and (b) SA3-CASSCF methods. Reprinted with permission from ref 209. Copyright 2009 Elsevier.

5.2. Derivative Coupling in CIS and Post-CIS Methods

Derivative couplings have been developed for CIS wave functions. Subotnik focused on obtaining derivative couplings between excited states at the CIS level initially.[378] Herbert and co-workers extended to spin-flip CIS.[98] Analytic gradients and derivative couplings have also been implemented for the corrected CIS-1D approach.[296] There are no couplings however for many of the popular post-CIS methods, such as CC2 and ADC(2).

The NACs with SF-ORMAS have been implemented in GAMESS, and they have been compared with other multireference methods.[343] The NACs computed by SF-ORMAS display the same general trends as CASSCF NAC, suggesting that this approach will be a good choice for nonadiabatic dynamics.

5.3. Derivative Coupling in EOM-CCSD

The formulas for NAC in EOM-CCSD were derived in 1999,[398] but the first implementations were not done until 2009.[399,400] A recent implementation in QCHEM includes derivatives for EOM-IP, EOM-EE, and EOM-EA versions.[361]

Specific aspects that need to be considered in EOM-CC are the consequences of the nonhermitian nature of the theory and normalization. Since the EOM-CC theory is non-Hermitian, the left and right eigenstates are not the conjugate of each other but they form a biorthogonal set

$$\langle 0|L_J R_I|0\rangle = \delta_{IJ} \tag{76}$$

Furthermore, the norms of left or right states are arbitrary, and thus the effect of normalization has to be taken into account. Normalized wave functions need to be used

https://doi.org/10.1021/acs.chemrev.1c00074
Chem. Rev. XXXX, XXX, XXX−XXX

$$|\Psi_I^{EOM}\rangle \rightarrow N_I^R|\Psi_I^{EOM}\rangle \tag{77}$$

$$\langle\tilde{\Psi}_I^{EOM}| \rightarrow N_I^L\langle\tilde{\Psi}_I^{EOM}| \tag{78}$$

where N_I^R and N_I^L are the normalization factors for the right and left wave functions, respectively. Expressions for N_I^L can be found in previous publications, while the relationship between the two is $N_I^R = 1/N_I^L$.[361,399,400]

Because of the non-Hermitian nature of the theory, matrix elements A_{IJ} are not the same as A_{JI}. Consequently, the nonadiabatic coupling vectors are being defined in two ways:

$$\langle N_I^L\tilde{\Psi}_I^{EOM}|\nabla_R N_J^R\Psi_J^{EOM}\rangle \neq \langle\nabla_R N_J^L\tilde{\Psi}_J^{EOM}|N_I^R\Psi_I^{EOM}\rangle \tag{79}$$

Since there is no reason to choose one of these expressions, a geometric or arithmetic mean can be used. Both of these approaches have been adopted before and they showed insignificant differences.[399,400] An arithmetic mean will be given by

$$\mathbf{f}_{IJ} = \frac{N_I^L N_J^R\langle\tilde{\Psi}_I^{EOM}|\nabla_R\Psi_J^{EOM}\rangle + N_J^L N_I^R\langle\nabla_R\tilde{\Psi}_J^{EOM}|\Psi_I^{EOM}\rangle}{2} \tag{80}$$

Furthermore, it was shown that the computed $W_I = N_I^L N_J^R$ are always almost equal to one and have a very small effect on the NACs.[361]

Similarly to all the other methods discussed here, the derivative coupling in EOM-CC is split into two terms,

$$\mathbf{f}_{IJ} = \mathbf{f}_{IJ}^C + \mathbf{f}_{IJ}^\phi \tag{81}$$

where the first includes the derivatives of the eigenvectors and cluster amplitudes and the second derivatives of the molecular orbitals. This term leads to translationally invariant coupling while $\mathbf{f}_{IJ}^\phi$ leads to translationally dependent terms.

The $\mathbf{h}_{IJ}^C = \mathbf{f}_{IJ}^C(E_J - E_I)$ is very similar to what Ichino et al.[399] refer to as quasidiabatic coupling strength λ_{IJ}

$$h_{IJ}^\alpha \approx \lambda_{IJ}^\alpha = \langle 0|L_I e^{-T}\frac{\partial H}{\partial R_\alpha}e^T R_J|0\rangle + \langle 0|L_I e^{-T}He^T\frac{\partial T}{\partial R_\alpha}R_J|0\rangle - \langle 0|L_I e^{-T}\frac{\partial T}{\partial R_\alpha}He^T R_J|0\rangle \tag{82}$$

The $\mathbf{f}_{IJ}^\phi$ term is given by[361,400]

$$\mathbf{f}_{IJ}^\phi = \sum_{pq}\langle\phi_p|\nabla\phi_q\rangle\tilde{D}_{pq}^{IJ} \tag{83}$$

where $\tilde{D}_{pq}^{IJ}$ is the antisymmetric one-particle transition density matrix as defined in CC, and $\nabla\phi_q$ is the derivative of MO ϕ_q.

In a recent publication, detailed comparisons were made between derivative couplings obtained from CCSD methods and MRCI or CASSCF using various metrics.[361] Both EOM-CC and MRCI include dynamical correlation, but the electronic structure of the states involved can differ, especially if nondynamical correlation is important, and comparison between these two methods can reveal that. Figure 19 shows the derivative coupling vectors for $NaNH_3$ using MRCI and EOM-EA-CCSD. The low-lying electronic states in this system and larger clusters of Na with NH_3 are described as *s*- and *p*-like states. The doublet states can be described by EOM-EA-CCSD starting from the closed shell cation as a reference. The NACs shown in the figure differ between the MRCI and EOM-EA-CCSD descriptions. The reason in this case is that the *p*-like states are almost degenerate in energy so they can mix, and small differences in the mixing between the different methods lead to the observed different directions of NACs.

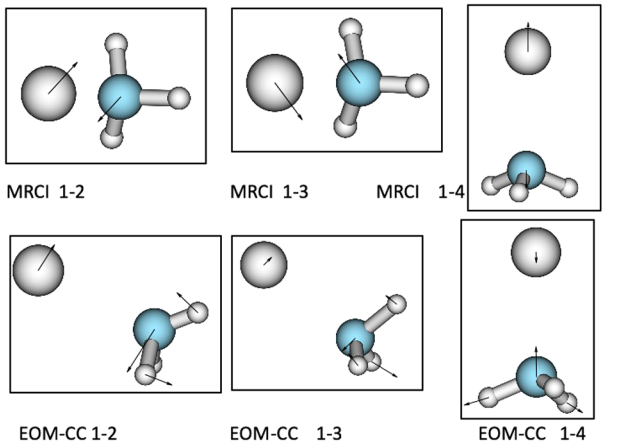

Figure 19. NAC forces in $NaNH_3$ computed using MRCI and EOM-EA-CCSD. Adapted from ref 361. Copyright 2018 AIP Publishing.

Another way to get information about the importance of the direction of the derivative coupling is inspired by how the coupling is used in nonadiabatic surface hopping dynamics, which is as a dot product of the coupling with the nuclear velocity. If we approximate the velocity by the initial slope of the initially populated surface $\mathbf{g}_I$, then the rate of transitions can be approximated from static electronic structure calculations using the dot product of the initial gradient with the derivative coupling ($r_{IJ} = \mathbf{f}_{IJ}\cdot\mathbf{g}_I$).[401]

Table 1 shows a comparison of the derivative coupling calculated with EOM-IP-CCSD and CASSCF for different pairs of states of uracil cation. The different metrics, magnitude, direction, and r_{IJ} are compared. Since the derivative coupling depends on the energy difference, a better measure of how sensitive the wave function is to the methodology is the vector $\mathbf{h}$, which is independent of the energy difference. The results in Table 1 show that the CASSCF and EOM-IP-CCSD results are quite similar. The directions of the coupling are always almost parallel, while the magnitudes are mostly similar, except for the D_0-D_2 and D_1-D_3 couplings which differ by about 30%. The metric r shows larger differences, but the trends agree qualitatively between the two methods.

Overall, EOM-CC agrees well with multireference results for couplings between excited and between ionic states. The results depend on the underlying wave functions, which are often very sensitive to correlation. EOM-CC methods provide a viable alternative to multireference approaches when applied to the appropriate systems and problems.

5.4. Derivative Coupling in TDDFT

There has been extensive work to implement nonadiabatic couplings within TDDFT during the past decade.[98,402−422] The most popular implementation of TDDFT is based on linear response theory of the density of the noninteracting Kohn−Sham reference system. For this reason, there are no electronic wave functions of the excited states defined which need to be differentiated to obtain the derivative coupling, making their derivation more problematic.

Within LR-TDDFT the first formulation of NAC between ground and excited states was done by Chernyak and Mukamel.[402,403] Chernyak and Mukamel using response theory derived closed expressions for the nonadiabatic coupling matrix

https://doi.org/10.1021/acs.chemrev.1c00074
Chem. Rev. XXXX, XXX, XXX−XXX

Table 1. Energy Gaps (ΔE), NAC Force (h), and Derivative Coupling Vector (f) between the Three Lowest Electronic States of the Uracil Cation[a]

States	ΔE^A	$\|h^A\|$	$\|f^A\|$	ΔE^B	$\|h^B\|$	$\|f^B\|$	Δ^{AB}	$\cos\theta^{AB}$	r^A	r^B
0−1	0.60	0.02	0.788	0.78	0.02	0.816	0.004	0.97	1.90×10^{-7}	1.30×10^{-4}
0−2	1.01	0.08	2.281	0.83	0.13	4.353	0.05	0.99	0.01	0.044
0−3	1.57	0.02	0.384	1.46	0.02	0.272	0.007	0.95	3.80×10^{-9}	8.0×10^{-5}
1−2	0.41	0.02	1.238	0.05	0.01	5.986	0.008	0.98	8×10^{-9}	3.50×10^{-6}
1−3	0.98	0.14	3.965	0.68	0.23	9.251	0.09	0.98	0.52	1.38
2−3	0.57	0.02	0.996	0.63	0.02	0.816	0.005	0.97	3.50×10^{-7}	3.10×10^{-4}

[a]Energy gaps are in eV; all other quantities are in a.u. Superscripts A and B denote the EOM-IP-CCSD/cc-pVDZ and CASSCF/cc-pVDZ values, respectively. $\Delta^{AB} = \|\mathbf{h}^A - \mathbf{h}^B\|$. $\cos\theta^{AB}$ is defined by the dot product of the **h** vectors produced by the two methods, so it is a metric of their differences in direction. Adapted with permission from ref 361. Copyright 2018 AIP Publishing.

elements based on computing the electronic response of the system to an external field. The Chernyak−Mukamel formula is equivalent to the Hellmann−Feynman contribution, and it is exact at the complete basis set limit. Although it was first developed for couplings between the ground and excited state, it can be extended to derivative couplings between excited states.[423] Chernyak and Mukamel used the following expression for the derivative coupling, first shown by Pauli[424]

$$f_{IJ}^{\alpha} = \frac{\langle \Psi_I | \frac{\partial V_{ne}}{\partial R_\alpha} | \Psi_J \rangle}{E_J - E_I} \tag{84}$$

where V_{ne} is the electron−nucleus attraction operator. This equation assumes that Ψ_I and Ψ_J are solutions to the exact Hamiltonian and that the Hamiltonian depends on the nuclear position R through the electron−nucleus potential only. In reality these assumptions are not satisfied, since approximate wave functions based on atom-centered finite basis sets are used. Using the above equation when one of the states is the ground state, it can be seen that the NAC can be expressed as follows

$$f_{0I}^{\alpha} = \frac{Tr[\gamma^{0I} \nabla_\alpha H]}{E_I - E_0} \tag{85}$$

using the electron−nucleus attraction potential, the excitation energy, and the transition density γ^{0I}.

However, Pulay terms, arising from atom centered basis functions, which are missing in the Hellmann−Feynman approach, are important in finite basis sets.[378,414] Send and Furche were the first to develop a consistent formulation and account for all Pulay terms.[414] They compared their results to FCI and found that TDDFT agreed well with FCI for regions of the PES where the Kohn−Sham ground state reference is stable and the character of the excitation can be correctly represented by the chosen functional. Their derivation only applies to coupling between ground and excited states.[414] TDDFT NACs were employed successfully in nonadiabatic studies of cyclohexadiene and other derivative molecules.[425]

As was already discussed extensively in section 4.2, TDDFT and all single reference methods are problematic when describing CoIn between the ground and excited states. Thus, the utility of TDDFT in dynamics is more important in describing couplings between excited states. Around the same time three different groups used time-dependent (quadratic) response theory to derive NAC between excited states and arrived at equivalent expressions.[415−417,421] In a succinct notation taken from Li and Liu[415,416] the couplings can be written as

$$f_{0I}^{\alpha} = \sum_{pq} d_{pq}^{\alpha} \gamma_{pq}^{0I} \tag{86}$$

$$f_{IJ}^{\alpha} = \omega_{JI}^{-1} \mathbf{t}_I^{\dagger} \mathbf{E}^{\alpha} \mathbf{t}_J + \sum_{pq} d_{pq}^{\alpha} \gamma_{pq}^{IJ} \tag{87}$$

where a generalized eigenvalue equation is used

$$\mathbf{E}\mathbf{t}_I = \omega_I \mathbf{S}\mathbf{t}_I \tag{88}$$

E can be the Hamiltonian matrix in the case of CIS or the orbital Hessian in TDHF or TDDFT. This is equivalent to eq 53 for TDDFT. γ_{pq}^{IJ} and γ_{pq}^{0I} are transition density matrices to be determined by TDDFT, and d_{pq}^{α} are the elements of the antisymmetric derivative matrix

$$d_{pq}^{\alpha} = \langle \phi_p | \frac{\partial}{\partial R_\alpha} | \phi_q \rangle \tag{89}$$

over orthonormal MO orbitals ϕ_p. The first term in eq 87 is the equivalent to the CI term in MRCI formalism while the second term corresponds to the CSF term. The CSF terms involve couplings between (O) and virtual (V) orbitals, giving rise to OV, VO, VV, and OO terms.

Alternatively, a pseudo-wave-function approach (PWA) can be used.[418,419] For spin-flip DFT the two approaches are formally equivalent,[417] but for spin-preserving treatments, it can be shown that in the PWA derivation the OV terms are not included.[417] Zhang and Herbert[417] and Ou et al.[421] explored the differences between the derivative coupling obtained from the quadratic response formalism and the PWA. Figure 20 compares the results from the two approaches. The derivative coupling obtained from the quadratic response theory is denoted as d_{IJ}^{KS} while the one obtained from the PWA is denoted d_{IJ}^{PWA}. The magnitude and the orientation of the vectors are compared. $\cos\theta$ is obtained from the dot product of the two vectors, so it is a measure of their orientation differences. A value of 1 denotes parallel vectors. The difference between the two couplings between excited states was compared as a function of the gap between the two states. When the gap is very small, the CI term is expected to dominate, and in this case the two vectors should be very similar. As seen in the figure, the magnitude of the two vectors differs by less than 1% for most of the cases, and only when the gap increases to about 5 eV do the vectors start to deviate. The orientation is always very similar. This indicates that the PWA can be used in most cases, and especially for a CoIn search. The PWA is marginally cheaper to calculate since a term is missing. On the other hand, when the energy difference between two excited states is equal to the excitation energy of a third excited state, the derivative couplings from adiabatic TDDFT response theory become problematic showing a

https://doi.org/10.1021/acs.chemrev.1c00074
Chem. Rev. XXXX, XXX, XXX−XXX

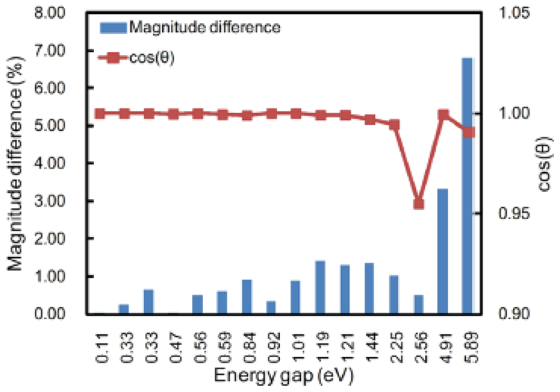

Figure 20. Differences between d_{IJ}^{KS} and d_{IJ}^{PWA} at various energy gaps. The derivative couplings were calculated by TDDFT/TDA at the PBE0/6-31G** level. Full (non-TDA) TDDFT results are similar and are omitted here. Note that the horizontal scale is not linear but rather consists of the 16 different gaps that were computed for the 8 molecules in the test set. Reprinted with permission from ref 417. Copyright 2015 AIP Publishing.

spurious pole. The PWA tend to give the correct qualitative behavior of the coupling, when the underlying excited states are described correctly with TDDFT, and it can be more useful in nonadiabatic dynamics, since it avoids the divergence seen in the quadratic response.[417,421] Efficient implementation of NACs between several pairs of states has been demonstrated on the noadiabatic dynamics of thymine involving three states, and it should be possible for molecules with up to 100 atoms and 10 ps simulation times on single workstation nodes.[422]

Figure 21 compares the derivative coupling vectors obtained in a loop around the CoIn on the branching plane x−y. TDHF

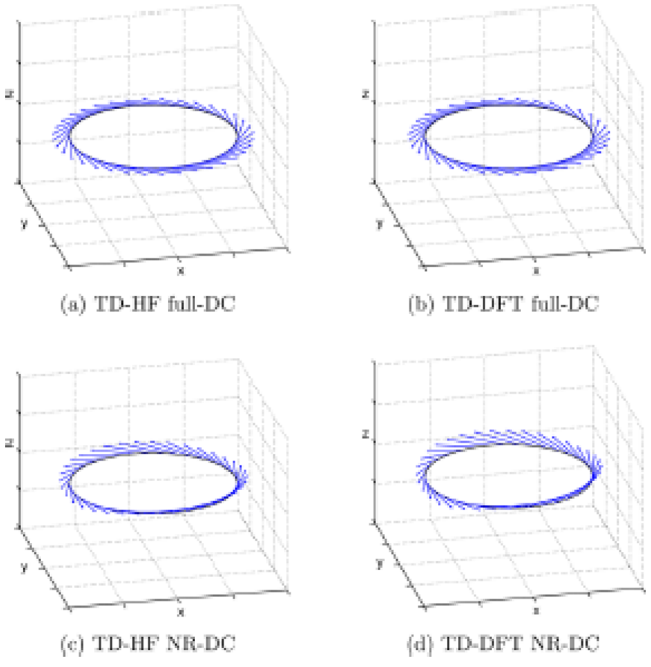

Figure 21. $CH_2NH_2^+$ S_1/S_2 derivative coupling vectors on the circular loop (r = 0.001 Å) around the CoIn point in the branching plane given by TDHF (left) and TDDFT (right). 36 single-point calculations were performed. NR-DC stands for no response derivative coupling. Reprinted with permission from ref 418. Copyright 2015 American Chemical Society.

and TDDFT derivative couplings were calculated with and without the orbital response (Pulay) terms. The full NAC is on the branching plane while when response terms are missing there are components out of the plane, indicating that the branching plane is not fully represented by them. TDDFT NAC was calculated with the PWA.

Figure 22 demonstrates the problems that can be encountered when using TDDFT to treat NAC with the ground state. Figure

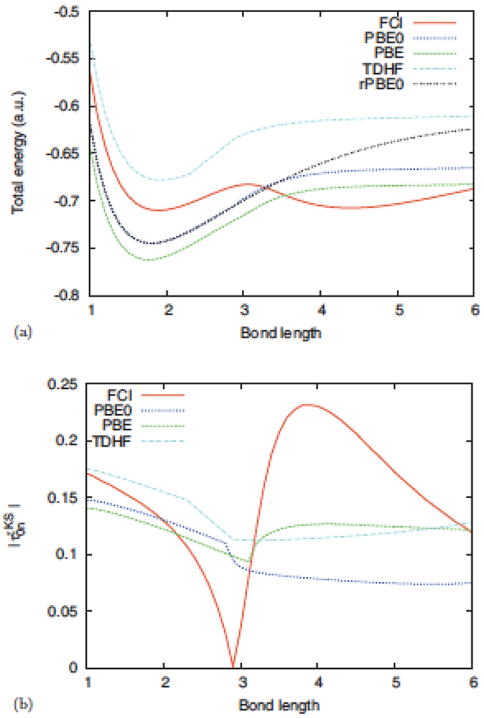

Figure 22. Absolute value of the z-component of KS for the coupling between the ground and EF $^1\Sigma_g^+$ excited state of H_2. The molecule is aligned along the *z*-axis. The spin unrestricted PBE0, PBE, and TDHF results are compared with FCI results. (a) Excited state potential energy curves. (b) Coupling elements. Reprinted with permission from ref 414. Copyright 2010 AIP Publishing.

22 shows the potential energy surface of the second excited singlet state, $^1\Sigma_g^+$, of H_2 using FCI, TDHF, and TDDFT. FCI shows that the state has two minima, but the other methods (TDHF and TDDFT) cannot reproduce the second minimum because it has a significant double excitation character. Figure 22b shows the NACs calculated at the same levels of theory. This picture shows that NACs display the same effect as the energies, namely that the TDDFT and TDHF fail to reproduce the correct behavior of the state at distances longer than 2.5 Å, where the double excitation character is important. The NAC with FCI is very different from the ones produced from TDHF and TDDFT at long distances.

There have not been many studies exploring how the different functionals affect the derivative coupling. The magnitude of NAC on the choice of functional has been tested using numerical time derivatives using the Hammes-Schiffer−Tully formula.[426] The NACs were computed numerically for small silicon clusters and silicon hydrides. It was found that pure functionals can significantly overestimate NAC magnitudes in comparison to those obtained with hybrid functionals. The ratio of the two magnitudes increases with the system size and differs by an order of magnitude even for small Si_7 and Si_{26} clusters.

https://doi.org/10.1021/acs.chemrev.1c00074
Chem. Rev. XXXX, XXX, XXX−XXX

6. SUMMARY AND OUTLOOK

Nonadiabatic effects are ubiquitous in photophysics and photochemistry, and there have been many theoretical developments to properly describe these effects. CoIns are central in nonadiabatic processes, as they promote efficient and ultrafast nonadiabatic transitions between electronic PES. A proper theoretical description requires developments in nonadiabatic dynamics, as well as in the description of the electronic structure of the ground and excited electronic states, the CoIns between them, and nonadiabatic coupling terms. In this review we focused on the electronic structure developments, which have been numerous in the last years. Both multireference and single reference methods have advanced in their description of CoIns, and there have been many new implementations of NACs. Several methods, however, do not describe properly CoIns, and particularly their topology, so one has to be very careful in choosing the appropriate method. Multireference methods have traditionally been the methods of choice for CoIns and nonadiabatic dynamics; nevertheless, even within this group of methods, there are some problematic ones. On the other hand, single reference methods are more problematic by design, especially for CoIns between the ground and excited states, but there has been enormous progress recently and many corrections and extensions have been developed. The current developments and interest in the field make us optimistic that progress will continue, and we will be able to study nonadiabatic processes quite accurately in the future, despite the many challenges involved.

ASSOCIATED CONTENT

Special Issue Paper

This paper is an additional review for *Chem. Rev.* **2018**, volume *118*, issue 15, "Theoretical Modeling of Excited State Processes".

AUTHOR INFORMATION

Corresponding Author

Spiridoula Matsika − *Department of Chemistry, Temple University, Philadelphia, Pennsylvania 19122, United States;* orcid.org/0000-0003-2773-3979; Email: smatsika@temple.edu

Complete contact information is available at: https://pubs.acs.org/10.1021/acs.chemrev.1c00074

Notes

The author declares no competing financial interest.

Biography

Spiridoula Matsika received a B.Sc. in Chemistry from the National and Kapodistrian University of Athens, Greece, in 1994, and a Ph.D. in Chemical Physics from The Ohio State University in 2000. After completing her Ph.D. she spent three years as a postdoctoral fellow at Johns Hopkins University. She joined Temple University in Philadelphia in 2003 where she is currently a Professor of Chemistry. Her research focuses on the theoretical description of excited states, nonadiabatic events, and conical intersections in molecular systems.

ACKNOWLEDGMENTS

Support from the National Science Foundation under grant CHE-1800171 is gratefully acknowledged. I wish to thank David Yarkony for useful discussions, and Todd Martinez, Donald Truhlar, and Joe Subotnik for providing feedback on the manuscript.

ABBREVIATIONS

2-RDM = two-electron reduced density matrix
ACSE = anti-Hermitian contracted Schrödinger equation
ADC = algebraic-diagrammatic-construction method
AO = atomic orbital
B3LYP = hybrid functional, Becke's 3 paramater exchange, and LYP correlation functional
BH&HLYP = Becke-half and-half-LYP functional
BLA = bond length alternation
BO = Born−Oppenheimer
BP = branching plane
CAS = complete active space
CASCI = complete active space configuration interaction
CASPT2 = complete active space second-order perturbation theory
CASSCF = complete active space self-consistent field
CC2 = approximate coupled-cluster method of second order
CCSD = coupled cluster singles and doubles
CDFT-CI = configuration interaction based on constrained density functional theory
CI = configuration interaction
CIC-TDA = configuration interaction-corrected Tamm−Dancoff approximation
CIS-1D = CIS with one doubly excited configuration added
CIS(2) = a doubles correction to CIS based on quasidegenerate perturbation theory that includes coupling with the ground state
CIS(D) = size-consistent doubles correction to CIS
CIS(D_n) = doubles correction to CIS based on quasi-degenerate perturbation theory
CISNO = configuration interaction singles natural orbitals
CoIn = conical intersection
CP-MCSCF = coupled perturbed MCSCF
CSF = configuration state function
DF-TDA = dual-functional Tamm−Dancoff approximation
DMRG = density matrix renormalization group
DOCC = doubly occupied orbitals
EOM-CCSD = equation of motion coupled cluster with single and double excitations
EOM-EA = equation of motion for electron attachment
EOM-EE = equation of motion for excitation energies
EOM-IP = equation of motion for ionization potential
FCI = full configuration interaction
FOMO = floating occupation molecular orbitals
FORS = full optimized reaction space
GPU = graphical processing unit
GUGA = graphical unitary group approach
GVVPT = generalized Van Vleck perturbation theory
hh-TDA = hole hole Tamm−Dancoff approximation
HMNO = high multiplicity natural orbitals
IPEA = empirical shift parameter used in multiconfigurational perturbation theory
LSDA = local spin density approximation
LR-TDDFT = linear response TDDFT
MCQDPT2 = multiconfiguration quasi-degenerate second-order perturbation theory
MCSCF = multiconfigurational self-consistent field
MC-PDFT = multiconfiguration pair-density functional theory
MECI = minimum energy conical intersection

MP2 = Møller−Plesset second-order perturbation theory
MRCI = multireference configuration interaction
MRCI+Q = MRCI with Davidson correction
MRCISD = multireference configuration interaction with single and double excitations
MRPT = multireference perturbation theory
MRSF-TDDFT = mixed-reference spin-flip time-dependent density functional theory
MS-CASPT2 = multistate CASPT2
NAC = nonadiabatic coupling
NEVPT2 = N-electron valence state perturbation theory
OO-CIS = orbital optimized CIS
OMx = orthogonalization models (semiempirical methods)
ORMAS = occupation-restricted-multiple-active-space
PBE1PBE = hybrid functional using the Perdew, Burke, and Ernzerhof functional
PES = potential energy surface
pp-RPA = particle−particle random phase approximation
pp-TDA = particle−particle Tamm−Dancoff approximation
PSB3 = penta-2,4-dieniminium cation
PWA = pseudo-wave-function approach
QD-NEVPT2 = quasidegenerate n-electron valence state perturbation theory
QD-PC-NEVPT2 = quasidegenerate partially contracted NEVPT2
QD-SC-NEVPT2 = quasidegenerate strongly contracted NEVPT2
QM/MM = combined quantum mechanics and classical mechanics
RASPT2 = restricted active space perturbation theory
RASSCF = restricted active space self-consistent field
RAS-SF = restricted active space spin-flip
REKS = spin-restricted ensemble referenced Kohn−Sham
RI-CC2 = resolution of the identity approximation CC2
ROKS = spin-restricted open-shell Kohn−Sham
SA-REKS = state-averaged spin-restricted ensemble referenced Kohn−Sham
SA-SFCIS = spin-adapted SF-CIS
SA-SF-DFT = spin-adapted SF-DFT
SCCSD = similarity constrained CCSD
SCF = self-consistent field
SCS = spin component-scaled
SC-SF-CIS = spin-complete SF-CIS
SF = spin-flip
SFPCIS = spin-flip projected CIS
SF-ORMAS = spin-flip ORMAS
SF-XCIS = spin-flip extended configuration interaction singles
SI-SA-REKS = state-interaction state-averaged spin-restricted ensemble referenced Kohn−Sham
SS-NEB = seam space nudged elastic band
SS-NEVPT2 = state specific NEVPT2
SORCI = spectroscopy oriented configuration interaction
SOS = spin-opposite-scaled
TDA = Tamm−Dancoff approximation
TDDFT = time-dependent density functional theory
TDDFT-1D = time-dependent density functional theory with one double excited configuration
TDHF = time-dependent Hartree−Fock
VOA-CIS = variationally orbital-adapted configuration interaction singles
XMS-CASPT2 = extended multistate complete active space second-order perturbation theory
XMCQDPT2 = extended multiconfiguration quasi-degenerate second-order perturbation theory
XDW-CASPT2 = dynamic weighting XMS-CASPT2

SOFTWARE

Bagel
Columbus
Firefly QC
Gamess
Gaussian
Molcas
Molpro
openMolcas
QChem
TeraChem

REFERENCES

(1) Born, M.; Oppenheimer, R. Zur Quantentheorie der Molekeln. *Ann. Phys.* **1927**, *84*, 457−484.
(2) Yarkony, D. R. Conical Intersections: Diabolical and Often Misunderstood. *Acc. Chem. Res.* **1998**, *31*, 511−518.
(3) Yarkony, D. R. Diabolical Conical Intersections. *Rev. Mod. Phys.* **1996**, *68*, 985−1013.
(4) Yarkony, D. R. Current Issues in Nonadiabatic Chemistry. *J. Phys. Chem.* **1996**, *100*, 18612−18628.
(5) Yarkony, D. R. Conical Intersections: The New Conventional Wisdom. *J. Phys. Chem. A* **2001**, *105*, 6277−6293.
(6) Bernardi, F.; Olivucci, M.; Robb, M. A. Predicting Forbidden and Allowed Cycloaddition Reactions: Potential Surface Topology and its Rationalization. *Acc. Chem. Res.* **1990**, *23*, 405−412.
(7) Bernardi, F.; Olivucci, M.; Robb, M. A. Potential Energy Surface Crossings in Organic Photochemistry. *Chem. Soc. Rev.* **1996**, *25*, 321−328.
(8) Robb, M. A.; Garavelli, M.; Olivucci, M.; Bernardi, F. In *Reviews in Computational Chemistry*; Lipkowitz, K. B., Boyd, D. B., Eds.; Wiley-VCH: New York, 2000; Vol. *15*, pp 87−146.
(9) Barckholtz, T. A.; Miller, T. A. Quantitative Insights about Molecules Exhibiting Jahn-Teller and Related Effects. *Int. Rev. Phys. Chem.* **1998**, *17*, 435−524.
(10) Jasper, A. W.; Zhu, C.; Nangia, S.; Truhlar, D. G. Introductory Lecture: Nonadiabatic Effects in Chemical Dynamics. *Faraday Discuss.* **2004**, *127*, 1−22.
(11) Matsika, S. In *Reviews in Computational Chemistry*; Lipkowitz, K. B., Cundari, T. R., Eds.; Wiley-VCH: NJ, 2007; Vol. *23*, pp 83−124.
(12) Worth, G. A.; Cederbaum, L. S. Beyond Born-Oppenheimer: Molecular Dynamics Through a Conical Intersection. *Annu. Rev. Phys. Chem.* **2004**, *55*, 127−158.
(13) Levine, B. G.; Martínez, T. J. Isomerization Through Conical Intersections. *Annu. Rev. Phys. Chem.* **2007**, *58*, 613−634.
(14) Matsika, S.; Krause, P. Nonadiabatic Events and Conical Intersections. *Annu. Rev. Phys. Chem.* **2011**, *62*, 621−643.
(15) Domcke, W.; Yarkony, D. R. Role of Conical Intersections in Molecular Spectroscopy and Photoinduced Chemical Dynamics. *Annu. Rev. Phys. Chem.* **2012**, *63*, 325−352.
(16) Yarkony, D. R. Nonadiabatic Quantum Chemistry - Past, Present, and Future. *Chem. Rev.* **2012**, *112*, 481−498.
(17) Domcke, W.; Yarkony, D. R.; Köppel, H. *Conical Intersections*; World Scientific: Singapore, 2004.
(18) Domcke, W.; Yarkony, D. R.; Köppel, H. *Conical Intersections: Theory, Computation and Experiment*; World Scientific: Singapore, 2011.
(19) Malhado, J. P.; Bearpark, M. J.; Hynes, J. T. Non-adiabatic Dynamics Close to Conical Intersections and the Surface Hopping Perspective. *Front. Chem.* **2014**, *2*, 97.
(20) Curchod, B. F. E.; Martínez, T. J. Ab Initio Nonadiabatic Quantum Molecular Dynamics. *Chem. Rev.* **2018**, *118*, 3305−3336.

https://doi.org/10.1021/acs.chemrev.1c00074
Chem. Rev. XXXX, XXX, XXX−XXX

(21) Crespo-Otero, R.; Barbatti, M. Recent Advances and Perspectives on Nonadiabatic Mixed Quantum-Classical Dynamics. *Chem. Rev.* **2018**, *118*, 7026−7068.
(22) Nelson, T. R.; White, A. J.; Bjorgaard, J. A.; Sifain, A. E.; Zhang, Y.; Nebgen, B.; Fernandez-Alberti, S.; Mozyrsky, D.; Roitberg, A. E.; Tretiak, S. Non-adiabatic Excited-State Molecular Dynamics: Theory and Applications for Modeling Photophysics in Extended Molecular Materials. *Chem. Rev.* **2020**, *120*, 2215−2287.
(23) Meek, G. A.; Levine, B. G. Wave Function Continuity and the Diagonal Born-Oppenheimer Correction at Conical Intersections. *J. Chem. Phys.* **2016**, *144*, 184109.
(24) Meek, G. A.; Levine, B. G. The Best of Both Reps-Diabatized Gaussians on Adiabatic Surfaces. *J. Chem. Phys.* **2016**, *145*, 184103.
(25) Lichten, W. Resonant Charge Exchange in Atomic Collisions. *Phys. Rev.* **1963**, *131*, 229−238.
(26) O'Malley, T. F. In *Advances in Atomic and Molecular Physics*; Bates, D., Esterman, I., Eds.; Academic Press: New York, 1971; Vol. *7*, pp 223−249.
(27) Smith, F. T. Diabatic and Adiabatic Representations for Atomic Collision Problems. *Phys. Rev.* **1969**, *179*, 111−123.
(28) Pacher, T.; Cederbaum, L. S.; Köppel, H. Adiabatic and Quasidiabatic States in a Gauge Theoretical Framework. *Adv. Chem. Phys.* **2007**, *84*, 293−391.
(29) Köppel, H. In *Conical Intersections*; Domcke, W., Yarkony, D. R., Köppel, H., Eds.; World Scientific: Singapore, 2004; pp 175−204.
(30) Truhlar, D. G.; Mead, C. A. Conditions for the Definition of a Strictly Diabatic Electronic Basis for Molecular Systems. *J. Chem. Phys.* **1982**, *77*, 6090−6098.
(31) von Neumann, J.; Wigner, E. P. On the Behaviour of Eigenvalues in Adiabatic Processes. *Phys. Z.* **1929**, *30*, 467.
(32) Teller, E. The Crossing of Potential Surfaces. *J. Phys. Chem.* **1937**, *41*, 109−116.
(33) Mead, C. A.; Truhlar, D. G. Relative Likelihood of Encountering Conical Intersections and Avoided Intersections on the Potential Energy Surfaces of Polyatomic Molecules. *Phys. Rev. A: At., Mol., Opt. Phys.* **2003**, *68*, 1−2.
(34) Atchity, G. J.; Xantheas, S. S.; Ruedenberg, K. Potential Energy Surfaces Near Intersections. *J. Chem. Phys.* **1991**, *95*, 1862−1876.
(35) Matsika, S.; Yarkony, D. R. Beyond Two-State Conical Intersections. Three-State Conical Intersections in Low Symmetry Molecules: The Allyl Radical. *J. Am. Chem. Soc.* **2003**, *125*, 10672−10676.
(36) Matsika, S.; Yarkony, D. R. Accidental Conical Intersections of Three States of the Same Symmetry. I. Location and Relevance. *J. Chem. Phys.* **2002**, *117*, 6907−6910.
(37) Matsika, S. In *Conical Intersections: Theory, Computation and Experiment*; Domcke, W., Yarkony, D. R., Köppel, H., Eds.; World Scientific, 2011; Vol. *17*, pp 83−116.
(38) Matsika, S.; Yarkony, D. R. Conical Intersections of Three Electronic States Affect the Ground State of Radical Species with Little Or No Symmetry: Pyrazolyl. *J. Am. Chem. Soc.* **2003**, *125*, 12428−12429.
(39) Matsika, S. Three-State Conical Intersections in Nucleic Acid Bases. *J. Phys. Chem. A* **2005**, *109*, 7538−7545.
(40) Matsika, S. Two and Three-State Conical Intersections in Uracil Cation Radical. *Chem. Phys.* **2008**, *349*, 356−362.
(41) Kistler, K. A.; Matsika, S. Three-State Conical Intersections in Cytosine and Pyrimidinone Bases. *J. Chem. Phys.* **2008**, *128*, 215102.
(42) Coe, J. D.; Martínez, T. J. Competitive Decay at Two- and Three-State Conical Intersections in Excited-State Intramolecular Proton Transfer. *J. Am. Chem. Soc.* **2005**, *127*, 4560−4561.
(43) Coe, J. D.; Martínez, T. J. Ab Initio Molecular Dynamics of Excited-State Intramolecular Proton Transfer Around a Three-State Conical Intersection in Malonaldehyde. *J. Phys. Chem. A* **2006**, *110*, 618−630.
(44) Coe, J. D.; Ong, M. T.; Levine, B. G.; Martínez, T. J. On the Extend and Connectivity of Conical Intersection Seams and the Effects of Three-State Intersections. *J. Phys. Chem. A* **2008**, *112*, 12559−12567.
(45) Ichino, T.; Gianola, A. J.; Lineberger, W. C.; Stanton, J. F. Nonadiabatic Effects in the Photoelectron Spectrum of the Pyrazolide-d(3) Anion: Three-State Interactions in the Pyrazolyl-d(3) Radical. *J. Chem. Phys.* **2006**, *125*, 084312.
(46) Blancafort, L.; Robb, M. A. Key Role of a Threefold State Crossing in the Ultrafast Decay of Electronically Excited Cytosine. *J. Phys. Chem. A* **2004**, *108*, 10609−10614.
(47) Gámez, J. A.; Serrano-Andrés, L.; Yáñez, M. Two- and Three-State Conical Intersections in the Electron Capture Dissociation of Disulfides: The Importance of Multireference Calculations. *Int. J. Quantum Chem.* **2011**, *111*, 3316−3323.
(48) González-Vázquez, J.; González, L. A Time-Dependent Picture of the Ultrafast Deactivation of keto-Cytosine Including Three-State Conical Intersections. *ChemPhysChem* **2010**, *11*, 3617−3624.
(49) Longuet-Higgins, H. C.; Opik, U.; Pryce, M. H. L.; Sack, R. A. Studies of the Jahn-Teller Effect. II. The Dynamical Problem. *Proc. R. Soc. London Ser. A* **1958**, *244*, 1−16.
(50) Herzberg, G.; Longuet-Higgins, H. C. Intersection of Potential Energy Surfaces in Polyatomic Molecules. *Discuss. Faraday Soc.* **1963**, *35*, 77−82.
(51) Mead, C. A.; Truhlar, D. G. On the Determination of Born-Oppenheimer Nuclear Motion Wave Functions Including Complications Due to Conical Intersection and Identical Nuclei. *J. Chem. Phys.* **1979**, *70*, 2284−2296.
(52) Berry, M. V. Quantal Phase Factors Accompanying Adiabatic Changes. *Proc. R. Soc. London Ser. A* **1984**, *392*, 45−57.
(53) Mead, C. A. Superposition of Reactive and Nonreactive Scattering-Amplitudes in the Presence of a Conical Intersection. *J. Chem. Phys.* **1980**, *72*, 3839−3840.
(54) Kuppermann, A. In *Dynamics of Molecules and Chemical Reactions*; Wyatt, R. E., Zhang, J. Z., Eds.; Marcel Dekker: New York, 1996; pp 411−472.
(55) Kendrick, B. K. Geometric Phase Effects in Chemical Reaction Dynamics and Molecular Spectra. *J. Phys. Chem. A* **2003**, *107*, 6739−6756.
(56) Xie, C.; Malbon, C. L.; Yarkony, D. R.; Xie, D.; Guo, H. Signatures of a Conical Intersection in Adiabatic Dissociation on the Ground Electronic State. *J. Am. Chem. Soc.* **2018**, *140*, 1986−1989.
(57) Yarkony, D. R. In *Conical Intersections*; Domcke, W., Yarkony, D. R., Köppel, H., Eds.; World Scientific: Singapore, 2004; pp 41−128.
(58) Köppel, H.; Domcke, W.; Cederbaum, L. S. Multimode Molecular Dynamics Beyond the Born-Oppenheimer Approximation. *Adv. Chem. Phys.* **1984**, *57*, 59−246.
(59) Domcke, W.; Stock, G. Theory of Ultrafast Nonadiabatic Excited-State Processes and their Spectroscopic Detection in Real Time. *Adv. Chem. Phys.* **2007**, *100*, 1−170.
(60) Yarkony, D. R. Nuclear Dynamics Near Conical Intersections in the Adiabatic Representation. I. The Effects of Local Topography on Interstate Transition. *J. Chem. Phys.* **2001**, *114*, 2601−2613.
(61) Ben-Nun, M.; Molnar, F.; Schulten, K.; Martínez, T. J. The Role of Intersection Topography in Bond Selectivity of Cis-trans Photoisomerization. *Proc. Natl. Acad. Sci. U. S. A.* **2002**, *99*, 1769−1773.
(62) Migani, A.; Sinicropi, A.; Ferre, N.; Cembran, A.; Garavelli, M.; Olivucci, M. Structure of the Intersection Space Associated with Z/E Photoisomerization of Retinal in Rhodopsin Proteins. *Faraday Discuss.* **2004**, *127*, 179−191.
(63) Dempsey, L. P.; Sechler, T. D.; Murray, C.; Lester, M. I.; Matsika, S. State-Resolved Distribution of OH X $^2\Pi$ Products Arising from Electronic Quenching of OH A $^2\Sigma^+$ by N_2. *J. Chem. Phys.* **2009**, *130*, 104307.
(64) Asturiol, D.; Lasorne, B.; Worth, G. A.; Robb, M. A.; Blancafort, L. Exploring the Sloped-to-Peaked S2/S1 Seam of Intersection of Thymine with Electronic Structure and Direct Quantum Dynamics Calculations. *Phys. Chem. Chem. Phys.* **2010**, *12*, 4949−4958.
(65) Virshup, A. M.; Chen, J.; Martínez, T. J. Nonlinear Dimensionality Reduction for Nonadiabatic Dynamics: The Influence of Conical Intersection Topography on Population Transfer Rates. *J. Chem. Phys.* **2012**, *137*, 22A519.

https://doi.org/10.1021/acs.chemrev.1c00074
Chem. Rev. XXXX, XXX, XXX−XXX

(66) Malhado, J. P.; Hynes, J. T. Non-Adiabatic Transition Probability Dependence on Conical Intersection Topography. *J. Chem. Phys.* **2016**, *145*, 194104.
(67) Farfan, C. A.; Turner, D. B. A Systematic Model Study Quantifying How Conical Intersection Topography Modulates Photochemical Reactions. *Phys. Chem. Chem. Phys.* **2020**, *22*, 20265−20283.
(68) Paterson, M. J.; Bearpark, M. J.; Robb, M. A.; Blancafort, L. J. The Curvature of the Conical Intersection Seam: An Approximate Second-Order Analysis. *J. Chem. Phys.* **2004**, *121*, 11562.
(69) Paterson, M. J.; Bearpark, M. J.; Robb, M. A.; Blancafort, L. J.; Worth, G. A. Conical Intersections: A Perspective on the Computation of Spectroscopic Jahn-Teller Parameters and the Degenerate Intersection Space. *Phys. Chem. Chem. Phys.* **2005**, *7*, 2100−2115.
(70) Sicilia, F.; Blancafort, L.; Bearpark, M. J.; Robb, M. A. Quadratic Description of Conical Intersections: Characterization of Critical Points on the Extended Seam. *J. Phys. Chem. A* **2007**, *111*, 2182−2192.
(71) Yarkony, D. R. Escape from the Double Cone: Optimized Descriptions of the Seam Space using Gateway Modes. *J. Chem. Phys.* **2005**, *123*, 134106.
(72) Yarkony, D. R. On the Connectivity of Seams of Conical Intersections: Seam Curvature. *J. Chem. Phys.* **2005**, *123*, 204101.
(73) Yarkony, D. R. On the Adiabatic to Diabatic States Transformation Near Intersections of Conical Intersections. *J. Chem. Phys.* **2000**, *112*, 2111−2120.
(74) Koga, N.; Morokuma, K. Determination of the Lowest Energy Point on the Crossing Seam Between Two Potential Surfaces Using the Energy Gradient. *Chem. Phys. Lett.* **1985**, *119*, 371−374.
(75) Farazdel, A.; Dupuis, M. On the Determination of the Minimum on the Crossing Seam of Two Potential Energy Surfaces. *J. Comput. Chem.* **1991**, *12*, 276−282.
(76) Yarkony, D. R. On the Characterization of Regions of Avoided Surface Crossings Using an Analytic Gradient Based Method. *J. Chem. Phys.* **1990**, *92*, 2457−2463.
(77) Manaa, M. R.; Yarkony, D. R. On the Intersection of Two Potential Energy Surfaces of the Same Symmetry. Systematic Characterization Using a Lagrange Multiplier Constrained Procedure. *J. Chem. Phys.* **1993**, *99*, 5251−5256.
(78) Anglada, J. M.; Bofill, J. M. A Reduced-Restricted-Quasi-Newton-Raphson Method for Locating and Optimizing Energy Crossing Points between Two Potential Energy Surfaces. *J. Comput. Chem.* **1997**, *18*, 992−1003.
(79) Ragazos, I. N.; Robb, M. A.; Bernardi, F.; Olivucci, M. Optimization and Characterization of the Lowest Energy Point on a Conical Intersection Using an MC-SCF Lagrangian. *Chem. Phys. Lett.* **1992**, *119*, 217−223.
(80) Bearpark, M. J.; Robb, M. A.; Schlegel, H. B. A Direct Method for the Location of the Lowest Energy Point on a Potential Surface Crossing. *Chem. Phys. Lett.* **1994**, *223*, 269−274.
(81) Zilberg, S.; Hass, Y. Molecular Photochemistry: A General Method for Localizing Conical Intersections Using the Phase-Change Rule. *Chem. - Eur. J.* **1999**, *5*, 1755−1765.
(82) Ciminelli, C.; Granucci, G.; Persico, M. The Photoisomerization Mechanism of Azobenzene: A Semiclassical Simulation of Nonadiabatic Dynamics. *Chem. - Eur. J.* **2004**, *10*, 2327−2341.
(83) De Vico, L.; Olivucci, M.; Lindh, R. New General Tools for Constrained Geometry Optimizations. *J. Chem. Theory Comput.* **2005**, *1*, 1029−1037.
(84) Levine, B. G.; Coe, J. D.; Martínez, T. J. Optimizing Conical Intersections without Derivative Coupling Vectors: Application to Multistate Multireference Second-Order Perturbation Theory (MS-CASPT2). *J. Phys. Chem. B* **2008**, *112*, 405−413.
(85) Chachiyo, T.; Rodriguez, J. H. A Direct Method for Locating Minimum-Energy Crossing Points (MECPs) in Spin-Forbidden Transitions and Nonadiabatic Reactions. *J. Chem. Phys.* **2005**, *123*, 094711.
(86) Sicilia, F.; Blancafort, L.; Bearpark, M. J.; Robb, M. A. New Algorithms for Optimizing and Linking Conical Intersection Points. *J. Chem. Theory Comput.* **2008**, *4*, 257−266.
(87) Ruiz-Barragan, S.; Robb, M. A.; Blancafort, L. Conical Intersection Optimization Based on a Double Newton-Raphson Algorithm Using Composed Steps. *J. Chem. Theory Comput.* **2013**, *9*, 1433−1442.
(88) Harabuchi, Y.; Maeda, S.; Taketsugu, T.; Minezawa, N.; Morokuma, K. Automated Search for Minimum Energy Conical Intersection Geometries between the Lowest Two Singlet States S0/S1-MECIs by the Spin-Flip TDDFT Method. *J. Chem. Theory Comput.* **2013**, *9*, 4116−4123.
(89) Maeda, S.; Taketsugu, T.; Morokuma, K. Exploring Pathways of Photoaddition Reactions by Artificial Force Induced Reaction Method: A Case Study on the Paternó-Büchi Reaction. *Z. Phys. Chem.* **2013**, *227*, 1421−1433.
(90) Maeda, S.; Harahuchi, Y.; Taketsugu, T.; Morokuma, K. Systematic Exploration of Minimum Energy Conical Intersection Structures near the Franck-Condon Region. *J. Phys. Chem. A* **2014**, *118*, 12050−12058.
(91) Maeda, S.; Taketsugu, T.; Ohno, K.; Morokuma, K. From Roaming Atoms to Hopping Surfaces: Mapping Out Global Reaction Routes in Photochemistry. *J. Am. Chem. Soc.* **2015**, *137*, 3433−3445.
(92) Aldaz, C.; Kammeraad, J. A.; Zimmerman, P. M. Discovery of Conical Intersection Mediated Photochemistry with Growing String Methods. *Phys. Chem. Chem. Phys.* **2018**, *20*, 27394−27405.
(93) Toniolo, A.; Ben-Nun, M.; Martínez, T. J. Optimization of Conical Intersections with Floating Occupation Semiempirical Configuration Interaction Wave Functions. *J. Phys. Chem. A* **2002**, *106*, 4679−4689.
(94) Izzo, R.; Klessinger, M. Optimization of Conical Intersections Using the Semiempirical MNDOC-CI Method with Analytic Gradients. *J. Comput. Chem.* **2000**, *21*, 52−62.
(95) Keal, T. W.; Koslowski, A.; Thiel, W. Comparison of Algorithms for Conical Intersection Optimisation Using Semiempirical Methods. *Theor. Chem. Acc.* **2007**, *118*, 837−844.
(96) Shen, L.; Xie, B.; Li, Z.; Liu, L.; Cui, G.; Fang, W.-H. Role of Multistate Intersections in Photochemistry. *J. Phys. Chem. Lett.* **2020**, *11*, 8490−8501.
(97) Liu, X.-Y.; Cui, G.; Fang, W.-H. Three-State Conical Intersection Optimization Methods: Development and Implementation at QM/MM Level. *Theor. Chem. Acc.* **2017**, *136*, 8.
(98) Zhang, X.; Herbert, J. M. Analytic Derivative Couplings for Spin-Flip Configuration Interaction Singles and Spin Flip Time-Dependent Density Functional Theory. *J. Chem. Phys.* **2014**, *141*, 064104.
(99) Winslow, M.; Cross, W. B.; Robinson, D. Comparison of Spin-Flip TDDFT-Based Conical Intersection Approaches with XMS-CASPT2. *J. Chem. Theory Comput.* **2020**, *16*, 3253−3263.
(100) Garavelli, M.; Celani, P.; Fato, M.; Bearpark, M.; Smith, B.; Olivucci, M.; Robb, M. Relaxation Paths from a Conical Intersection: The Mechanism of Product Formation in the Cyclohexadiene/Hexatriene Photochemical Interconversion. *J. Phys. Chem. A* **1997**, *101*, 2023−2032.
(101) Migani, A.; Olivucci, M. In *Conical Intersections*; Domcke, W., Yarkony, D. R., Köppel, H., Eds.; World Scientific: Singapore, 2004; pp 271−320.
(102) Migani, A.; Robb, M. A.; Olivucci, M. Relationship between Photoisomerization Path and Intersection Space in a Retinal Chromophore Model. *J. Am. Chem. Soc.* **2003**, *125*, 2804−2808.
(103) Matsika, S.; Yarkony, D. R. Conical Intersections and the Nonadiabatic Reactions $H_2O+O(^3P) \leftrightarrow OH(A^2\Sigma^+)+OH(X^2\Pi)$. *J. Chem. Phys.* **2002**, *117*, 3733.
(104) Celani, P.; Robb, M. A.; Garavelli, M.; Bernardi, F.; Olivucci, M. Geometry Optimisation on a Hypersphere. Application to Finding Reaction Paths from a Conical Intersection. *Chem. Phys. Lett.* **1995**, *243*, 1−8.
(105) Frutos, L. M.; Andrunio, T.; Santoro, F.; Ferre, N.; Olivucci, M. Tracking the Excited-State Time Evolution of the Visual Pigment with Multiconfigurational Quantum Chemistry. *Proc. Natl. Acad. Sci. U. S. A.* **2007**, *104*, 7764−7769.
(106) Vreven, T.; Bernardi, F.; Garavelli, M.; Olivucci, M.; Robb, M. A.; Schlegel, H. B. Ab Initio Photoisomerization Dynamics of a Simple

https://doi.org/10.1021/acs.chemrev.1c00074
Chem. Rev. XXXX, XXX, XXX−XXX

Retinal Chromophore Model. *J. Am. Chem. Soc.* **1997**, *119*, 12687−12688.
(107) Mori, T.; Martinez, T. J. Exploring the Conical Intersection Seam: The Seam Space Nudged Elastic Band Method. *J. Chem. Theory Comput.* **2013**, *9*, 1155−1163.
(108) Weingart, O.; Migani, A.; Olivucci, M.; Robb, M. A.; Buss, V.; Hunt, P. Probing the Photochemical Funnel of a Retinal Chromophore Model via Zero-Point Energy Sampling Semiclassical Dynamics. *J. Phys. Chem. A* **2004**, *108*, 4685−4693.
(109) Jahn, H. A.; Teller, E. Stability of Polyatomic Molecules in Degenerate Electronic States. I. Orbital Degeneracy. *Proc. R. Soc. London Ser. A* **1937**, *161*, 220−235.
(110) Bersuker, I. B. *The Jahn-Teller Effect*; Cambridge University Press: Cambridge, UK, 2006.
(111) Applegate, B. E.; Barckholtz, T. A.; Miller, T. A. Exploration of Conical Intersections and Their Ramifications for Chemistry Through the Jahn-Teller Effect. *Chem. Soc. Rev.* **2003**, *32*, 38−49.
(112) Szalay, P. G.; Müller, T.; Gidofalvi, G.; Lischka, H.; Shepard, R. Multiconfiguration Self-Consistent Field and Multireference Configuration Interaction Methods and Applications. *Chem. Rev.* **2012**, *112*, 108−181.
(113) Lischka, H.; Nachtigallova, D.; Aquino, A. J. A.; Szalay, P. G.; Plasser, F.; Machado, F. B. C.; Barbatti, M. Multireference Approaches for Excited States of Molecules. *Chem. Rev.* **2018**, *118*, 7293−7361.
(114) Park, J. W.; Al-Saadon, R.; MacLeod, M. K.; Shiozaki, T.; Vlaisavljevich, B. Multireference Electron Correlation Methods: Journeys along Potential Energy Surfaces. *Chem. Rev.* **2020**, *120*, 5878−5909.
(115) Ghosh, S.; Verma, P.; Cramer, C. J.; Gagliardi, L.; Truhlar, D. G. Combining Wave Function Methods with Density Functional Theory for Excited States. *Chem. Rev.* **2018**, *118*, 7249−7292.
(116) Bao, J. J.; Zhou, C.; Varga, Z.; Kanchanakungwankul, S.; Gagliardi, L.; Truhlar, D. G. Multi-State Pair-Density Functional Theory. *Faraday Discuss.* **2020**, *224*, 348−372.
(117) Bao, J. J.; Zhou, C.; Truhlar, D. G. Compressed-State Multistate Pair-Density Functional Theory. *J. Chem. Theory Comput.* **2020**, *16*, 7444−7452 PMID: 33141587.
(118) Shavitt, I. In *Methods of Electronic Structure Theory*; Schaefer, H. F., III, Ed.; Modern Theoretical Chemistry; Plenum Press: New York, 1977; Vol. 4, pp 189−275.
(119) Shavitt, I. The History and Evolution of Configuration Interaction. *Mol. Phys.* **1998**, *94*, 3−17.
(120) Siegbahn, P. E. M. Direct Configuration Interaction with a Reference State Composed of Many Reference Configurations. *Int. J. Quantum Chem.* **1980**, *18*, 1229−1242.
(121) Werner, H.; Reinsch, E. The Self-Consistent Electron Pairs Method for Multiconfiguration Reference State Functions. *J. Chem. Phys.* **1982**, *76*, 3144−3156.
(122) Werner, H.-J.; Knowles, P. J. An Efficient Internally Contracted Multiconfiguration Reference CI Method. *J. Chem. Phys.* **1988**, *89*, 5803−5814.
(123) Pople, J. A.; Binkley, J. S.; Seeger, R. Theoretical Model Incorporating Electron Correlation. *Int. J. Quantum Chem.* **1976**, *10*, 1−19.
(124) Bartlett, R. J. Many-Body Perturbation Theory and Coupled Cluster Theory for Electron Correlation in Molecules. *Annu. Rev. Phys. Chem.* **1981**, *32*, 359−401.
(125) Langhoff, S. R.; Davidson, E. R. Configuration Interaction Calculations on the Nitrogen Molecule. *Int. J. Quantum Chem.* **1974**, *8*, 61−72.
(126) Amor, N. B.; Maynau, D.; Malrieu, J.-P.; Monari, A. Restoring the Size Consistency of Multireference Configuration Interactions through Class Dressings: Applications to Ground and Excited States. *J. Chem. Phys.* **2008**, *129*, 064112.
(127) Lischka, H.; et al. *COLUMBUS, an Ab Initio Electronic Structure Program*, Release 7.0; 2012.
(128) Lischka, H.; Shepard, R.; Müller, T.; Szalay, P.; Pitzer, R.; Aquino, A.; do Nascimento, M.; Barbatti, M.; Belcher, L.; Blaudeau, J.; et al. The Generality of the GUGA MRCI Approach in COLUMBUS for Treating Complex Quantum Chemistry. *J. Chem. Phys.* **2020**, *152*, 134110.
(129) Shepard, R. Geometrical Energy Derivative Evaluation with MRCI Wave Functions. *Int. J. Quantum Chem.* **1987**, *31*, 33−44.
(130) Shepard, R. In *Modern Electronic Structure Theory Part I*; Yarkony, D. R., Ed.; World Scientific: Singapore, 1995; pp 345−458.
(131) Lischka, H.; Dallos, M.; Shepard, R. Analytic MRCI Gradient for Excited States: Formalism and Application to the $n\pi$ Valence- and n-(3*s* 3*p*) Rydberg States of Formaldehyde. *Mol. Phys.* **2002**, *100*, 1647−1658.
(132) Lischka, H.; Dallos, M.; Szalay, P. G.; Yarkony, D. R.; Shepard, R. Analytic Evaluation of Nonadiabatic Coupling Terms at the MR-CI Level. I. Formalism. *J. Chem. Phys.* **2004**, *120*, 7322−7329.
(133) Dallos, M.; Lischka, H.; Shepard, R.; Yarkony, D. R.; Szalay, P. G. Analytic Evaluation of Nonadiabatic Coupling Terms at the MR-CI Level. II. Minima on the Crossing Seam: Formaldehyde and the Photodimerization of Ethylene. *J. Chem. Phys.* **2004**, *120*, 7330−7339.
(134) Werner, H. J. Matrix-Formulated Direct Multiconfiguration Self-Consistent Field and Multiconfiguration Reference Configuration Interaction Methods. *Adv. Chem. Phys.* **2007**, *69*, 1−62.
(135) Roos, B. O. The Complete Active Space Self Consistent Field Method and its Applications in Electronic Structure Calculations. *Adv. Chem. Phys.* **2007**, *69*, 399−445.
(136) Shepard, R. The Multiconfiguration Self-Consistent Field Method. *Adv. Chem. Phys.* **2007**, *69*, 63−200.
(137) Roos, B. O.; Taylor, P. R. A Complete Active Space SCF Method (CASSCF) using a Density-Matrix Formulated Super-CI Approach. *Chem. Phys.* **1980**, *48*, 157−173.
(138) Ruedenberg, K.; Schmidt, M. W.; Gilbert, M. M.; Elbert, S. T. Are Atoms Intrinsic to Molecular Electronic Wavefunctions? I. The FORS Model. *Chem. Phys.* **1982**, *71*, 41−49.
(139) Malmqvist, P. Å.; Rendell, A.; Roos, B. O. The Restricted Active Space Self-Consistent-Field Method, Implemented with a Split Graph Unitary Group Approach. *J. Phys. Chem.* **1990**, *95*, 5477−5482.
(140) Hohenstein, E. G.; Luehr, N.; Ufimtsev, I. S.; Martínez, T. J. An Atomic Orbital-Based Formulation of the Complete Active Space Self-Consistent Field Method on Graphical Processing Units. *J. Chem. Phys.* **2015**, *142*, 224103.
(141) Snyder, J. W., Jr.; Hohenstein, E. G.; Luehr, N.; Martinez, T. J. An Atomic Orbital-Based Formulation of Analytical Gradients and Nonadiabatic Coupling Vector Elements for the State-Averaged Complete Active Space Self-Consistent Field Method on Graphical Processing Units. *J. Chem. Phys.* **2015**, *143*, 154107.
(142) Hohenstein, E. G.; Bouduban, M. E. F.; Song, C.; Luehr, N.; Ufimtsev, I. S.; Martínez, T. J. Analytic First Derivatives of Floating Occupation Molecular Orbital-Complete Active Space Configuration Interaction on Graphical Processing Units. *J. Chem. Phys.* **2015**, *143*, 014111.
(143) Ivanic, J. Direct Configuration Interaction and Multiconfigurational Self-Consistent-Field Method for Multiple Active Spaces with Variable Occupations. I. Method. *J. Chem. Phys.* **2003**, *119*, 9364−9376.
(144) West, A. C.; Windus, T. L. Can ORMAS Be Used for Nonadiabatic Coupling Calculations? $SiCH_4$ and Butadiene Contours. *Theor. Chem. Acc.* **2012**, *131*, 1251.
(145) Mato, J.; Gordon, M. S. A General Spin-Complete Spin-Flip Configuration Interaction Method. *Phys. Chem. Chem. Phys.* **2018**, *20*, 2615−2626.
(146) Mato, J.; Gordon, M. S. Analytic Gradients for the Spin-Flip ORMAS-CI Method: Optimizing Minima, Saddle Points, and Conical Intersections. *J. Phys. Chem. A* **2019**, *123*, 1260−1272.
(147) Potts, D. M.; Taylor, C. M.; Chaudhuri, R. K.; Freed, K. F. The Improved Virtual Orbital-Complete Active Space Configuration Interaction Method, a "Packageable" Efficient Ab Initio Many-Body Method for Describing Electronically Excited States. *J. Chem. Phys.* **2001**, *114*, 2592−2600.
(148) Abrams, M. L.; Sherrill, C. D. Natural Orbitals as Substituents for Optimized Orbitals in Complete Active Space Wavefunctions. *Chem. Phys. Lett.* **2004**, *395*, 227−232.

https://doi.org/10.1021/acs.chemrev.1c00074
Chem. Rev. XXXX, XXX, XXX−XXX

(149) Lu, Z.; Matsika, S. High-Multiplicity Natural Orbitals in Multireference Configuration Interaction for Excited States. *J. Chem. Theory Comput.* **2012**, *8*, 509−517.
(150) Shu, Y.; Levine, B. G. Reducing the Propensity for Unphysical Wavefunction Symmetry Breaking in Multireference Calculations of the Excited States of Semiconductor Clusters. *J. Chem. Phys.* **2013**, *139*, 074102.
(151) Fales, B. S.; Shu, Y.; Levine, B. G.; Hohenstein, E. G. Configuration Interaction Singles Natural Orbitals: An Orbital Basis for an Efficient and Size Intensive Multireference Description of Electronic Excited States. *J. Chem. Phys.* **2015**, *142*, 024102.
(152) Slavicek, P.; Martínez, T. J. Ab Initio Floating Occupation Molecular Orbital-Complete Active Space Configuration Interaction: An Efficient Approximation to CASSCF. *J. Chem. Phys.* **2010**, *132*, 234102.
(153) Casanova, D.; Head-Gordon, M. Restricted Active Space Spin-Flip Configuration Interaction Approach: Theory, Implementation and Examples. *Phys. Chem. Chem. Phys.* **2009**, *11*, 9779−9790.
(154) Fales, B. S.; Shu, Y.; Levine, B. G.; Hohenstein, E. G. Complete Active Space Configuration Interaction from State-Averaged Configuration Interaction Singles Natural Orbitals: Analytic First Derivatives and Derivative Coupling Vectors. *J. Chem. Phys.* **2017**, *147*, 094104.
(155) Lu, Z.; Matsika, S. High-Multiplicity Natural Orbitals in Multireference Configuration Interaction for Excited State Potential Energy Surfaces. *J. Phys. Chem. A* **2013**, *117*, 7421−7430.
(156) Chien, A. D.; Zimmerman, P. M. Recovering Dynamic Correlation in Spin Flip Configuration Interaction through a Difference Dedicated Approach. *J. Chem. Phys.* **2017**, *146*, 014103.
(157) Granucci, G.; Toniolo, A. Molecular Gradients for Semiempirical CI Wavefunctions with Floating Occupation Molecular Orbitals. *Chem. Phys. Lett.* **2000**, *325*, 79−85.
(158) Hohenstein, E. G. Analytic Formulation of Derivative Coupling Vectors for Complete Active Space Configuration Interaction Wavefunctions with Floating Occupation Molecular Orbitals. *J. Chem. Phys.* **2016**, *145*, 174110.
(159) Hollas, D.; Sistik, L.; Hohenstein, E. G.; Martinez, T. J.; Slavicek, P. Nonadiabatic Ab Initio Molecular Dynamics with the Floating Occupation Molecular Orbital-Complete Active Space Configuration Interaction Method. *J. Chem. Theory Comput.* **2018**, *14*, 339−350.
(160) Levine, B. G.; Durden, A. S.; Esch, M. P.; Liang, F.; Shu, Y. CAS Without SCF—Why to Use CASCI and Where to Get the Orbitals. *J. Chem. Phys.* **2021**, *154*, 090902.
(161) Mazziotti, D. A. Anti-Hermitian Contracted Schrödinger Equation: Direct Determination of the Two-Electron Reduced Density Matrices of Many-Electron Molecules. *Phys. Rev. Lett.* **2006**, *97*, 143002.
(162) Snyder, J. W., Jr.; Rothman, A. E.; IV, J. J. F.; Mazziotti, D. A. Conical Intersections in Triplet Excited States of Methylene from the Anti-Hermitian Contracted Schrödinger Equation. *J. Chem. Phys.* **2010**, *132*, 154109.
(163) Snyder, J. W.; Mazziotti, D. A. Conical Intersection of the Ground and First Excited States of Water: Energies and Reduced Density Matrices from the Anti-Hermitian Contracted Schrödinger Equation. *J. Phys. Chem. A* **2011**, *115*, 14120−14126.
(164) Snyder, J. W., Jr.; Mazziotti, D. A. Photoexcited Tautomerization of Vinyl Alcohol to Acetylaldehydevia a Conical Intersection from Contracted Schrödinger Theory. *Phys. Chem. Chem. Phys.* **2012**, *14*, 1660−1667.
(165) Chan, G. K.-L.; Sharma, S. The Density Matrix Renormalization Group in Quantum Chemistry. *Annu. Rev. Phys. Chem.* **2011**, *62*, 465−481.
(166) Yanai, T.; Kurashige, Y.; Mizukami, W.; Chalupsky, J.; Lan, T. N.; Saitow, M. Density Matrix Renormalization Group for ab initio Calculations and Associated Dynamic Correlation Methods: A Review of Theory and Applications. *Int. J. Quantum Chem.* **2015**, *115*, 283−299.
(167) Kurashige, Y.; Yanai, T. Second-Order Perturbation Theory with a Density Matrix Renormalization Group Self-Consistent Field Reference Function: Theory and Application to the Study of Chromium Dimer. *J. Chem. Phys.* **2011**, *135*, 094104.
(168) Kurashige, Y. Multireference Electron Correlation Methods with Density Matrix Renormalisation Group Reference Functions. *Mol. Phys.* **2014**, *112*, 1485−1494.
(169) Saitow, M.; Kurashige, Y.; Yanai, T. Multireference Configuration Interaction Theory using Cumulant Reconstruction with Internal Contraction of Density Matrix Renormalization Group Wave Function. *J. Chem. Phys.* **2013**, *139*, 044118.
(170) Liu, F.; Kurashige, Y.; Yanai, T.; Morokuma, K. Multireference Ab Initio Density Matrix Renormalization Group (DMRG)-CASSCF and DMRG-CASPT2 Study on the Photochromic Ring Opening of Spiropyran. *J. Chem. Theory Comput.* **2013**, *9*, 4462−4469.
(171) Hu, W.; Chan, G. K.-L. Excited-State Geometry Optimization with the Density Matrix Renormalization Group, as Applied to Polyenes. *J. Chem. Theory Comput.* **2015**, *11*, 3000−3009.
(172) Freitag, L.; Ma, Y.; Baiardi, A.; Knecht, S.; Reiher, M. Approximate Analytical Gradients and Nonadiabatic Couplings for the State-Average Density Matrix Renormalization Group Self-Consistent-Field Method. *J. Chem. Theory Comput.* **2019**, *15*, 6724−6737.
(173) Andersson, K.; Malmqvist, P. A.; Roos, B. O.; Sadlej, A. J.; Wolinski, K. Second-Order Perturbation-Theory with a CASSCF Reference Function. *J. Phys. Chem.* **1990**, *94*, 5483−5488.
(174) Anderson, K.; Malmqvist, P. A.; Roos, B. O. Second-Order Perturbation Theory with a Complete Active Space Self-Consistent Field Reference Function. *J. Chem. Phys.* **1992**, *96*, 1218−1226.
(175) Andersson, K.; Barysz, M.; Bernhardsson, A.; et al. *MOLCAS 6.0*; 2004.
(176) Werner, H.-J.; et al. *MOLPRO*, version 2002.6, a Package of Ab Initio programs; 2003; see http://www.molpro.net.
(177) Finley, J.; Malmqvist, P.; Roos, B.; Serrano-Andres, L. The Multi-State CASPT2Method. *Chem. Phys. Lett.* **1998**, *288*, 299−306.
(178) Serrano-Andrès, L.; Merchán, M.; Lindh, R. Computation of Conical Intersections by Using Perturbation Techniques. *J. Chem. Phys.* **2005**, *122*, 104107.
(179) Hirao, K. Multireference Möller-Plesset Method. *Chem. Phys. Lett.* **1992**, *190*, 374−380.
(180) Nakano, H. Quasidegenerate Perturbation Theory with Multiconfigurational Self-Consistent-Field Reference Functions. *J. Chem. Phys.* **1993**, *99*, 7983−7992.
(181) Nakano, H. MCSCF Reference Quasidegenerate Perturbation Theory with Epstein-Nesbet Partitioning. *Chem. Phys. Lett.* **1993**, *207*, 372−378.
(182) Nakano, H.; Hirao, K.; Gordon, M. Analytic Energy Gradients for Multiconfigurational Self-Consistent Field Second-Order Quasidegenerate Perturbation Theory (MC-QDPT). *J. Chem. Phys.* **1998**, *108*, 5660−5669.
(183) Angeli, C.; Cimiraglia, R.; Evangelisti, S.; Leininger, T.; Malrieu, J. Introduction of N-Electron Valence States for Multireference Perturbation Theory. *J. Chem. Phys.* **2001**, *114*, 10252−10264.
(184) Angeli, C.; Cimiraglia, R.; Malrieu, J. P. N-Electron Valence State Perturbation Theory: A Fast Implementation of the Strongly Contracted Variant. *Chem. Phys. Lett.* **2001**, *350*, 297−305.
(185) Angeli, C.; Cimiraglia, R.; Malrieu, J. N-Electron Valence State Perturbation Theory: A Spinless Formulation and an Efficient Implementation of the Strongly Contracted and of the Partially Contracted Variants. *J. Chem. Phys.* **2002**, *117*, 9138−9153.
(186) Angeli, C.; Borini, S.; Cestari, M.; Cimiraglia, R. A Quasidegenerate Formulation of the Second Order N-Electron Valence State Perturbation Theory Approach. *J. Chem. Phys.* **2004**, *121*, 4043−4049.
(187) Schmidt, M. W.; Baldridge, K. K.; Boatz, J. A.; Elbert, S. T.; Gordon, M. S.; Jensen, J. H.; Koseki, S.; Matsunaga, N.; Nguyen, K. A.; Su, S.; et al. , General Atomic and Molecular Electronic Structure System. *J. Comput. Chem.* **1993**, *14*, 1347−1363.
(188) Gordon, M. S.; Schmidt, M. W. In *Theory and Applications of Computational Chemistry: the first forty years*; Dykstra, C.E., Frenking, G., Kim, K.S., Scuseria, G.E., Eds.; Elsevier: Amsterdam, 2005; pp 1167−1189.

https://doi.org/10.1021/acs.chemrev.1c00074
Chem. Rev. XXXX, XXX, XXX−XXX

(189) Malrieu, J.; Heully, J.; Zaitsevskii, A. Multiconfigurational 2nd-Order Perturbative Methods - Overview and Comparison of Basic Properties. *Theor. Chim. Acta* **1995**, *90*, 167−187.
(190) Granovsky, A. A. Extended Multi-Configuration Quasi-Degenerate Perturbation Theory: The New Approach to Multi-Atate Multi-Reference Perturbation Theory. *J. Chem. Phys.* **2011**, *134*, 214113.
(191) Granovsky, A. *Firefly*, version 8 (http://classic.chem.msu.su/gran/firefly/index.html).
(192) Shiozaki, T.; Gyorffy, W.; Celani, P.; Werner, H.-J. Communication: Extended Multi-State Complete Active Space Second-Order Perturbation Theory: Energy and Nuclear Gradients. *J. Chem. Phys.* **2011**, *135*, 174111.
(193) Dyall, K. G. The Choice of a Zeroth-Order Hamiltonian for Second-Order Perturbation Theory with a Complete Active Space Self-Consistent-Field Reference Function. *J. Chem. Phys.* **1995**, *102*, 4909−4918.
(194) Ghigo, G.; Roos, B. O.; Malmqvist, P. A. A Modified Definition of the Zeroth-Order Hamiltonian in Multiconfigurational Perturbation Theory (CASPT2). *Chem. Phys. Lett.* **2004**, *396*, 142−149.
(195) Zobel, J. P.; Nogueira, J. J.; González, L. The IPEA Dilemma in CASPT2. *Chem. Sci.* **2017**, *8*, 1482−1499.
(196) Forsberg, N.; Malmqvist, P. A. Multiconfiguration Perturbation Theory with Imaginary Level Shift. *Chem. Phys. Lett.* **1997**, *274*, 196−204.
(197) Celani, P.; Werner, H. J. Multireference Perturbation Theory for Large Restricted and Selected Active Space Reference Wave Functions. *J. Chem. Phys.* **2000**, *112*, 5546−5557.
(198) Schreiber, M.; Silva-Junior, M. R.; Sauer, S. P. A.; Thiel, W. Benchmarks for Electronically Excited States: CASPT2, CC2, CCSD, and CC3. *J. Chem. Phys.* **2008**, *128*, 134110.
(199) Silva-Junior, M. R.; Schreiber, M.; Sauer, S. P. A.; Thiel, W. Benchmarks of Electronically Excited States: Basis Set Effects on CASPT2 Results. *J. Chem. Phys.* **2010**, *133*, 174318.
(200) Battaglia, S.; Lindh, R. Extended Dynamically Weighted CASPT2: The Best of Two Worlds. *J. Chem. Theory Comput.* **2020**, *16*, 1555−1567.
(201) Battaglia, S.; Lindh, R. On the Role of Symmetry in XDW-CASPT2. *J. Chem. Phys.* **2021**, *154*, 034102.
(202) MacLeod, M. K.; Shiozaki, T. Communication: Automatic Code Generation Enables Nuclear Gradient Computations for Fully Internally Contracted Multireference Theory. *J. Chem. Phys.* **2015**, *142*, 051103.
(203) Park, J. W.; Al-Saadon, R.; Strand, N. E.; Shiozaki, T. Imaginary Shift in CASPT2 Nuclear Gradient and Derivative Coupling Theory. *J. Chem. Theory Comput.* **2019**, *15*, 4088−4098.
(204) Vlaisavljevich, B.; Shiozaki, T. Nuclear Energy Gradients for Internally Contracted Complete Active Space Second-Order Perturbation Theory: Multistate Extensions. *J. Chem. Theory Comput.* **2016**, *12*, 3781−3787.
(205) Park, J. W.; Shiozaki, T. Analytical Derivative Coupling for Multistate CASPT2 Theory. *J. Chem. Theory Comput.* **2017**, *13*, 2561−2570.
(206) Park, J. W.; Shiozaki, T. On-the-Fly CASPT2 Surface-Hopping Dynamics. *J. Chem. Theory Comput.* **2017**, *13*, 3676−3683.
(207) Shiozaki, T. BAGEL: Brilliantly Advanced General Electronic-Structure Library. *Wiley Interdiscip. Rev.: Comput. Mol. Sci.* **2018**, *8*, No. e1331.
(208) Celani, P.; Werner, H.-J. Analytical Energy Gradients for Internally Contracted Second-Order Multireference Perturbation Theory. *J. Chem. Phys.* **2003**, *119*, 5044−5057.
(209) Mori, T.; Kato, S. Dynamic Electron Correlation Effect on Conical Intersections in Photochemical Ring-Opening Reaction of Cyclohexadiene: MS-CASPT2 Study. *Chem. Phys. Lett.* **2009**, *476*, 97−100.
(210) Mori, T.; Nakano, K.; Kato, S. Conical Intersections of Free Energy Surfaces in Solution: Effect of Electron Correlation on a Protonated Schiff Base in Methanol Solution. *J. Chem. Phys.* **2010**, *133*, 064107.
(211) Mori, T.; Glover, W. J.; Schuurman, M. S.; Martínez, T. J. Role of Rydberg States in the Photochemical Dynamics of Ethylene. *J. Phys. Chem. A* **2012**, *116*, 2808−2818 PMID: 22148837..
(212) Nishimoto, Y. Analytic First-Order Derivatives of Partially Contracted N-Electron Valence State Second-Order Perturbation Theory (PC-NEVPT2). *J. Chem. Phys.* **2019**, *151*, 114103.
(213) Park, J. W. Analytical Gradient Theory for Strongly Contracted (SC) and Partially Contracted (PC) N-Electron Valence State Perturbation Theory (NEVPT2). *J. Chem. Theory Comput.* **2019**, *15*, 5417−5425.
(214) Park, J. W. Analytical Gradient Theory for Quasidegenerate N-Electron Valence State Perturbation Theory (QD-NEVPT2). *J. Chem. Theory Comput.* **2020**, *16*, 326−339.
(215) Song, C.; Neaton, J. B.; Martínez, T. J. Reduced Scaling Formulation of CASPT2 Analytical Gradients using the Supporting Subspace Method. *J. Chem. Phys.* **2021**, *154*, 014103.
(216) Matsika, S. Radiationless Decay of Excited States of Uracil Through Conical Intersections. *J. Phys. Chem. A* **2004**, *108*, 7584.
(217) Kistler, K. A.; Matsika, S. Radiationless Decay Mechanism of Cytosine: An Ab Initio Study with Comparisons to the Fluorescent Analogue 5-Methyl-2-pyrimidinone. *J. Phys. Chem. A* **2007**, *111*, 2650−2661.
(218) Barbatti, M.; Aquino, A. J. A.; Szymczak, J. J.; Nachtigallova, D.; Hobza, P.; Lischka, H. Relaxation Mechanisms of UV-Photoexcited DNA and RNA Nucleobases. *Proc. Natl. Acad. Sci. U. S. A.* **2010**, *107*, 21453−21458.
(219) Siddique, F.; Barbatti, M.; Cui, Z.; Lischka, H.; Aquino, A. J. A. Nonadiabatic Dynamics of Charge-Transfer States Using the Anthracene -Tetracyanoethylene Complex as a Prototype. *J. Phys. Chem. A* **2020**, *124*, 3347−3357.
(220) Ismail, N.; Blancafort, L.; Olivucci, M.; Kohler, B.; Robb, M. A. Ultrafast Decay of Electronically Excited Singlet Cytosine via $\pi\pi$ to $n\pi$ State Switch. *J. Am. Chem. Soc.* **2002**, *124*, 6818−6819.
(221) Merchán, M.; Serrano-Andrés, L.; Robb, M.; Blancafort, L. Triplet-State Formation along the Ultrafast Decay of Excited Singlet Cytosine. *J. Am. Chem. Soc.* **2005**, *127*, 1820−1825.
(222) Blancafort, L. Energetics of Cytosine Singlet Excited-State Decay Paths - A Difficult Case for CASSCF and CASPT2. *Photochem. Photobiol.* **2007**, *83*, 603−610.
(223) Nakayama, A.; Harabuchi, Y.; Yamazaki, S.; Taketsugu, T. Photophysics of Cytosine Tautomers: New Insights into the Non-radiative Decay Mechanisms from MS-CASPT2 Potential Energy Calculations and Excited-State Molecular Dynamics Simulations. *Phys. Chem. Chem. Phys.* **2013**, *15*, 12322−12329.
(224) Improta, R.; Santoro, F.; Blancafort, L. Quantum Mechanical Studies on the Photophysics and the Photochemistry of Nucleic Acids and Nucleobases. *Chem. Rev.* **2016**, *116*, 3540−3593.
(225) Segarra-Martí, J.; Tran, T.; Bearpark, M. J. Ultrafast and Radiationless Electronic Excited State Decay of Uracil and Thymine Cations: Computing the Effects of Dynamic Electron Correlation. *Phys. Chem. Chem. Phys.* **2019**, *21*, 14322−14330.
(226) Nishimoto, Y. Locating Conical Intersections using the Quasidegenerate Partially and Strongly Contracted NEVPT2Methods. *Chem. Phys. Lett.* **2020**, *744*, 137219.
(227) Gozem, S.; Huntress, M.; Schapiro, I.; Lindh, R.; Granovsky, A. A.; Angeli, C.; Olivucci, M. Dynamic Electron Correlation Effects on the Ground State Potential Energy Surface of a Retinal Chromophore Model. *J. Chem. Theory Comput.* **2012**, *8*, 4069−4080.
(228) Gozem, S.; Krylov, A. I.; Olivucci, M. Conical Intersection and Potential Energy Surface Features of a Model Retinal Chromophore: Comparison of EOM-CC and Multireference Methods. *J. Chem. Theory Comput.* **2013**, *9*, 284−292.
(229) Gozem, S.; Melaccio, F.; Lindh, R.; Krylov, A. I.; Granovsky, A. A.; Angeli, C.; Olivucci, M. Mapping the Excited State Potential Energy Surface of a Retinal Chromophore Model with Multireference and Equation-of-Motion Coupled-Cluster Methods. *J. Chem. Theory Comput.* **2013**, *9*, 4495−4506.
(230) Huix-Rotllant, M.; Filatov, M.; Gozem, S.; Schapiro, I.; Olivucci, M.; Ferré, N. Assessment of Density Functional Theory for

https://doi.org/10.1021/acs.chemrev.1c00074
Chem. Rev. XXXX, XXX, XXX−XXX

Describing the Correlation Effects on the Ground and Excited State Potential Energy Surfaces of a Retinal Chromophore Model. *J. Chem. Theory Comput.* **2013**, *9*, 3917−3932.
(231) Gozem, S.; Melaccio, F.; Valentini, A.; Filatov, M.; Huix-Rotllant, M.; Ferre, N.; Manuel Frutos, L.; Angeli, C.; Krylov, A. I.; Granovsky, A. A.; Lindh, R.; Olivucci, M. Shape of Multireference, Equation-of-Motion Coupled-Cluster, and Density Functional Theory Potential Energy Surfaces at a Conical Intersection. *J. Chem. Theory Comput.* **2014**, *10*, 3074−3084.
(232) Tuna, D.; Lefrancois, D.; Wolanski, L.; Gozem, S.; Schapiro, I.; Andruniow, T.; Dreuw, A.; Olivucci, M. Assessment of Approximate Coupled-Cluster and Algebraic-Diagrammatic-Construction Methods for Ground- and Excited-State Reaction Paths and the Conical-Intersection Seam of a Retinal-Chromophore Model. *J. Chem. Theory Comput.* **2015**, *11*, 5758−5781.
(233) Schapiro, I.; Neese, F. SORCI for Photochemical and Thermal Reaction Paths: A Benchmark Study. *Comput. Theor. Chem.* **2014**, *1040-1041*, 84−98.
(234) Gozem, S.; Schapiro, I.; Ferre, N.; Olivucci, M. The Molecular Mechanism of Thermal Noise in Rod Photoreceptors. *Science* **2012**, *337*, 1225−1228.
(235) Werner, H.-J.; Kállay, M.; Gauss, J. The Barrier Height of the F + H_2 Reaction Revisited: Coupled-Cluster and Multireference Configuration-Interaction Benchmark Calculations. *J. Chem. Phys.* **2008**, *128*, 034305.
(236) Rozgonyi, T.; González, L. On the Location of Conical Intersections in CH2BrCl Using MS-CASPT2Methods. *J. Phys. Chem. A* **2006**, *110*, 10251−10259.
(237) Neese, F. A Spectroscopy Oriented Configuration Interaction Procedure. *J. Chem. Phys.* **2003**, *119*, 9428−9443.
(238) Liu, X.; Fatehl, S.; Shao, Y.; Veldkamp, B. S.; Subotnik, J. E. Communication: Adjusting Charge Transfer State Energies for Configuration Interaction Singles: Without Any Parameterization and with Minimal Cost. *J. Chem. Phys.* **2012**, *136*, 161101.
(239) Liu, X.; Subotnik, J. E. The Variationally Orbital-Adapted Configuration Interaction Singles (VOA-CIS) Approach to Electronically Excited States. *J. Chem. Theory Comput.* **2014**, *10*, 1004−1020.
(240) Liu, X.; Subotnik, J. E. Erratum: ÒThe Variationally Orbital-Adapted Configuration Interaction Singles (VOA-CIS) Approach to Electronically Excited States. *J. Chem. Theory Comput.* **2014**, *10*, 1835−1835.
(241) Teh, H.-H.; Subotnik, J. E. The Simplest Possible Approach for Simulating S-0-S-1 Conical Intersections with DFT/TDDFT: Adding One Doubly Excited Configuration. *J. Phys. Chem. Lett.* **2019**, *10*, 3426−3432.
(242) Levine, B. G.; Ko, C.; Quenneville, J.; Martínez, T. J. Conical Intersections and Double Excitations in Time-Dependent Density Functional Theory. *Mol. Phys.* **2006**, *104*, 1039−1051.
(243) Head-Gordon, M.; Rico, R. J.; Oumi, M.; Lee, T. J. A Doubles Correction to Electronic Excited States from Configuration Interaction in the Space of Single Substitutions. *Chem. Phys. Lett.* **1994**, *219*, 21−29.
(244) Head-Gordon, M.; Oumi, M.; Maurice, D. Quasidegenerate Second-Order Perturbation Corrections to Single-Excitation Configuration Interaction. *Mol. Phys.* **1999**, *96*, 593−602.
(245) Hättig, C. Structure Optimizations for Excited States with Correlated Second-Order Methods: CC2 and ADC(2). *Adv. Quantum Chem.* **2005**, *50*, 37−60.
(246) Laikov, D.; Matsika, S. Inclusion of Second-Order Correlation Effects for the Ground and Singly-Excited States Suitable for the Study of Conical Intersections: The CIS(2) Model. *Chem. Phys. Lett.* **2007**, *448*, 132−137.
(247) Christiansen, O.; Koch, H.; Jorgensen, P. The Second-Order Approximate Coupled Cluster Singles and Doubles Model CC2. *Chem. Phys. Lett.* **1995**, *243*, 409−418.
(248) Hättig, C.; Weigend, F. CC2 Excitation Energy Calculations on Large Molecules using the Resolution of the Identity Approximation. *J. Chem. Phys.* **2000**, *113*, 5154−5161.
(249) Hohenstein, E. G.; Kokkila, S. I. L.; Parrish, R. M.; Martínez, T. J. Quartic Scaling Second-Order Approximate Coupled Cluster Singles and Doubles via Tensor Hypercontraction: THC-CC2. *J. Chem. Phys.* **2013**, *138*, 124111.
(250) Hohenstein, E. G.; Kokkila, S. I. L.; Parrish, R. M.; Martínez, T. J. Tensor Hypercontraction Equation-of-Motion Second-Order Approximate Coupled Cluster: Electronic Excitation Energies in O(N4) Time. *J. Phys. Chem. B* **2013**, *117*, 12972−12978.
(251) Dreuw, A.; Wormit, M. The Algebraic Diagrammatic Construction Scheme for the Polarization Propagator for the Calculation of Excited States. *WIREs Comput. Mol. Sci.* **2015**, *5*, 82−95.
(252) Schirmer, J. Beyond the Random-Phase Approximation: A New Approximation Scheme for the Polarization Propagator. *Phys. Rev. A: At., Mol., Opt. Phys.* **1982**, *26*, 2395−2416.
(253) Trofimov, A. B.; Schirmer, J. An Efficient Polarization Propagator Approach to Valence Electron Excitation Spectra. *J. Phys. B: At., Mol. Opt. Phys.* **1995**, *28*, 2299−2324.
(254) Schirmer, J. Closed-Form Intermediate Representations of Many-Body Propagators and Resolvent Matrices. *Phys. Rev. A: At., Mol., Opt. Phys.* **1991**, *43*, 4647−4659.
(255) Grimme, S.; Goerigk, L.; Fink, R. F. Spin-Component-Scaled Electron Correlation Methods. *WIREs Comput. Mol. Sci.* **2012**, *2*, 886−906.
(256) Hellweg, A.; Gruan, S.; Hättig, C. Benchmarking the Performance of Spin-Component Scaled CC2 in Ground and Electronically Excited States. *Phys. Chem. Chem. Phys.* **2008**, *10*, 4119−4127.
(257) Krauter, C. M.; Pernpointner, M.; Dreuw, A. Application of the Scaled-Opposite-Spin Approximation to Algebraic Diagrammatic Construction Schemes of Second Order. *J. Chem. Phys.* **2013**, *138*, 044107.
(258) Grimme, S. Improved Second-Order M?ller-Plesset Perturbation Theory by Separate Scaling of Parallel- and Antiparallel-Spin Pair Correlation Energies. *J. Chem. Phys.* **2003**, *118*, 9095−9102.
(259) Casanova, D.; Rhee, Y. M.; Head-Gordon, M. Quasidegenerate Scaled Opposite Spin Second Order Perturbation Corrections to Single Excitation Configuration Interaction. *J. Chem. Phys.* **2008**, *128*, 164106.
(260) Plasser, F.; Crespo-Otero, R.; Pederzoli, M.; Pittner, J.; Lischka, H.; Barbatti, M. Surface Hopping Dynamics with Correlated Single-Reference Methods: 9H-Adenine as a Case Study. *J. Chem. Theory Comput.* **2014**, *10*, 1395−1405.
(261) Stojanovic, L.; Bai, S.; Nagesh, J.; Izmaylov, A. F.; Crespo-Otero, R.; Lischka, H.; Barbatti, M. New Insights into the State Trapping of UV-Excited Thymine. *Molecules* **2016**, *21*, 1603.
(262) Lischka, H.; Barbatti, M.; Siddique, F.; Das, A.; Aquino, A. J. A. The Effect of Hydrogen Bonding on the Nonadiabatic Dynamics of a Thymine-Water Cluster. *Chem. Phys.* **2018**, *515*, 472−479.
(263) Hu, D.; Liu, Y. F.; Sobolewski, A. L.; Lan, Z. Nonadiabatic Dynamics Simulation of Keto Isocytosine: a Comparison of Dynamical Performance of Different Electronic-Structure Methods. *Phys. Chem. Chem. Phys.* **2017**, *19*, 19168−19177.
(264) Du, L.; Lan, Z. An On-the-Fly Surface-Hopping Program JADE for Nonadiabatic Molecular Dynamics of Polyatomic Systems: Implementation and Applications. *J. Chem. Theory Comput.* **2015**, *11*, 1360−1374.
(265) Köhn, A.; Tajti, A. Can Coupled-Cluster Theory Treat Conical Intersections? *J. Chem. Phys.* **2007**, *127*, 044105.
(266) Lefrancois, D.; Wormit, M.; Dreuw, A. Adapting Algebraic Diagrammatic Construction Schemes for the Polarization Propagator to Problems with Multi-Reference Electronic Ground States Exploiting the Spin-Flip Ansatz. *J. Chem. Phys.* **2015**, *143*, 124107.
(267) Bartlett, R. J. Coupled-Cluster Approach to Molecular-Structure and Spectra - a Step Toward Predictive Quantum-Chemistry. *J. Phys. Chem.* **1989**, *93*, 1697−1708.
(268) Bartlett, R. J.; Musial, M. Coupled-Cluster Theory in Quantum Chemistry. *Rev. Mod. Phys.* **2007**, *79*, 291−352.
(269) Crawford, T. D.; Schaefer, H. F., III In *Reviews in Computational Chemistry*; Lipkowitz, K. B., Boyd, D. B., Eds.; Wiley-VCH: New York, 1999; Vol. *14*, pp 33−136.

https://doi.org/10.1021/acs.chemrev.1c00074
Chem. Rev. XXXX, XXX, XXX−XXX

(270) Stanton, J. F.; Bartlett, R. J. The Equation of Motion Coupled-Cluster Method. A Systematic Biorthogonal Approach to Molecular Excitation Energies, Transition Probabilities, and Excited State Properties. *J. Chem. Phys.* **1993**, *98*, 7029−7039.
(271) Comeau, D. C.; Bartlett, R. J. The Equation-of-Motion Coupled-Cluster Method. Applications to Open- and Closed-Shell Reference States. *Chem. Phys. Lett.* **1993**, *207*, 414−423.
(272) Sneskov, K.; Christiansen, O. Excited State Coupled Cluster Methods. *WIREs Comput. Mol. Sci.* **2012**, *2*, 566−584.
(273) Krylov, A. I. Equation-of-Motion Coupled-Cluster Methods for Open-Shell and Electronically Excited Species: The Hitchhiker's Guide to Fock Space. *Annu. Rev. Phys. Chem.* **2008**, *59*, 433−462.
(274) Benda, Z.; Szalay, P. G. Details of the Excited-State Potential Energy Surfaces of Adenine by Coupled Cluster Techniques. *J. Phys. Chem. A* **2014**, *118*, 6197−6207.
(275) Kjonstad, E. F.; Myhre, R. H.; Martínez, T. J.; Koch, H. Crossing Conditions in Coupled Cluster Theory. *J. Chem. Phys.* **2017**, *147*, 164105.
(276) Kjonstad, E. F.; Koch, H. Resolving the Notorious Case of Conical Intersections for Coupled Cluster Dynamics. *J. Phys. Chem. Lett.* **2017**, *8*, 4801−4807.
(277) Krylov, A. I. Size-Consistent Wave Functions for Bond-Breaking: The Equation-of-Motion Spin-Flip Model. *Chem. Phys. Lett.* **2001**, *338*, 375−384.
(278) Krylov, A. I. Spin-Flip Equation-of-Motion Coupled-Cluster Electronic Structure Method for a Description of Excited States, Bond Breaking, Diradicals, and Triradicals. *Acc. Chem. Res.* **2006**, *39*, 83−91.
(279) Casida, M. E.; Huix-Rotllant, M. Progress in Time-Dependent Density-Functional Theory. *Annu. Rev. Phys. Chem.* **2012**, *63*, 287−323.
(280) Dreuw, A.; Head-Gordon, M. Single-Reference ab Initio Methods for the Calculation of Excited States of Large Molecules. *Chem. Rev.* **2005**, *105*, 4009−4037.
(281) Cordova, F.; Doriol, L. J.; Ipatov, A.; Casida, M. E.; Filippi, C.; Vela, A. Troubleshooting Time-Dependent Density-Functional Theory for Photochemical Applications: Oxirane. *J. Chem. Phys.* **2007**, *127*, 164111.
(282) Tapavicza, E.; Tavernelli, I.; Rothlisberger, U.; Filippi, C.; Casida, M. E. Mixed Time-Dependent Density-Functional Theory/Classical Trajectory Surface Hopping Study of Oxirane Photochemistry. *J. Chem. Phys.* **2008**, *129*, 124108.
(283) Huix-Rotllant, M.; Natarajan, B.; Ipatov, A.; Wawire, C. M.; Deutsch, T.; Casida, M. E. Assessment of Noncollinear Spin-Flip Tamm-Dancoff Approximation Time-Dependent Density-Functional Theory for the Photochemical Ring-Opening of Oxirane. *Phys. Chem. Chem. Phys.* **2010**, *12*, 12811−12825.
(284) Huix-Rotllant, M.; Nikiforov, A.; Thiel, W.; Filatov, M. Description of Conical Intersections with Density Functional Methods. *Top. Curr. Chem.* **2015**, *368*, 445−476.
(285) Barbatti, M.; Crespo-Otero, R. Surface Hopping Dynamics with DFT Excited States. *Top. Curr. Chem.* **2014**, *368*, 415−444.
(286) Maitra, N.; Zhang, F.; Cave, R.; Burke, K. Double Excitations within Time-Dependent Density Functional Theory Linear Response. *J. Chem. Phys.* **2004**, *120*, 5932−5937.
(287) Cave, R.; Zhang, F.; Maitra, N.; Burke, K. A Dressed TDDFT Treatment of the 2^1A_g States of Butadiene and Hexatriene. *Chem. Phys. Lett.* **2004**, *389*, 39−42.
(288) Li, S. L.; Marenich, A. V.; Xu, X.; Truhlar, D. G. Configuration Interaction-Corrected Tamm-Dancoff Approximation: A Time-Dependent Density Functional Method with the Correct Dimensionality of Conical Intersections. *J. Phys. Chem. Lett.* **2014**, *5*, 322−328.
(289) Shu, Y.; Parker, K. A.; Truhlar, D. G. Dual-Functional Tamm-Dancoff Approximation: A Convenient Density Functional Method that Correctly Describes S-1/S-0 Conical Intersections. *J. Phys. Chem. Lett.* **2017**, *8*, 2107−2112.
(290) van Aggelen, H.; Yang, Y.; Yang, W. Exchange-Correlation Energy from Pairing Matrix Fluctuation and the Particle-Particle Random Phase Approximation. *Phys. Rev. A: At., Mol., Opt. Phys.* **2013**, *88*, 030501.
(291) Yang, Y.; van Aggelen, H.; Yang, W. Double, Rydberg and Charge Transfer Excitations from Pairing Matrix Fluctuation and Particle-Particle Random Phase Approximation. *J. Chem. Phys.* **2013**, *139*, 224105.
(292) Yang, Y.; Shen, L.; Zhang, D.; Yang, W. Conical Intersections from Particle-Particle Random Phase and Tamm-Dancoff Approximations. *J. Phys. Chem. Lett.* **2016**, *7*, 2407−2411.
(293) Bannwarth, C.; Yu, J. K.; Hohenstein, E. G.; Martinez, T. J. Hole-hole Tamm-Dancoff-approximated density functional theory: A highly efficient electronic structure method incorporating dynamic and static correlation. *J. Chem. Phys.* **2020**, *153*, 024110.
(294) Yu, J. K.; Bannwarth, C.; Hohenstein, E. G.; Martinez, T. J. Ab Initio Nonadiabatic Molecular Dynamics with Hole-Hole Tamm-Dancoff Approximated Density Functional Theory. *J. Chem. Theory Comput.* **2020**, *16*, 5499−5511.
(295) Yu, J. K.; Bannwarth, C.; Liang, R.; Hohenstein, E. G.; Martinez, T. J. Nonadiabatic Dynamics Simulation of the Wavelength-Dependent Photochemistry of Azobenzene Excited to the n pi* and pi pi* Excited States. *J. Am. Chem. Soc.* **2020**, *142*, 20680−20690.
(296) Teh, H.-H.; Subotnik, J. E. Analytic Gradients and Derivative Couplings for Configuration Interaction with All Single Excitations and One Double Excitation-En Route to Nonadiabatic Dynamics. *J. Chem. Phys.* **2020**, *153*, 184106.
(297) Kaduk, B.; Kowalczyk, T.; Voorhis, T. V. Constrained Density Functional Theory. *Chem. Rev.* **2012**, *112*, 321−370.
(298) Wu, Q.; Cheng, C.-L.; Van Voorhis, T. Configuration Interaction Based on Constrained Density Functional Theory: A Multireference Method. *J. Chem. Phys.* **2007**, *127*, 164119.
(299) Kaduk, B.; Van Voorhis, T. Communication: Conical Intersections using Constrained Density Functional Theory-Configuration Interaction. *J. Chem. Phys.* **2010**, *133*, 061102.
(300) Kaduk, B.; Tsuchimochi, T.; Van Voorhis, T. Analytic Energy Gradients for Constrained DFT-Configuration Interaction. *J. Chem. Phys.* **2014**, *140*, 18A503.
(301) Lieb, E. Density Functionals for Coulomb Systems. *Int. J. Quantum Chem.* **1983**, *24*, 243−277.
(302) Gross, E.; Oliveira, L.; Kohn, W. Rayleigh-Ritz Variational Principle for Ensembles of Fractionally Occupied States. *Phys. Rev. A: At., Mol., Opt. Phys.* **1988**, *37*, 2805−2808.
(303) Gross, E.; Oliveira, L.; Kohn, W. Density-Functional Theory for Ensembles of Fractionally Occupied States. I. Basic Formalism. *Phys. Rev. A: At., Mol., Opt. Phys.* **1988**, *37*, 2809−2820.
(304) Oliveira, L.; Gross, E.; Kohn, W. Density-Functional Theory for Ensembles of Fractionally Occupied States. II. Application to the He Atom. *Phys. Rev. A: At., Mol., Opt. Phys.* **1988**, *37*, 2821−2833.
(305) Frank, I.; Hutter, J.; Marx, D.; Parrinello, M. Molecular Dynamics in Low-Spin Excited States. *J. Chem. Phys.* **1998**, *108*, 4060−4069.
(306) Filatov, M.; Shaik, S. Spin-Restricted Density Functional Approach to the Open-Shell Problem. *Chem. Phys. Lett.* **1998**, *288*, 689−697.
(307) Kowalczyk, T.; Tsuchimochi, T.; Chen, P.-T.; Top, L.; Voorhis, T. V. Excitation Energies and Stokes Shifts from a Restricted Open-Shell Kohn-Sham Approach. *J. Chem. Phys.* **2013**, *138*, 164101.
(308) Filatov, M.; Shaik, S. A Spin-Restricted Ensemble-Referenced Kohn-Sham Method and its Application to Diradicaloid Situations. *Chem. Phys. Lett.* **1999**, *304*, 429−437.
(309) Billeter, S. R.; Egli, D. Calculation of Nonadiabatic Couplings with Restricted Open-Shell Kohn-Sham Density- Functional Theory. *J. Chem. Phys.* **2006**, *125*, 224103.
(310) Kazaryan, A.; Heuver, J.; Filatov, M. Excitation Energies from Spin-Restricted Ensemble-Referenced Kohn-Sham Method: A State-Average Approach. *J. Phys. Chem. A* **2008**, *112*, 12980−12988.
(311) Nikiforov, A.; Gamez, J. A.; Thiel, W.; Huix-Rotllant, M.; Filatov, M. Assessment of Approximate Computational Methods for Conical Intersections and Branching Plane Vectors in Organic Molecules. *J. Chem. Phys.* **2014**, *141*, 124122.

https://doi.org/10.1021/acs.chemrev.1c00074
Chem. Rev. XXXX, XXX, XXX−XXX

(312) Filatov, M. Assessment of Density Functional Methods for Obtaining Geometries at Conical Intersections in Organic Molecules. *J. Chem. Theory Comput.* **2013**, *9*, 4526−4541.
(313) Filatov, M. Spin-Restricted Ensemble-Referenced Kohn-Sham Method: Basic Principles and Application to Strongly Correlated Ground and Excited States of Molecules. *WIREs Comput. Mol. Sci.* **2015**, *5*, 146−167.
(314) Filatov, M.; Liu, F.; Martinez, T. J. Analytical Derivatives of the Individual State Energies in Ensemble Density Functional Theory Method. I. General formalism. *J. Chem. Phys.* **2017**, *147*, 034113.
(315) Filatov, M.; Min, S. K.; Kim, K. S. Direct Nonadiabatic Dynamics by Mixed Quantum-Classical Formalism Connected with Ensemble Density Functional Theory Method: Application to Trans-Penta-2,4-dieniminium Cation. *J. Chem. Theory Comput.* **2018**, *14*, 4499−4512.
(316) Filatov, M.; Min, S. K.; Kim, K. S. Non-Adiabatic Dynamics of Ring Opening in Cyclohexa-1,3-diene Described by an Ensemble Density-Functional Theory Method. *Mol. Phys.* **2019**, *117*, 1128−1141.
(317) Liu, F.; Filatov, M.; Martínez, T. J. Analytical Derivatives of the Individual State Energies in Ensemble Density Functional Theory. II. Implementation on Graphical Processing Units (GPUs). *J. Chem. Phys.* **2021**, *154*, 104108.
(318) Liang, R.; Liu, F.; Martínez, T. J. Nonadiabatic Photodynamics of Retinal Protonated Schiff Base in Channelrhodopsin 2. *J. Phys. Chem. Lett.* **2019**, *10*, 2862−2868.
(319) Yu, J. K.; Liang, R.; Liu, F.; Martínez, T. J. First-Principles Characterization of the Elusive I Fluorescent State and the Structural Evolution of Retinal Protonated Schiff Base in Bacteriorhodopsin. *J. Am. Chem. Soc.* **2019**, *141*, 18193−18203.
(320) Peters, L. D. M.; Kussmann, J.; Ochsenfeld, C. A Fermi Smearing Variant of the Tamm-Dancoff Approximation for Non-adiabatic Dynamics Involving S1-S0 Transitions: Validation and Application to Azobenzene. *J. Chem. Phys.* **2020**, *153*, 094104.
(321) Slipchenko, L. V.; Krylov, A. I. Singlet-Triplet Gaps in Diradicals by the Spin-Flip Approach: A Benchmark Study. *J. Chem. Phys.* **2002**, *117*, 4694−4708.
(322) Krylov, A. Spin-Flip Configuration Interaction: An Electronic Structure Model that is Both Variational and Size-Consistent. *Chem. Phys. Lett.* **2001**, *350*, 522−530.
(323) Shao, Y.; Head-Gordon, M.; Krylov, A. I. The Spin-Flip Approach Within Time-Dependent Density Functional Theory: Theory and Applications to Diradicals. *J. Chem. Phys.* **2003**, *118*, 4807−4818.
(324) Bernard, Y. A.; Shao, Y.; Krylov, A. I. General Formulation of Spin-Flip Time-Dependent Density Functional Theory Using Non-Collinear Kernels: Theory, Implementation, and Benchmarks. *J. Chem. Phys.* **2012**, *136*, 204103.
(325) Manohar, P. U.; Krylov, A. A Noniterative Perturbative Triples Correction for the Spin-Flipping and Spin-Conserving Equation-of-Motion Coupled-Cluster Methods with Single and Double Substitutions. *J. Chem. Phys.* **2008**, *129*, 194105.
(326) Levchenko, S. V.; Krylov, A. I. Equation-of-Motion Spin-Flip Coupled-Cluster Model with Single and Double Substitutions: Theory and Application to Cyclobutadiene. *J. Chem. Phys.* **2004**, *120*, 175−185.
(327) Herbert, J. M.; Zhang, X.; Morrison, A. F.; Liu, J. Beyond Time-Dependent Density Functional Theory Using Only Single Excitations: Methods for Computational Studies of Excited States in Complex Systems. *Acc. Chem. Res.* **2016**, *49*, 931−941.
(328) Minezawa, N.; Gordon, M. S. Optimizing Conical Intersections by Spin-Flip Density Functional Theory: Application to Ethylene. *J. Phys. Chem. A* **2009**, *113*, 12749−12753.
(329) Zhang, X.; Herbert, J. M. Spin-Flip, Tensor Equation-of-Motion Configuration Interaction with a Density-Functional Correction: A Spin-Complete Method for Exploring Excited-State Potential Energy Surfaces. *J. Chem. Phys.* **2015**, *143*, 234107.
(330) Lefrancois, D.; Tuna, D.; Martínez, T. J.; Dreuw, A. The Spin-Flip Variant of the Algebraic-Diagrammatic Construction Yields the Correct Topology of S1/S0 Conical Intersections. *J. Chem. Theory Comput.* **2017**, *13*, 4436−4441.
(331) Harabuchi, Y.; Keipert, K.; Zahariev, F.; Taketsugu, T.; Gordon, M. S. Dynamics Simulations with Spin-Flip Time-Dependent Density Functional Theory: Photoisomerization and Photocyclization Mechanisms of Cis-Stilbene in $\pi\pi$ States. *J. Phys. Chem. A* **2014**, *118*, 11987−11998.
(332) Minezawa, N.; Gordon, M. S. Optimizing Conical Intersections of Solvated Molecules: The Combined Spin-Flip Density Functional Theory/Effective Fragment Potential Method. *J. Chem. Phys.* **2012**, *137*, 034116.
(333) Casanova, D.; Slipchenko, L. V.; Krylov, A. I.; Head-Gordon, M. Double Spin-Flip Approach within Equation-of-Motion Coupled Cluster and Configuration Interaction Formalisms: Theory, Implementation and Examples. *J. Chem. Phys.* **2009**, *130*, 044103.
(334) Casanova, D.; Krylov, A. I Spin-Flip Methods in Quantum Chemistry. *Phys. Chem. Chem. Phys.* **2020**, *22*, 4326−4342.
(335) Liu, J.; Koslowski, A.; Thiel, W. Analytic Gradient and Derivative Couplings for the Spin-Flip Extended Configuration Interaction Singles Method: Theory, Implementation, and Application to Proton Transfer. *J. Chem. Phys.* **2018**, *148*, 244108.
(336) Sears, J. S.; Sherrill, C. D.; Krylov, A. I. A Spin-Complete Version of the Spin-Flip Approach to Bond Breaking: What is the Impact of Obtaining Spin Eigenfunctions? *J. Chem. Phys.* **2003**, *118*, 9084−9094.
(337) Casanova, D.; Head-Gordon, M. The Spin-Flip Extended Single Excitation Configuration Interaction Method. *J. Chem. Phys.* **2008**, *129*, 064104.
(338) Bell, F.; Zimmerman, P. M.; Casanova, D.; Goldey, M.; Head-Gordon, M. Restricted Active Space Spin-Flip (RAS-SF) with Arbitrary Number of Spin-Flips. *Phys. Chem. Chem. Phys.* **2013**, *15*, 358−366.
(339) Shoji, M.; Koizumi, K.; Kitagawa, Y.; Kawakami, T.; Yamanaka, S.; Okumura, M.; Yamaguchi, K. A. General Algorithm for Calculation of Heisenberg Exchange Integrals J in Multispin Systems. *Chem. Phys. Lett.* **2006**, *432*, 343−347.
(340) Tsuchimochi, T. Spin-Flip Configuration Interaction Singles with Exact Spin-Projection: Theory and Applications to Strongly Correlated Systems. *J. Chem. Phys.* **2015**, *143*, 144114.
(341) Xu, X.; Gozem, S.; Olivucci, M.; Truhlar, D. G. Combined Self-Consistent-Field and Spin-Flip Tamm-Dancoff Density Functional Approach to Potential Energy Surfaces for Photochemistry. *J. Phys. Chem. Lett.* **2013**, *4*, 253−258.
(342) Li, Z.; Liu, W. Spin-Adapted Open-Shell Random Phase Approximation and Time-Dependent Density Functional Theory. I. Theory. *J. Chem. Phys.* **2010**, *133*, 064106.
(343) Mato, J.; Gordon, M. S. Analytic Non-Adiabatic Couplings for the Spin-Flip ORMAS Method. *Phys. Chem. Chem. Phys.* **2020**, *22*, 1475−1484.
(344) Feng, X.; Luzanov, A. V.; Krylov, A. I. Fission of Entangled Spins: An Electronic Structure Perspective. *J. Phys. Chem. Lett.* **2013**, *4*, 3845−3852.
(345) Matsika, S.; Feng, X.; Luzanov, A. V.; Krylov, A. I. What We Can Learn from the Norms of One-particle Density Matrices, and What We Can't. *J. Phys. Chem. A* **2014**, *118*, 11943−11955.
(346) Lee, S.; Filatov, M.; Lee, S.; Choi, C. H. Eliminating Spin-Contamination of Spin-Flip Time Dependent Density Functional Theory within Linear Response Formalism by the Use of Zeroth-Order Mixed- Reference (MR) Reduced Density Matrix. *J. Chem. Phys.* **2018**, *149*, 104101.
(347) Lee, S.; Shostak, S.; Filatov, M.; Choi, C. H. Conical Intersections in Organic Molecules: Benchmarking Mixed-Reference Spin-Flip Time-Dependent DFT (MRSF-TD-DFT) vs Spin-Flip TD-DFT. *J. Phys. Chem. A* **2019**, *123*, 6455−6462.
(348) Thiel, W. Semiempirical Quantum Chemical Methods. *Wiley Interdiscip. Rev.: Comput. Mol. Sci.* **2014**, *4*, 145−157.
(349) Koslowski, A.; Beck, M. E.; Thiel, W. Implementation of a General Multireference Configuration Interaction Procedure with Analytic Gradients in a Semiempirical Context Using the Graphical Unitary Group Approach. *J. Comput. Chem.* **2003**, *24*, 714−726.
(350) Tuna, D.; Lu, Y.; Koslowski, A.; Thiel, W. Semiempirical Quantum-Chemical Orthogonalization-Corrected Methods: Bench-

https://doi.org/10.1021/acs.chemrev.1c00074
Chem. Rev. XXXX, XXX, XXX−XXX

marks of Electronically Excited States. *J. Chem. Theory Comput.* **2016**, *12*, 4400−4422.
(351) Gerber, R. B.; Shemesh, D.; Varner, M. E.; Kalinowski, J.; Hirshberg, B. Ab Initio and Semi-Empirical Molecular Dynamics Simulations of Chemical Reactions in Isolated Molecules and in Clusters. *Phys. Chem. Chem. Phys.* **2014**, *16*, 9760−9775.
(352) Liu, J.; Thiel, W. An Efficient Implementation of Semiempirical Quantum-Chemical Orthogonalization-Corrected Methods for Excited-State Dynamics. *J. Chem. Phys.* **2018**, *148*, 154103.
(353) Toniolo, A.; Granucci, G.; Martínez, T. J. Conical Intersections in Solution: A QM/MM Study Using Floating Occupation Semiempirical Configuration Interaction Wave Functions. *J. Phys. Chem. A* **2003**, *107*, 3822−3830.
(354) Virshup, A. M.; Punwong, C.; Pogorelov, T. V.; Lindquist, B. A.; Ko, C.; Martínez, T. J. Photodynamics in Complex Environments: Ab Initio Multiple Spawning Quantum Mechanical/Molecular Mechanical Dynamics. *J. Phys. Chem. B* **2009**, *113*, 3280−3291.
(355) Thongyod, W.; Buranachai, C.; Pengpan, T.; Punwong, C. Fluorescence Quenching by Photoinduced Electron Transfer between 7-Methoxycoumarin and Guanine Base Facilitated by Hydrogen Bonds: An In Silico Study. *Phys. Chem. Chem. Phys.* **2019**, *21*, 16258−16269.
(356) Grimme, S.; Waletzke, M. A Combination of Kohn-Sham Density Functional Theory and Multi-Reference Configuration Interaction Methods. *J. Chem. Phys.* **1999**, *111*, 5645−5655.
(357) Lyskov, I.; Kleinschmidt, M.; Marian, C. M. Redesign of the DFT/MRCI Hamiltonian. *J. Chem. Phys.* **2016**, *144*, 034104.
(358) Marian, C. M.; Heil, A.; Kleinschmidt, M. The DFT/MRCI Method. *Wiley Interdiscip. Rev.: Comput. Mol. Sci.* **2019**, *9*, No. e1394.
(359) Heil, A.; Marian, C. M. DFT/MRCI Hamiltonian for Odd and Even Numbers of Electrons. *J. Chem. Phys.* **2017**, *147*, 194104.
(360) Pohler, L.; Kleinschmidt, M.; Etinski, M.; Marian, C. M. In Search of the Dark State of 5-Methyl-2-hydroxypyrimidine using a Numerical DFT/MRCI Gradient. *Mol. Phys.* **2012**, *110*, 2429−2438.
(361) Faraji, S.; Matsika, S.; Krylov, A. I. Calculations of Non-Adiabatic Couplings within Equation-of-Motion Coupled-Cluster Framework: Theory, Implementation, and Validation Against Multi-Reference Methods. *J. Chem. Phys.* **2018**, *148*, 044103.
(362) Galloy, C.; Lorquet, J. C. Nonadiabatic Interaction in Unimolecular Decay. III. Selection and Propensity Rules for Polyatomic Molecules. *J. Chem. Phys.* **1977**, *67*, 4672−4680.
(363) Desouter-Lecomte, M.; Galloy, C.; Lorquet, J. C.; Pires, M. V. Nonadiabatic Interactions in Unimolecular decay. V. Conical and Jahn-Teller Intersections. *J. Chem. Phys.* **1979**, *71*, 3661−3672.
(364) Hirsch, G.; Bruna, P. J.; Buenker, R. J.; Peyerimhoff, S. D. Non-Adiabatic Coupling Matrix Elements $< \Psi^{\alpha}|\Psi^{\beta} >$ for Large CI Wavefunctions. *Chem. Phys.* **1980**, *45*, 335−347.
(365) Hammes-Schiffer, S.; Tully, J. C. Proton Transfer in Solution: Molecular Dynamics with Quantum Transitions. *J. Chem. Phys.* **1994**, *101*, 4657−4667.
(366) Shu, Y.; Zhang, L.; Sun, S.; Truhlar, D. G. Time-Derivative Couplings for Self-Consistent Electronically Nonadiabatic Dynamics. *J. Chem. Theory Comput.* **2020**, *16*, 4098−4106.
(367) Meek, G. A.; Levine, B. G. Evaluation of the Time-Derivative Coupling for Accurate Electronic State Transition Probabilities from Numerical Simulations. *J. Phys. Chem. Lett.* **2014**, *5*, 2351−2356.
(368) Ryabinkin, I. G.; Nagesh, J.; Izmaylov, A. F. Fast Numerical Evaluation of Time-Derivative Nonadiabatic Couplings for Mixed Quantum-Classical Methods. *J. Phys. Chem. Lett.* **2015**, *6*, 4200−4203.
(369) Garrett, B. C.; Truhlar, D. G. The Coupling of Electronically Adiabatic States in Atomic and Molecular Collisions. In *Theoretical Chemistry: Advances and Perspectives*; Henderson, D., Ed.; Academic Press: New York, 1981; Vol. *6A*, pp 215−289.
(370) Saxe, P.; Lengsfield, B. H.; Yarkony, D. R. On the Evaluation of Non-Adiabatic Coupling Matrix Elements for Large Scale CI Wavefunctions. *Chem. Phys. Lett.* **1985**, *113*, 159−164.
(371) Yarkony, D. R. On the Reaction $Na(^2P) + H \rightarrow Na(^2S) + H_2$ Nonadiabatic Effects. *J. Chem. Phys.* **1986**, *84*, 3206−3211.
(372) Russek, A. Rotationally Induced Transitions in Atomic Collisions. *Phys. Rev. A: At., Mol., Opt. Phys.* **1971**, *4*, 1918−1924.
(373) Buenker, R. J.; Peric, M.; Peyerimhoff, S. D.; Marian, R. Ab Initio Treatment of the Renner-Teller Effect for the X $^2B_1$ and A $^2A_1$ Electronic States of NH_2. *Mol. Phys.* **1981**, *43*, 987−1014.
(374) Yarkony, D. R. Nonadiabatic Effects in the Vicinity of Multiple Surface Crossings. Evaluation of Derivative Couplings with Respect to Rotational and Internal Degrees of Freedom. Application to the Charge Transfer Reaction $H^+ + NO \rightarrow H + NO^+$. *J. Chem. Phys.* **1989**, *90*, 1657−1665.
(375) Lengsfield, B. H.; Saxe, P.; Yarkony, D. R. On the Evaluation of Non-Adiabatic Coupling Matrix Elements using SA-MCSCF/CI Wavefunctions and Analytic Gradient Techniques. *J. Chem. Phys.* **1984**, *81*, 4549−4553.
(376) Delos, J. B. Theory of Electronic Transitions in Slow Atomic Collisions. *Rev. Mod. Phys.* **1981**, *53*, 287−357.
(377) Kutzelnigg, W. Which Masses are Vibrating or Rotating in a Molecule? *Mol. Phys.* **2007**, *105*, 2627−2647.
(378) Fatehi, S.; Alguire, E.; Shao, Y.; Subotnik, J. E. Analytic Derivative couplings between Configuration-Interaction-Singles States with Built-In Electron-Translation Factors for Translational Invariance. *J. Chem. Phys.* **2011**, *135*, 234105.
(379) Fatehi, S.; Subotnik, J. E. Derivative Couplings with Built-In Electron-Translation Factors: Application to Benzene. *J. Phys. Chem. Lett.* **2012**, *3*, 2039−2043.
(380) Lengsfield, B. H.; Yarkony, D. R. In *State-Selected and State-to-State Ion−Molecule Reaction Dynamics: Part 2 Theory*; Baer, M., Ng, C. Y., Eds.; Advances in Chemical Physics; John Wiley and Sons: New York, 1992; Vol. *82*, pp 1−71.
(381) Bak, K. L.; Jorgensen, P.; Jorgen, A.; Jensen, H.; Olsen, J.; Helgaker, T. First-Order Nonadiabatic coupling Matrix Elements from Multiconfigurational Self- Consistent-Field Response Theory. *J. Chem. Phys.* **1992**, *97*, 7573−7584.
(382) Rice, J.; Amos, R. On the Efficient Evaluation of Analytic Energy Gradients. *Chem. Phys. Lett.* **1985**, *122*, 585−590.
(383) Page, M.; Saxe, P.; Adams, G. F.; Lengsfield, B. H. Multireference CI Gradients and MCSCF Second Derivatives. *J. Chem. Phys.* **1984**, *81*, 434−439.
(384) Handy, N. C.; Schaefer, H. F., III On the Evaluation of Analytic Energy Derivatives for Correlated Wave Functions. *J. Chem. Phys.* **1984**, *81*, 5031−5033.
(385) Lischka, H.; Shepard, R.; Pitzer, R. M.; Shavitt, I.; Dallos, M.; Müller, T.; Szalay, P. G.; Seth, M.; Kedziora, G. S.; Yabushita, S.; Zhang, Z. High-Level Multireference Methods in the Quantum-Chemistry Program System COLUMBUS: Analytic MR-CISD and MR-AQCC Gradients and MR-AQCC-LRT for Excited States, GUGA Spin-Orbit CI and Parallel CI Density. *Phys. Chem. Chem. Phys.* **2001**, *3*, 664−673.
(386) Belcher, L. T.; Kedziora, G. S.; Weeks, D. E. Analytic Non-Adiabatic Derivative Coupling Terms for Spin-Orbit MRCI Wavefunctions. I. Formalism. *J. Chem. Phys.* **2019**, *151*, 234104.
(387) Belcher, L. T.; Lewis, C. D., III; Kedziora, G. S.; Weeks, D. E. Analytic Non-Adiabatic Derivative Coupling Terms for Spin-Orbit MRCI Wavefunctions. II. Derivative Coupling Terms and Coupling Angle for $KHe(A^2\Pi_{1/2}) \rightarrow KHe(B^2\Sigma_{1/2})$. *J. Chem. Phys.* **2019**, *151*, 234109.
(388) Khait, Y. G.; Theis, D.; Hoffmann, M. R. Lagrangian Approach for Geometrical Derivatives and Nonadiabatic Coupling Terms in MRCISD. *Mol. Phys.* **2010**, *108*, 2703−2716.
(389) Frisch, M. J.; Trucks, G. W.; Schlegel, H. B.; Scuseria, G. E.; Robb, M. A.; Cheeseman, J. R.; Scalmani, G.; Barone, V.; Petersson, G. A.; Nakatsuji, H.; et al. *Gaussian16*, Revision C.01; Gaussian Inc.: Wallingford, CT, 2016.
(390) Galvan, I. F.; et al. OpenMolcas: From Source Code to Insight. *J. Chem. Theory Comput.* **2019**, *15*, 5925−5964.
(391) Galvan, I. F.; Delcey, M. G.; Pedersen, T. B.; Aquilante, F.; Lindh, R. Analytical State-Average Complete-Active-Space Self-Consistent Field Nonadiabatic Coupling Vectors: Implementation with Density-Fitted Two-Electron Integrals and Application to Conical Intersections. *J. Chem. Theory Comput.* **2016**, *12*, 3636−3653.

https://doi.org/10.1021/acs.chemrev.1c00074
Chem. Rev. XXXX, XXX, XXX−XXX

(392) Ufimtsev, I.; Martinez, T. J. Quantum Chemistry on Graphical Processing Units. 3. Analytical Energy Gradients and First Principles Molecular Dynamics. *J. Chem. Theory Comput.* **2009**, *5*, 2619−2628.
(393) Titov, A. V.; Ufimtsev, I. S.; Luehr, N.; Martínez, T. J. Generating Efficient Quantum Chemistry Codes for Novel Architectures. *J. Chem. Theory Comput.* **2013**, *9*, 213−221.
(394) Seritan, S.; Bannwarth, C.; Fales, B. S.; Hohenstein, E. G.; Isborn, C. M.; Kokkila-Schumacher, S. I. L.; Li, X.; Liu, F.; Luehr, N.; Snyder, J. W., Jr.; et al. TeraChem: A Graphical Processing Unit-Accelerated Electronic Structure Package for Large-Scale Ab Initio Molecular Dynamics. *Wiley Interdiscip. Rev.: Comput. Mol. Sci.* **2021**, *11*, No. e1494.
(395) Tao, H.; Levine, B. G.; Martínez, T. J. Ab Initio Multiple Spawning Dynamics Using Multi-State Second-Order Perturbation Theory. *J. Phys. Chem. A* **2009**, *113*, 13656−13662.
(396) Redmon, L. Perturbative Determination of Nonadiabatic Coupling Matrix Elements. *Phys. Rev. A: At., Mol., Opt. Phys.* **1982**, *25*, 2453−2466.
(397) Khait, Y. G.; Theis, D.; Hoffmann, M. R. Nonadiabatic Coupling Terms for the GVVPT2 Variant of Multireference Perturbation Theory. *Chem. Phys.* **2012**, *401*, 88−94.
(398) Christiansen, O. First-Order Nonadiabatic Coupling Matrix Elements using Coupled Cluster Methods. I. Theory. *J. Chem. Phys.* **1999**, *110*, 711−723.
(399) Ichino, T.; Gauss, J.; Stanton, J. F. Quasidiabatic States Described by Coupled-Cluster Theory. *J. Chem. Phys.* **2009**, *130*, 174105.
(400) Tajti, A.; Szalay, P. G. Analytic Evaluation of the Nonadiabatic Coupling Vector between Excited States using Equation-of-Motion Coupled-Cluster Theory. *J. Chem. Phys.* **2009**, *131*, 124104.
(401) Assmann, M.; Weinacht, T.; Matsika, S. Surface Hopping Investigation of the Relaxation Dynamics in Radical Cations. *J. Chem. Phys.* **2016**, *144*, 034301.
(402) Chernyak, V.; Mukamel, S. Density-Matrix Representation of Nonadiabatic Couplings in Time-Dependent Density Functional (TDDFT) Theories. *J. Chem. Phys.* **2000**, *112*, 3572−3579.
(403) Tommasini, M.; Chernyak, V.; Mukamel, S. Electronic Density-Matrix Algorithm for Non-Adiabatic Couplings in Molecular Dynamics Simulations. *Int. J. Quantum Chem.* **2001**, *85*, 225−238.
(404) Baer, R. Non-Adiabatic Couplings by Time-Dependent Density Functional Theory. *Chem. Phys. Lett.* **2002**, *364*, 75−79.
(405) Billeter, S. R.; Curioni, A. Calculation of Nonadiabatic Couplings in Density-Functional Theory. *J. Chem. Phys.* **2005**, *122*, 034105.
(406) Hu, C.; Hirai, H.; Sugino, O. Nonadiabatic Couplings from Time-Dependent Density Functional Theory: Formulation in the Casida Formalism and Practical Scheme within Modified Linear Response. *J. Chem. Phys.* **2007**, *127*, 064103.
(407) Hu, C.; Hirai, H.; Sugino, O. Nonadiabatic Couplings from Time-Dependent Density Functional Theory. II. Successes and Challenges of the Pseudopotential Approximation. *J. Chem. Phys.* **2008**, *128*, 154111.
(408) Hu, C.; Sugino, O.; Tateyama, Y. All-Electron Calculation of Nonadiabatic Couplings from Time-Dependent Density Functional Theory: Probing with the Hartree-Fock Exact Exchange. *J. Chem. Phys.* **2009**, *131*, 114101.
(409) Hu, C.; Sugino, O.; Hirai, H.; Tateyama, Y. Nonadiabatic Couplings from the Kohn-Sham Derivative Matrix: Formulation by Time-Dependent Density-Functional Theory and Evaluation in the Pseudopotential Framework. *Phys. Rev. A: At., Mol., Opt. Phys.* **2010**, *82*, 062508.
(410) Tavernelli, I.; Tapavicza, E.; Rothlisberger, U. Trajectory Surface Hopping within Linear Response Time-Dependent Density-Functional Theory. *Phys. Rev. Lett.* **2007**, *98*, 023001.
(411) Tavernelli, I.; Tapavicza, E.; Rothlisberger, U. Nonadiabatic Coupling Vectors within Linear Response Time-Dependent Density Functional Theory. *J. Chem. Phys.* **2009**, *130*, 124107.
(412) Tavernelli, I.; Curchod, B. F. E.; Rothlisberger, U. On Nonadiabatic Coupling Vectors in Time-Dependent Density Functional Theory. *J. Chem. Phys.* **2009**, *131*, 196101.
(413) Tavernelli, I.; Curchod, B. F. E.; Laktionov, A.; Rothlisberger, U. Nonadiabatic Coupling Vectors for Excited States within Time-Dependent Density Functional Theory in the Tamm-Dancoff Approximation and Beyond. *J. Chem. Phys.* **2010**, *133*, 194104.
(414) Send, R.; Furche, F. First-Order Nonadiabatic Couplings from Time-Dependent Hybrid Density Functional Response Theory: Consistent Formalism, Implementation, and Performance. *J. Chem. Phys.* **2010**, *132*, 033107.
(415) Li, Z.; Liu, W. First-Order Nonadiabatic Coupling Matrix Elements between Excited States: A Lagrangian Formulation at the CIS, RPA, TD-HF, and TD-DFT Levels. *J. Chem. Phys.* **2014**, *141*, 014110.
(416) Li, Z.; Liu, W. First-Order Nonadiabatic Coupling Matrix Elements between Excited States: Implementation and Application at the TD-DFT and pp-TDA Levels. *J. Chem. Phys.* **2014**, *141*, 244105.
(417) Zhang, X.; Herbert, J. M. Analytic Derivative Couplings in Time-Dependent Density Functional Theory: Quadratic Response Theory Versus Pseudo-Wavefunction Approach. *J. Chem. Phys.* **2015**, *142*, 064109.
(418) Ou, Q.; Alguire, E. C.; Subotnik, J. E. Derivative Couplings between Time-Dependent Density Functional Theory Excited States in the Random-Phase Approximation Based on Pseudo-Wavefunctions: Behavior around Conical Intersections. *J. Phys. Chem. B* **2015**, *119*, 7150−7161.
(419) Ou, Q.; Fatehi, S.; Alguire, E.; Shao, Y.; Subotnik, J. E. Derivative Couplings between TDDFT Excited States Obtained by Direct Differentiation in the Tamm-Dancoff Approximation. *J. Chem. Phys.* **2014**, *141*, 024114.
(420) Subotnik, J. E.; Alguire, E. C.; Ou, Q.; Landry, B. R.; Fatehi, S. The Requisite Electronic Structure Theory To Describe Photoexcited Nonadiabatic Dynamics: Nonadiabatic Derivative Couplings and Diabatic Electronic Couplings. *Acc. Chem. Res.* **2015**, *48*, 1340−1350.
(421) Ou, Q.; Bellchambers, G. D.; Furche, F.; Subotnik, J. E. First-Order Derivative Couplings between Excited States from Adiabatic TDDFT Response Theory. *J. Chem. Phys.* **2015**, *142*, 064114.
(422) Parker, S. M.; Roy, S.; Furche, F. Multistate Hybrid Time-Dependent Density Functional Theory with Surface Hopping Accurately Captures Ultrafast Thymine Photodeactivation. *Phys. Chem. Chem. Phys.* **2019**, *21*, 18999−19010.
(423) Nelson, T.; Fernandez-Alberti, S.; Chernyak, V.; Roitberg, A. E.; Tretiak, S. Nonadiabatic Excited-State Molecular Dynamics Modeling of Photoinduced Dynamics in Conjugated Molecules. *J. Phys. Chem. B* **2011**, *115*, 5402−5414.
(424) Pauli, W. *Handbuch der Physik*; Springer: New York, 1933; Vol. *24*.
(425) Tapavicza, E.; Bellchambers, G. D.; Vincent, J. C.; Furche, F. Ab Initio Non-Adiabatic Molecular Dynamics. *Phys. Chem. Chem. Phys.* **2013**, *15*, 18336−18348.
(426) Lin, Y.; Akimov, A. V. Dependence of Nonadiabatic Couplings with Kohn-Sham Orbitals on the Choice of Density Functional: Pure vs Hybrid. *J. Phys. Chem. A* **2016**, *120*, 9028−9041.

https://doi.org/10.1021/acs.chemrev.1c00074
Chem. Rev. XXXX, XXX, XXX−XXX